Cellulose nanopaper as reinforcement for sustainable polymer composites

2018

Martin Hervy

A dissertation submitted to Imperial College London

for the degree of Doctor of Philosophy

in the Department of Aeronautics

Abstract

The use of cellulose nanopapers as reinforcement to produce high performance polymer composites is investigated in this thesis. Cellulose nanopapers are dense networks of nanofibrils that uses the hydrogen bonding ability of cellulose nanofibres. Both microbially synthesised cellulose nanofibres (known as bacterial cellulose or BC) and wood derived cellulose nanofibrils (CNF), were used in this work.

This thesis starts with the investigation of the influence of test specimen geometries on the measured tensile properties of both CNF and BC nanopapers is investigated. Miniaturised specimens are often used for the tensile testing of cellulose nanopapers as there are no standardised test geometries to evaluate their tensile properties Four test specimen geometries were studied: (i) miniaturised dog bone specimen with 2 mm width, (ii) miniaturised rectangular specimen with 5 mm width, (iii) standard dog bone specimen with 5 mm width and (iv) standard rectangular specimen with 15 mm width. It was found that the tensile moduli of both CNF and BC nanopapers were not significantly influenced by the test specimen geometries if an independent strain measurement system (video extensometer) was employed. The average tensile strength of the cellulose nanopapers is also influenced by test specimen geometries. It was observed that the smaller the test specimen width, the higher the average tensile strength of the cellulose nanopapers. This can be described by the weakest link theory, whereby the probability of defects present in the cellulose nanopapers increases with increasing test specimen width. The Poisson's ratio and fracture resistance of nanopapers are also discussed.

The use of (ultra-)low grammage nanopaper as polymer reinforcement is also investigated. Bacterial cellulose (BC) nanopapers of 5, 10, 25 and 50 g m^{-2} were manufactured. Vacuum filtration to produce a 5 g m^{-2} nanopaper was found to be 3 times faster than that of a 50 g m^{-2}. Low grammage nanopapers possessed a tensile modulus and strength as low as 2.4 GPa and 31 MPa respectively, against 11.8 GPa and 111 MPa for the 50 g m^{-2}. Laminated composites containing 10, 5, 2 and 1 layer(s) of 5, 10, 25 and 50 g m^{-2} nanopapers were produced using a polylactide (PLLA) matrix. With a fibre loading fractions of $v_f \geq 39\%$, the manufactured composites all possessed a tensile

modulus and strength of ~10 GPa and ~100 MPa, respectively. The porosity of the nanopapers increased from 48% to 78% from 50 g m^{-2} to 5 g m^{-2}. The porosity of the composites was ~10% independently of the layup. Finally, SEM images of the fracture surfaces of the composites revealed a layered morphology with little or no impregnation.

The mechanical response of PLLA reinforced with multiple layers of BC nanopaper is then discussed. Laminated composites consisting of 1, 3, 6 and 12 sheet(s) of BC nanopaper were produced. It was observed that increasing the number of BC nanopaper led to an increase in the porosity of the resulting BC nanopaper-reinforced PLLA laminated composites. The tensile moduli of the laminated composites were found to be ~12.5 – 13.5 GPa, insensitive to the number of sheets of BC nanopaper in the composites but the tensile strength of the laminated composites decreased by up to 25% (from 121 MPa to 95 MPa) when the number of reinforcing BC nanopaper increased from 1 to 12 sheets. This was attributed to the presence and severity of the scale-induced defects increased with increasing number of sheets of BC nanopaper in the PLLA laminated composites.

Finally, the environmental impacts of BC- and CNF-reinforced epoxy composites were evaluated using life cycle assessment (LCA). Neat polylactide (PLA) and 30% randomly oriented glass fibre-reinforced polypropylene (GF/PP) composites were used as benchmark materials for comparison. A cradle-to-gate LCA showed that BC- and CNF-reinforced epoxy composites have higher global warming potential (GWP) and abiotic depletion potential of fossil fuels (ADf) compared to neat PLA and GF/PP even though the specific tensile moduli of the nanocellulose-reinforced epoxy composites are higher than neat PLA and GF/PP. However, when the use phase and the end-of-life of nanocellulose-reinforced epoxy composites are considered, their “green credentials” are comparable to that of neat PLA and GF/PP composites. The life cycle scenario analysis showed that the cradle-to-grave GWP and ADf of BC- and CNF-reinforced epoxy composites could be lower than neat PLA when the composites contains more than 60 vol.-% nanocellulose. The LCA model suggests that nanocellulose-reinforced epoxy composites with high nanocellulose loading is desired to produce materials with “greener credentials” than the best performing commercially available bio-derived polymer.

Copyright declaration

Declaration of originality

I declare that this report and the work presented in it are my own and has been generated by me as the result of my own research. Where I have consulted the published work of others, this is always clearly attributed; where I have quoted the work of others, the source is always given. This work was done wholly in candidature for a research degree at Imperial College London.

Martin HERVY

Acknowledgement

I would like to express my sincere gratitude to Dr. Koon-Yang Lee for enabling me to pursue this doctoral degree. His constant support and guidance throughout this PhD punctuated with many discussions on the research or science in general are what made this entire work possible.

I also thank dearly the co-authors on the papers on which I collaborated which all helped my work in one way or another and particularly Frederic Bock for his implication and dedication to the work. Additionally, I want to mention the members of the Future Materials group for their help in the long term and friendship outside of research: Wenzhe Song, Alba Santmarti, Diyang Li, Nicolas Février and Jannah Noorol Daud.

Je remercie également mes parents qui m'ont toujours soutenu et m'ont permis de voyager en Angleterre en 2012 et ensuite en Australie en 2013 pour des projets de recherche qui m'ont amenés à poursuivre ce doctorat.

Acknowledgements are extended to the EPSRC, University College London and Imperial College London for funding the research and my scholarship.

Table of Contents

List of figures

List of tables

List of publications

Peer-reviewed Journal Papers

1. Hervy, M., Evangelisti, S., Lettieri, P., Lee, K.-Y., Life cycle assessment of nanocellulose-reinforced advanced fibre composites. Composites Science and Technology, 2015, 118, 154–162.

2. Hervy M., Santmarti, A., Lahtinen, P., Tammelin, T., Lee, K.-Y., Sample geometry dependency on the measured tensile properties of cellulose nanopapers. Materials & Design, 2017, 121, 421-429.

3. Mautner, A., Mayer, F., Hervy, M., Lee, K-Y., Bismarck, A. Better Together: Synergy in Nanocellulose Blends, Philosophical Transactions of the Royal Society A, 2018, 376.

4. Hervy M., Bock F., Lee, K.-Y., (Ultra-)Low grammage bacterial cellulose nanopaper-reinforced polylactide composite laminates, submitted.

5. Hervy M., Blaker J. J., Braz A. L., Lee, K.-Y., Mechanical response of multi-layer bacterial cellulose nanopaper-reinforced polylactide laminated composites, Composites Part A: Applied Science and Manufacturing, 2018, 107, 155-163.

Conference presentations

- ❖ Oral presentations at conferences

1. Hervy, M., Evangelisti, S., Lettieri, P., Lee, K.-Y., Life cycle assessment of high performance nanocellulose-reinforced advanced fibre composites. 249th American Chemical Society National Meeting & Exposition, 22-26th March 2015, Denver, Colorado, USA.

2. Hervy, M., Evangelisti, S., Lettieri, P., Lee, K.-Y., Life cycle assessment of high performance nanocellulose-reinforced advanced fibre composites. Nordic Polymer Days, 30th May to 1st June 2016, Helsinki, Finland.

3. Hervy M., Bock F., Lee, K.-Y., Thin ply bacterial cellulose-reinforced polylactide nanocomposites. 253rd American Chemical Society National Meeting & Exposition, 2-6th April 2017, San Francisco, California, USA.

- Poster presentations at conferences

1. Hervy, M., Evangelisti, S., Lettieri, P., Lee, K.-Y., Life cycle assessment of nanocellulose-reinforced polymer composites. Round Table of Ideas, Nanocellulose 2015, September 26-28th 2015, Vienna, Austria.

2. Hervy M., Santmarti, A., Lahtinen, P., Tammelin, T., Lee, K.-Y., Sample geometry dependency on the measured tensile properties of cellulose nanopapers. New horizons for nanocellulose technology, The Royal Society, 2-3rd May 2017, London, UK.

- Conference Proceeding

1. Hervy, M., Evangelisti, S., Lettieri, P., Lee, K.-Y. Life cycle assessment of high performance nanocellulose-reinforced advanced fibre composites. 20th International Conference on Composite Materials, 19-24th July 2015, Copenhagen, Denmark.

1 Introduction

Nanometre scale cellulose fibres, or nanocellulose, are emerging nano-reinforcement for polymers. The major driver for utilising nanocellulose as reinforcement is the possibility of exploiting the high tensile stiffness and strength of cellulose crystals [1]. Raman spectroscopy and X-ray diffraction have estimated the tensile moduli of a single nanocellulose fibre to be between 100-160 GPa [2–5]. The tensile strength of a single nanocellulose fibre was estimated to be 900 MPa based on experiments conducted on single elementary flax and hemp fibres [6]. More recently, Saito et al. [7] used ultrasound-induced fragmentation of nanocellulose fibres to estimate the tensile strength of a single 2,2,6,6-tetramethylpiperidinyl-1-oxyl (TEMPO) oxidised nanocellulose fibre. The authors estimated the tensile strength of single wood- and tunicate-derived nanocellulose fibre to be 1.6 GPa and 3.2 GPa, respectively based on this method.

Nanocellulose can be produced via two approaches: top-down or bottom-up. In the top-down approach, lignocellulosic biomass such as wood pulp can be exposed to high intensity ultrasound [8] to isolate the cellulose nanofibres from fibre bundles or passed through stone grinders [9,10] and high pressure homogenisers or microfluidisers [11,12] to fibrillate these fibres to the nanometre scale. This lignocellulosic biomass-derived nanocellulose is more commonly known as cellulose nanofibres* (CNF). In the bottom-up approach, nanocellulose is produced by the fermentation of low molecular weight sugars using cellulose-producing bacteria, such as from the *Acetobacter* species

* The term microfibrillated cellulose and nanofibrillated cellulose are also often used in literature.

[13]. Microbially synthesised cellulose, more commonly known as bacterial cellulose (BC), is secreted by the bacteria in the form of wet pellicles (thick biofilm). BC is synthesised directly as nanofibres of approximately ~50 nm in diameter and several micrometres in length [13]. Nanocellulose can also be extracted from certain algae and tunicates [14].

A pre-requisite to producing high performance CNF- and BC-reinforced polymer composites is to incorporate high loadings of nanocellulose (typically > 30 vol.-%) into the polymer matrix [15]. In this context, high performance cellulose networks or nanopapers can be used directly as reinforcement for polymers. Cellulose network in the form of cellulose nanopapers represents a conceptually important material structure [16] for various applications, including filtration membranes [17], packaging [18], electronics [19] and as nano-reinforcement for polymers [15]. Whilst cellulose nanopapers are dense and difficult to impregnate with resin, using nanopapers is the only *feasible and economically viable manufacturing technology* to achieve high nanocellulose loading fractions within composites, which is also a prerequisite to producing high performance nanocomposites.

1.1 Aim and objectives

The aim of this thesis is to make use of cellulose nanopapers to produce truly green, high-performance cellulose nanopaper-reinforced polymer composites. The specific objectives are:

- To produce high performance nanopaper-reinforced polymer composites
- To manufacture (ultra-)low grammage nanopapers that can be impregnated with a polymer at the single nanofibre level

- ❖ To assess and quantify the green credentials of cellulose nanopaper-reinforced polymer composites.

1.2 Structure of the thesis

This thesis is split into 8 chapters. Chapter 2 contains a state of the art of neat cellulose nanopaper-reinforced polymer composites. Chapter 3 describes the influence of sample geometry on the measured tensile properties of cellulose nanopapers. Chapter 4 discusses the use of (ultra-)low grammage BC nanopaper as reinforcement for polylactide (PLLA) composite laminates. Chapter 5 investigates the influence of the number of reinforcing BC nanopapers on the tensile properties of BC nanopaper-reinforced PLLA composite. The life cycle assessment of cellulose nanopaper-reinforced polymer composites is discussed in chapter 6. Finally, chapter 7 summarises the conclusions from this thesis and chapter 8 discusses possible directions for future work in the continuation of this thesis.

2 Literature review

2.1 Nanocellulose in polymer composites

2.1.1 Nanocellulose-reinforced polymer composites

The first use of nanocellulose as reinforcement for polymer, namely polypropylene (PP), polystyrene (PS) and polyethylene (PE) was reported by Boldizar et al. [20]. The authors reported that the incorporation of 40 wt.-% nanofibrillated cellulose in PS by melt compounding increased the tensile modulus of their injection moulded sample from 2.4 GPa to 5.2 GPa. This experimentally obtained tensile modulus was more than what they calculated theoretically using the Halpin-Tsai equation and was interpreted as a direct result of the high aspect ratio, modulus and strength of the nanofibrils.

Since then, many authors have produced nanocellulose-reinforced composites using different polymers, different nanocellulose contents as well as multiple manufacturing techniques. Figure 1 and Figure 2 show the tensile modulus and strength, respectively, of BC- and CNF-reinforced polymer composites found in the literature in function of their nanocellulose volume fraction. From Figure 1 and Figure 2, it can be concluded that high nanocellulose loading fractions must be achieved in order to produce composites with high mechanical performance [15]. Lee et al. [15] recommended fibre volume fractions of >30 vol.-% should be reached in order to surpass the tensile properties of PLLA (polylactide), a commercially available green polymer.

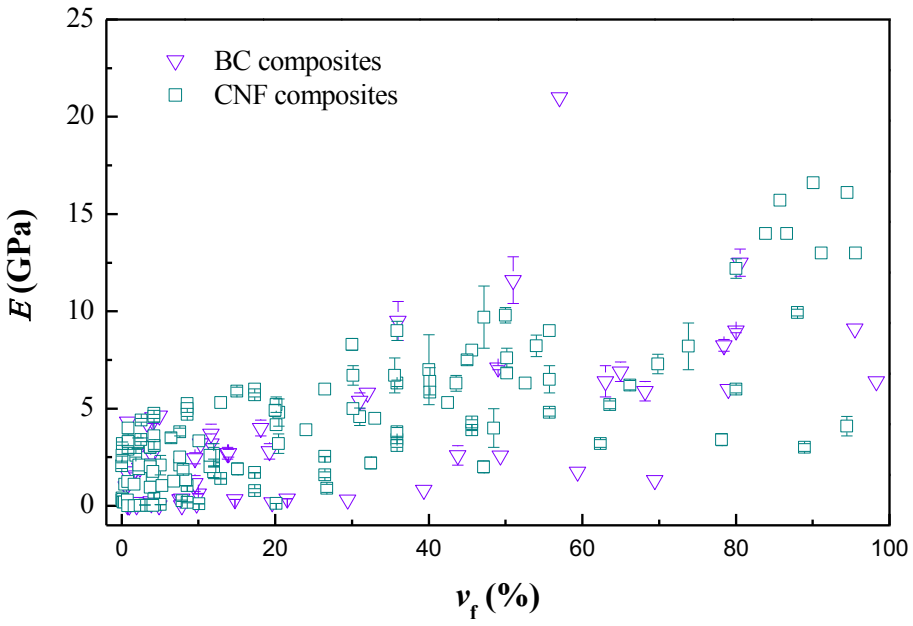

Figure 1: Tensile modulus of BC- and CNF-reinforced polymer composites found in the literature in function of their fibre volume fraction. Data obtained from [15] with the addition of recent relevant cellulose nanopaper-reinforced polymer composite data.

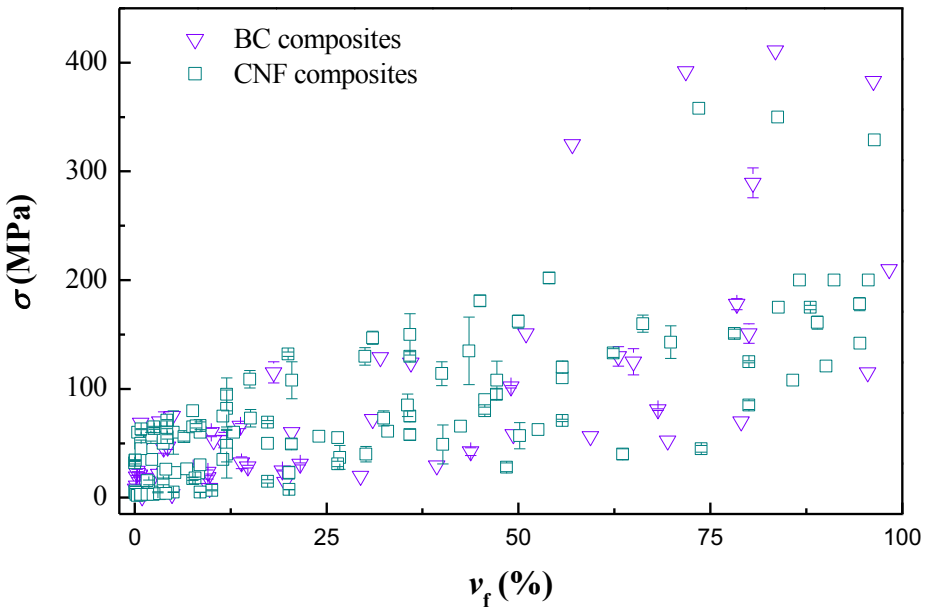

Figure 2: Tensile strength of BC- and CNF-reinforced polymer composites found in the literature in function of their fibre volume fraction. Data obtained from [15] with the addition of recent relevant cellulose nanopaper-reinforced polymer composite data.

The same group of authors also showed that the tensile properties of cellulose nanopaper-reinforced polymer composites are governed predominantly by the tensile properties of the cellulose nanopaper used [15]. Cellulose nanopapers are typically produced by vacuum filtration of a dilute nanocellulose-in-water suspension followed by water removal and heat consolidation. The tensile properties of the resulting cellulose nanopaper-reinforced polymer composites follow closely the prediction of the volume-weighted average between the tensile properties of the cellulose nanopaper and the polymer matrix:

$$E_{\text{composite}} = E_{\text{nanopaper}} v_{\text{f}} + E_{\text{matrix}} \times (1 - v_{\text{f}}) \tag{2.1}$$

$$\sigma_{\text{composite}} = \sigma_{\text{nanopaper}} v_{\text{f}} + \sigma_{\text{matrix}} \times (1 - v_{\text{f}}) \tag{2.2}$$

where $E_{\text{composite}}$, $E_{\text{nanopaper}}$ and E_{matrix} denote the tensile moduli of the cellulose nanopaper-reinforced polymer composites, cellulose nanopaper and matrix, respectively. $\sigma_{\text{nanocomposite}}$, $\sigma_{\text{nanopaper}}$ and σ_{matrix} are the tensile strengths of the composites, cellulose nanopaper and the matrix, respectively. v_{f} is the volume fraction of cellulose nanopaper in the composites.

2.1.2 BC nanopaper-reinforced polymer composites

Yano et al. [21] reported in 2005 among the highest tensile properties for a BC-reinforced polymer composite. In this work, the authors produced a 65 wt.-% BC-reinforced epoxy composite by the infusion of BC nanopaper under vacuum (vacuum assisted resin infusion or VARI). The tensile strength of the resulting composite was measured to be around 325 MPa, improving upon the 260 MPa measured for the BC

sheet alone. The tensile modulus of the BC nanopaper-reinforced epoxy composite was found to be around 20-21 GPa. Despite the high BC volume fraction, the transparency of the neat epoxy resin was well retained in the resulting BC-reinforced composite (Figure 3) with a light transmittance of >80% in the 500-800 nm range. This was attributed to the size of the BC nanofibres (~50 nm) which is postulated to be small enough not to induce light scattering, which is usually associated with the presence of a reinforcing phase in a polymer.

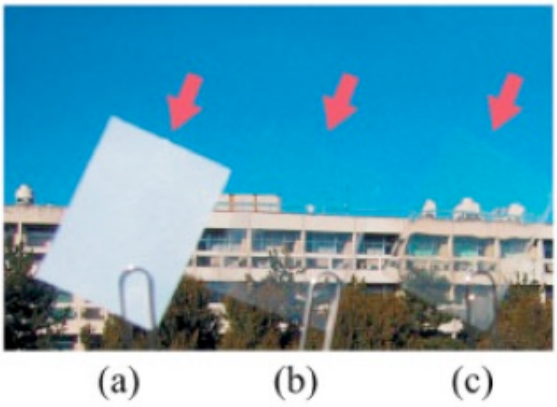

Figure 3: (a) BC nanopaper (b) 62 wt.-% with acrylic resin and (c) 65 wt.-% with epoxy resin taken from Yano et al. [21].

Contrarily to VARI, lamination constitutes a very simple and quick way to produce cellulose nanopaper-reinforced polymer composites. Quero et al. [22] used compression moulding to produce a laminated composite consisting of a dried and well consolidated sheet of BC (at v_f = 18 vol.-%) between sheets of PLLA. A tensile modulus and strength of 4 GPa modulus and 115 MPa, respectively, was obtained for the resulting BC nanopaper-reinforced PLLA composite. In this work, the differences induced by different cultivation time of BC was also studied. Higher mechanical properties of the

resulting dried and well consolidated BC network were positively correlated with longer cultivation times. However, the BC nanopaper-reinforced laminated composite containing the BC that was cultivated for the shortest time was found to possess the highest tensile properties. The authors further used Raman spectroscopy to demonstrate that stress transfer efficiency between the BC network and the matrix was better for BC network that were cultivated for the shortest time. Because no impregnation of the PLLA in the BC network was observed, it was postulated the thinner and less laminated morphology of these BC networks were the factors leading to better stress transfer.

Following up upon this work, high BC loading fraction and high performance BC nanopaper-reinforced PLLA composites with a laminated composite architecture (as observed in the SEM images in Figure 4) was produced by stacking and compression-moulding BC nanopaper between two thin PLA films [23]. A BC nanopaper loading of 65 vol.-% was achieved by producing extremely thin PLLA films using solvent casting. The resulting composites possessed a tensile modulus and strength of 6.9 GPa and 125 MPa, respectively, improving upon the work of Quero et al. [22]. Nevertheless, it was found that the tensile properties of the BC nanopaper-reinforced PLLA composite were closer to the prediction of equation 2.1 and 2.2 than prediction from micromechanical models relying on the single BC nanofibre properties. This led to the conclusion that the tensile properties of BC nanopaper-reinforced laminated composites are dominated by the tensile properties of the reinforcing cellulose nanopaper instead of that of the single BC nanofibre.

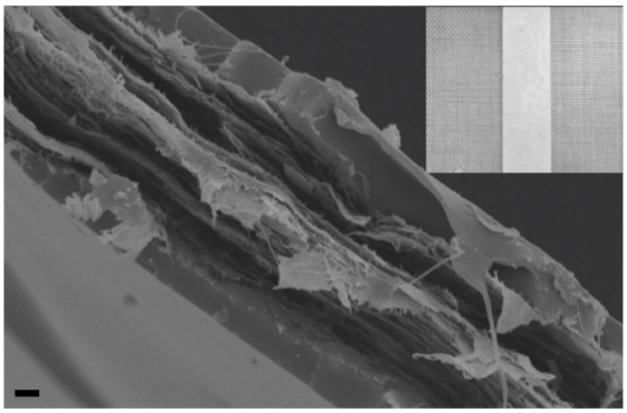

Figure 4: Fractured surface of a BC nanopaper-reinforced polylactide (v_f=65 vol.-%) produced by lamination observed by SEM [23]. The inset shows a photo of the produced laminated composite.

Cellulose nanopaper-reinforced polymer composites can also be produced by immersing nanopaper(s) in a liquid resin, followed by a consolidation/crosslinking step. This method has been used to reinforce polydiethylene glycol bis(allyl carbonate) (DEAC) [24], a castor oil based polyurethane [25] and a photocurable polyurethane [26], with BC nanopaper. In [24], the authors obtained a transparent composite with 88% light transmittance at 550 nm at 63 vol.-% BC. This was attributed to complete filling of the pores of the BC network. These results are comparable to the results obtained by Yano et al. [21]. It was also noted the photocuring of the DEAC was much quicker than the thermal curing of more traditional resins. The tensile modulus and strength measured for this composite was of 6.4 GPa and 130 MPa respectively.

In [25], a light transmittance of 82% at 700 nm was achieved for the BC nanopaper-reinforced PU composites with a BC loading of 79 vol.-%, which is also comparable to the two previous studies [21,24]. For this work, the tensile modulus and strength obtained for the BC nanopaper-reinforced composite were of 6 GPa and 70

MPa, respectively. This demonstrates the potential of BC nanopaper as reinforcement to produce transparent composites. In [26], the authors produced BC nanopaper-reinforced polyurethane composite by immersing the nanopaper in the resin for 1 min, followed by 3 min of photocuring. A tensile modulus and strength of 11.6 GPa and 151 MPa, respectively, were reported at a BC loading fraction of 51 vol.-%. The higher tensile properties obtained by these authors with PU compared to [25] can be attributed to the stronger polymer matrix used (0.19 GPa and 16 MPa modulus and strength respectively vs 0.016 GPa and 2 MPa in [25]). The authors also produced composites with more porous BC nanopapers by either using less pressure during consolidation or by drying the BC nanopaper from ethanol. The tensile properties of these composites, however, were not as high as those obtained with a well consolidated BC nanopaper.

2.1.3 CNF nanopaper-reinforced polymer composites

Wang et al. [27] also used an immersion technique to produce CNF-reinforced polyvinyl alcohol (PVA). The CNF nanopaper was immersed in a PVA solution for 12 h, followed by drying at 40°C overnight. The resulting composite (CNF loading fraction of 76 vol.-%) possessed a light transmittance of 84% at a wavelength of 600 nm, demonstrating that CNF nanopapers can also be used to produce optically transparent composites. The composite also possessed a tensile modulus and strength of 6 GPa and 123 MPa respectively (Figure 5b), which followed closely tensile properties predicted by equation 2.1 and equation 2.2. The strain at break of the composite, however, was limited to the strain-at-break of the CNF nanopaper (8.6%) and thus did not benefit to the high strain-at-break of PVA (Figure 5a).

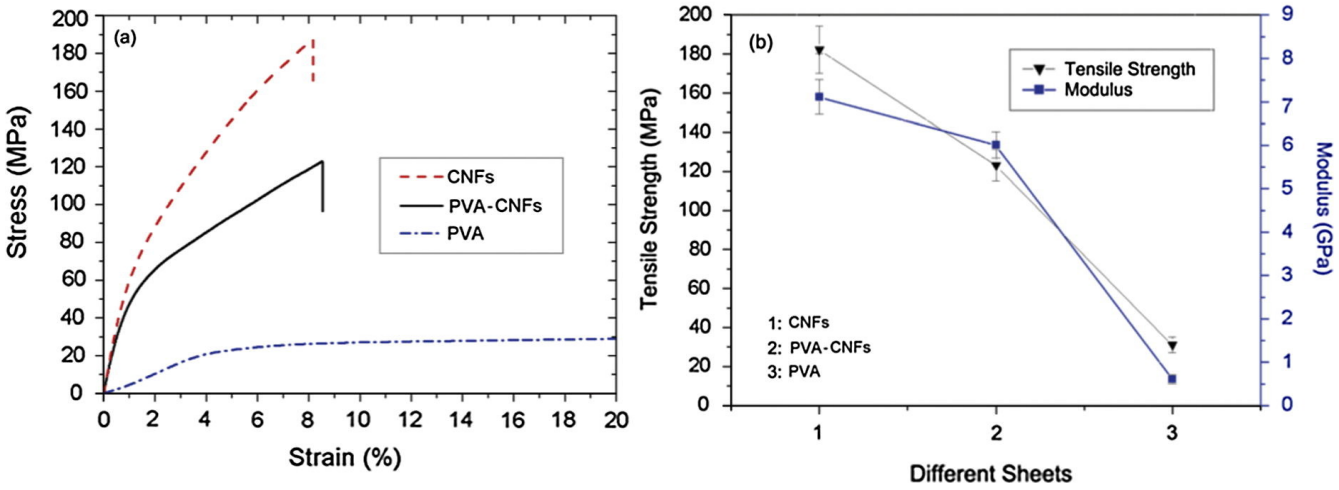

Figure 5: Stress/strain curves and tensile strength and modulus of the CNF nanopaper, neat PVA and CNF nanopaper-reinforced PVA composite obtained by Wang et al. [27].

Optically transparent composites were also produced using CNF nanopapers as the reinforcement for acrylic resin (Tricyclodecane dimethanol dimethacrylate TCDDMA) [28]. After immersing the CNF nanopaper for 24 h in the acrylic resin, the composites were cured using UV light, followed by drying for 2 h at 105 °C. In this work, the number of passes of the starting pulp through a grinder to produce CNF was studied to understand the influence of the degree of fibrillation on the properties of the resulting composites. A higher number of passes led to denser CNF nanopapers which ultimately increased light transmittance in the resulting composites (up to 85% transmittance for a composite containing 88 wt.-% CNF passed 30 times in the grinder). However, it was found that a large number of passes degraded the CNF and led to lower mechanical properties of the resulting CNF nanopaper-reinforced composites. The CNF nanopaper-reinforced composite resulting from the CNF that was passed 5 times in the grinder was found to possess the highest tensile properties. At 86 wt.-% CNF, this

composite possessed a tensile modulus and strength of 8.1 GPa and 94 MPa, respectively.

Henriksson et al. [29] produced CNF nanopaper-reinforced melamine formaldehyde (MF) composite by immersing CNF nanopaper in a water/MF solution. After a drying step to evaporate the water, the impregnated CNF nanopaper was pressed for 10 min at 160°C under a pressure of 30 MPa to cure the resin and produce a rigid and semi-transparent CNF nanopaper-reinforced composite. The authors produced a CNF nanopaper-reinforced composites at CNF loading fractions of 87, 91 and 95 vol.-%. No significant variation of the tensile modulus of the composites was observed (~16 GPa). However, the highest tensile strength of the CNF nanopaper-reinforced composite was obtained for composites reinforced with 95 vol.-% CNF (142 MPa). The authors also noted the higher transparency of the composites compared to neat CNF nanopapers suggested that porosity of the neat nanopapers decreased due to impregnation of MF.

CNF nanopaper-reinforced epoxy composites were also produced by immersing CNF nanopaper in epoxy diluted using acetone, followed by a curing cycle [30]. The CNF nanopaper-reinforced composites possessed a CNF loading fraction of ~20 vol.-%. In this study, an in-house made bio epoxy that possessed a high toughness (or work of fracture) was added to a commercial epoxy in order to increase toughness. Additionally, neat CNF nanopaper was also compared with acetone dried nanopaper. The neat CNF nanopaper reinforcing commercial epoxy possessed the highest tensile modulus at 7.7 GPa but a strength of only 81 MPa while acetone dried CNF nanopapers lead to composites with a modulus of 4.2 GPa and strength of 112 MPa. The addition of 10 wt.-% toughened bio epoxy in the composite reinforced with neat CNF nanopaper did not

result in a statistically significant increase in toughness. The authors also showed their experimental results were extremely close to predictions made using equation 2.1 and equation 2.2.

Aitomäki et al. [31] studied the impregnation of different types of CNF nanopapers by a low viscosity epoxy resin using vacuum assisted resin infusion (VARI). The authors produced CNF nanopapers with different porosities by drying them from acetone, methanol or using freeze drying and observed that higher network porosity caused faster impregnation by the resin. At v_f = 40 vol.-%, the water dried CNF nanopaper-reinforced epoxy composite possessed a tensile modulus and strength of 7.0 GPa and 114 MPa, respectively. However, higher porosity networks (80% for a freeze dried nanopaper) possessed lower tensile properties. It was observed that the lower porosity nanopaper (23% when dried from water) led to the highest tensile properties for the resulting composite.

2.1.4 BC nanopaper vs CNF nanopaper as reinforcement for polymers

Recently, both BC nanopaper- and CNF nanopaper-reinforced laminated composites were fabricated and compared [32]. In this study, two cellulose nanopapers with an intercalated layer of epoxy were hot-pressed at 120°C for 2 h. Both the BC- and CNF-reinforced epoxy composites possessed a loading fraction of ~80 vol.-%. The BC nanopaper-reinforced epoxy composite was found to possess a tensile modulus and strength of 9 GPa and 151 MPa, respectively, while the CNF nanopaper-reinforced epoxy composite possessed a higher tensile modulus 12.2 GPa but lower tensile strength (85 MPa). A brief comparison of the reinforcing ability of BC and CNF was given by the authors who linked the higher tensile modulus of the CNF nanopaper-reinforced

composite to better packing efficiency of the thinner CNF nanofibrils. The authors indicated the higher tensile strength of BC nanopaper-reinforced composites could be due to higher purity and better homogeneity of the fibrils.

Two other studies comparing the reinforcing abilities of CNF and BC nanopapers show slightly different results. In the work of Lee et al. [33], both CNF and BC nanopapers were manufactured (Figure 6). To produce, both CNF and BC nanopaper-reinforced composite, 11 sheets of cellulose nanopapers were stacked and infused with an epoxy resin using VARI. Very similar tensile mechanical performances were reported for both CNF and BC nanopaper-reinforced composites. At 49 vol.-% BC, the BC nanopaper-reinforced epoxy composite possessed a tensile modulus and strength of 102 MPa and 7.1 GPa, respectively. At 58 vol.-% CNF, the CNF nanopaper-reinforced epoxy composite possessed a tensile strength and modulus of 96 MPa and 8.5 GPa, respectively. When the tensile modulus and strength of the fabricated composites was normalised for 60 vol.-%, the tensile modulus of both BC and CNF composites was ~8.8 GPa. However, the authors reported a degree of crystallinity of 41% for CNF against 72% for BC, which was explained by the presence of impurities in the CNF. This led to a higher thermal degradation temperature for BC.

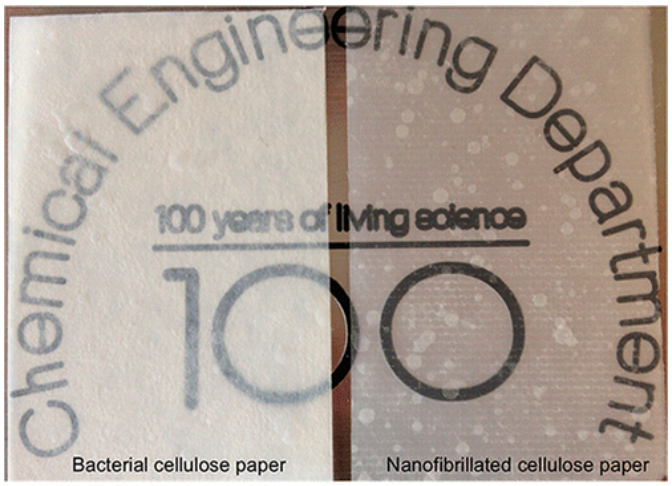

Figure 6: BC nanopaper (left) and CNF nanopaper (right). Taken from Lee et al. [33]

In the work of Nakagaito et al. [34], CNF and BC nanopapers were immersed in diluted phenol formaldehyde under vacuum before drying at ambient temperature and finally being cured at 50 °C for 6 h . At a nanocellulose loading fraction of ~79 vol.-%, the BC nanopaper-reinforced composite possessed a tensile modulus of 28 GPa when the modulus of the CNF nanopaper-reinforced composite was measured to be 19 GPa. While for both nanocellulose type, satisfying reinforcement was obtained, the authors explained the BC nanopaper-reinforced composite possessed a much higher Young's modulus than the CNF one because of "*extremely fine, pure, and dimensionally uniform ribbon-like cellulose microfibril bundles*".

The tensile modulus and tensile strength of (unmodified) cellulose nanopaper-reinforced composites found in the literature are summarised along their fibre volume fractions in Table 1. The tensile properties reported in Table 1 demonstrate that cellulose nanopaper-reinforced polymer composites can surpass a widely use biopolymer such as PLLA. However, the green credentials of these composites need to be verified.

Table 1: Tensile modulus (E) and strength (σ_{max}) of (unmodified) cellulose nanopaper-reinforced polymer composites found in the literature. The column labelled '#' indicates the number of BC nanopaper(s) in the composite.

Ref.	#	Type	Matrix	Method	v_f (%)	E (GPa)	σ_{max} (MPa)
[35]	1	BC	Epoxy	VARI[1]	~50	20.5 ± 0.5	325
[36]	1	BC	PLLA	Lamination	18	4.0 ± 0.4	115 ± 10
[33]	11	BC	Epoxy	VARI[1]	49	7.1 ± 0.1	102
[23]	1	BC	PLLA	Lamination	65	6.9 ± 0.5	125 ± 12
[25]	1	BC	Polyurethane	Immersion	79	6.0	70
[26]	1	BC	Polyurethane	Immersion	51	11.6	151
[24]	1	BC	DEAC[2]	Immersion	63	6.4 ± 0.8	130 ± 9
[32]	2	BC	Epoxy	Lamination	~80	9.0 ± 0.1	151 ± 9
[16]	1	CNF	MF[3]	Immersion	87	15.7	108
[28]	1	CNF	TCDDMA[4]	Immersion	~83	8.1	94
[33]	11	CNF	Epoxy	VARI[1]	58	8.5 ± 0.2	96 ± 1
[27]	1	CNF	PVA	Immersion	~76	6.0 ± 0.2	125 ± 1
[31]	1	CNF	Epoxy	VARI[1]	40	7.0 ± 1.8	114 ± 11
[30]	1	CNF	Epoxy	Immersion	20	4.9 ± 0.3	132 ± 2
[32]	2	CNF	Epoxy	Lamination	~80	12.2 ± 0.5	85 ± 4

[1]Vacuum assisted resin infusion
[2]Diethylene glycol bis(allyl carbonate)
[3]Melamine formaldehyde
[4]Tricyclodecane dimethanol dimethacrylate

2.2 Life cycle analysis and nanocellulose

2.2.1 Principles of Life Cycle Analysis

The life cycle analysis (LCA) tool has been considerably developed in the last fifteen years as part of the increasing interest toward environmental performance. An LCA is divided into 4 main phases [37] described below:

- Goal and scope definition**:** aims and objectives of the study. Definition of the system boundaries and main hypothesis and assumptions.
- Inventory analysis: data collection and allocation of the environmental burdens.
- Impact assessment: calculation of the different impacts and understanding of the significance of the results.
- Interpretation and recommendations: sensitivity and consistency check to reach a conclusion leading to recommendations.

One of the main factors that will vouch for the quality of an LCA is the quality of the data. Lack of data, to some extent, is part of any LCA. For this reason, imprecision of data, hypothesis and incompleteness must be described thoroughly to allow discussion. The separation of a foreground and background system also helps improving the results of an LCA. The foreground system is defined by the processes of main importance that are directly impacted by any decisions made for the study and the background system is defined by the processes used to support the foreground system (supply of energy and materials) [38]. The description of the assumptions should be based on either engineering estimates or carefully selected references.

One critical point of an LCA aiming at comparing products is the criterion used for a fair comparison. This criterion, called the functional unit, expresses the function in

quantitative terms [37]. For material-related LCA, a mass or volume are common functional units. However, when the material is destined for targeted applications, the functional unit should be linked to a performance indicator that considers the desired properties. A method for materials selection has been developed by Ashby and allows comparison of materials on a performance basis [39]. Comparing materials in LCA should be done using performance indicators related to the requirements for the material and part geometry, whether it is mechanical properties, thermal properties or any other material property.

The results of an LCA are obtained by applying factors to all the input and outputs. Different calculation methods exist (i.e. applying different factors) and can lead to significant results variations. However, Simoes et al. [40] demonstrated that this is not the case on the following impact categories: climate change, ozone layer depletion, acidification and eutrophication. For that reason, these four impacts constitute the core of many studies as they are the most trustworthy and are relatively independent of the calculation method. Also, it is important in any LCA study to show the results in different impact categories and not just cumulative energy demand and greenhouse gas emission as some processes can influence positively on one of these categories while being a burden in every other category. For example, Lazarevic et al. [41] showed that landfill at the end of life has smaller impact than incineration on greenhouse gas emissions but a more important impact in every other category. The impacts categories that are used in this thesis along with a brief description [42] are listed below:

- Global Warming Potential (CO_2 eq):

Greenhouse gases (GHG) increase the reflection of heat from sunrays and are responsible for global warming. An increase in GHG (CO_2, CH_4, N_2O and CFCs) will result in more heat "trapped" in the atmosphere and ultimately, climate change. Industrial activity, deforestation and pollution are responsible of the increase in GHG. The global warming effect will eventually lead to increasing sea level and various effects on biodiversity due to the warmer climate such as species extinctions, spreading of diseases, heavy rains and floods (as hot air can transport more humidity) or poor air quality.

- Acidification Potential (SO_2 eq):

The emissions of SO_2, HCl, HF, NO_x and NH_3 are responsible for the general acidification of soils and waters that ultimately leads to less available nutrients for plants, the death of marine animals and a general increase in corrosion.

- Abiotic Depletion Fossil (MJ):

This impact accounts for the consumption linked to non-renewable resources: fossil fuels, metals and minerals unlike CED (cumulative energy demand) that also takes into accounts the renewable energy consumption. This impact is strongly related to the two previous impacts described (GWP and AP) as energy demand is usually mostly met by burning fossil fuel that will result in the emission of CO_2 and SO_x.

- Photochemical Ozone Creation Potential (ethene eq):

Ozone creation at ground level (known commonly as summer smog) has a negative impact on both human and animal respiratory systems as well as ecosystems as it decreases photosynthesis capacity. Photochemical ozone formation occurs with the exposition to sunlight of volatile organic compounds (VOCs) and NO_2.

- Freshwater ecotoxicity Potential (DCB eq):

Measured in dichlorobenzene equivalent, the calculation of this impact is based on the maximum tolerable concentration in water, for aquatic organisms, of certain toxic substances. This impact category is particularly interesting in systems using large amounts of water that can become contaminated by chemicals.

2.2.2 LCA of nanocellulose production

Albeit not giving a full environmental report, some works do report the high energy consumption of the transformation of cellulose to nanocellulose. Spence et al. [43] compared the energy consumption of using a homogeniser, a microfluidiser and a micro-grinder with different process parameters (pre-treatment, number of passes and pressure/speed) to obtain nanocellulose. This study is particularly interesting as the authors tried to take into account the mechanical, optical and water interaction properties of the resulting CNF by testing them in network form. The conclusions that can be drawn of their results is that using a micro-grinder is the less energy consuming mechanical treatment (requiring only 1.5 kWh kg^{-1}) while the microfluidiser requires more energy but results in slightly higher tensile index for the CNF films as shown in Figure 7. Additionally, micro-grinding is the only method that does not require refining of the fibres as pre-treatment making it an overall simpler process.

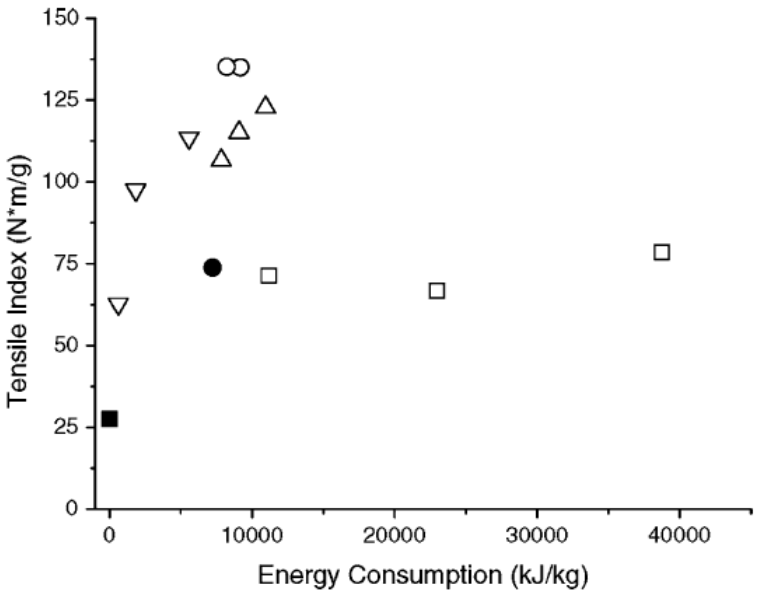

Figure 7: Unbleached hardwood films tensile indices based on energy consumption and processing method. Closed square: neat, closed circle: pre-treated, open square: homogenizer, open circle: microfluidizer, open triangle: grinder, open inverted triangle grinder with pre-treatment). Obtained with permission from [43].

In a similar study, Josset et al. [44] used micro-grinding to produce nanocellulose out of recycled materials (wheat straw and recycled newspaper) and wood pulp (elemental chlorine free bleached wood-pulp fibres). Only 1.25 kWh kg^{-1} were necessary to improve greatly the tensile modulus and tensile strength of the wood pulp based CNF but around 5 kWh kg^{-1} were necessary to get the overall best for all the tested properties. On the other hand, both recycled materials properties improved with increasing micro-grinding cycles and required around 5 kWh kg^{-1} to reach their best potential. Lee and Mani [45] used a dry grinding process to successfully extract CNF from cellulose powder using only 0.894 kWh kg^{-1}. However, with an average nanofibre diameter of 119 nm, this study shows it is difficult to compare raw energy consumption when significant variation

in the end product, here demonstrated by the relatively high fibre diameter, can be observed.

Focusing solely on environmental impact, Li et al. [46] used life cycle analysis (LCA) to study the production of CNF using high pressure homogenisation and high intensity sonication. TEMPO-oxidised or chloroacetic acid etherified Kraft pulp was chosen as the starting material for the analysis and the two chemical treatments were thus also compared. The authors found in their analysis that CNF obtained through the high pressure homogenisation of tempo-oxidised Kraft pulp presents the lowest environmental impact compared to all the production routes tested assuming that, no matter the route, the resulting CNF possesses the same properties. Piccinno et al. [47] conducted their LCA on CNF produced from carrot waste with the use of an enzymatic treatment. The energy consumption and CO_2 emissions were found to be comparable to those of Li et al. [46] but the authors also highlighted their water-based process had other environmental advantages over more traditional, chemical-heavy, processes. Arvidsson et al. [48] showed the environmental impact of CNF production could be much lower than found by the previous authors as seen in Table 2. The authors modelled a process that includes microfluidisation and homogenisation and showed that it is by using an enzymatic pre-treatment that the environmental impact could be greatly reduced. The addition of solvent recovery in their system also played a major role in the reduced impacts compared to the study of Li et al. [46]. However, in this study as well, the resulting CNF is assumed to be the same regardless of the manufacturing route.

Table 2: Lowest reported CED and GWP for the production of CNF at laboratory scale and at industrial scale.

Type	GWP Method	F.U. (kg)	CED (MJ)	GWP (kg CO_2 eq)
CNF [48]	ReCiPe	1	100[a]	1[a]
CNF [46]	IPCC 7	0.01	34.7	1.9
CNF [47]	IPCC 7	0.01	25.2	1.5
CNF[b] [49]	IPCC 7	1000	~8500[a,c]	750[a]

[a]values estimated from a graph
[b]at industrial scale
[c]based on ReCiPe "fossil depletion fossil" in kg oil eq

Another LCA focusing on a nanocellulose product was reported recently by Hohenthal et al. [49]. In their technical report, the authors found the fossil energy consumption of producing CNF at industrial scale to be approximately 107.5 MJ kg^{-1}. This is significantly higher than the production of PLA which consumes only 42 MJ kg^{-1} of fossil energy [50]. However, the global warming potential of the production of 1 kg of CNF paper was found to be lower than that of PLA with 1 kg CO_2 equivalent against 1.3 kg CO_2 equivalent for the production of 1 kg of PLA. This study shows the use of CNF as a green material is much more relevant than it appears from laboratory scale studies. To the best of the author's knowledge no work on the sustainability of BC production exist to this day.

3 Sample geometry dependency on the measured tensile properties of cellulose nanopapers

3.1 Introduction

Various researchers have reported the tensile properties of cellulose nanopapers (Table 3). It can be seen from Table 3 that the reported density of cellulose nanopapers varied between 0.72 and 1.61 g cm^{-3}. This variation could be attributed to the differences in the grammage of cellulose nanopapers, as well as the manufacturing process used to produce these cellulose nanopapers. Furthermore, the tensile moduli of cellulose nanopapers reported in the literature vary between 1.4 GPa and 22.5 GPa and the tensile strength of cellulose nanopapers vary between 23 MPa and 515 MPa, with various test specimen dimensions and geometries used. In addition to this, some studies employed an independent (video) strain measurement to monitor the strain experienced by the test specimens whilst others used a compliance correction method to back calculate the strain experienced by the test specimens. There are currently no standardised test methods for evaluating the tensile properties of cellulose nanopapers. The most appropriate tensile test standards for cellulose nanopapers are the test standards for papers and paperboards (such as BS EN ISO 1924 and TAPPI T494), which recommend rectangular tensile test specimens with dimensions of 180 mm between clamping lines and 15 mm width. Nevertheless, miniaturised tensile test specimens are still often used to quantify the tensile properties of cellulose nanopapers, presumably due to difficulties in producing larger samples for tensile testing.

Table 3: Tensile properties of CNF and BC nanopapers reported by various authors. ρ, l, w, t are the density, overall test specimen length, test specimen width and thickness of the cellulose nanopapers, respectively. E, σ_{max} and ε are the measured tensile moduli,

tensile strength and strain-to-failure of the cellulose nanopapers. All the reported tensile properties are measured on rectangular test specimen geometries unless specified.

Nanopaper	**Origin**	**ρ** (g cm^{-3})	$\boldsymbol{l \times w}$ (mm × mm)	$\boldsymbol{t}$ (μm)	**Testing Speed** (mm min^{-1})	$\boldsymbol{E}$ (GPa)	$\boldsymbol{\sigma_{max}}$ (MPa)	**ε** (%)	**Ref.**
BC	*A. aceti*					18	231	2.1	[51]
	A. xylinus	1.1	35 × 5	50	1	22.5*	515*		[52]
	G. xylinus		30 × 1	7	0.5	9.7 ± 2.1§	240 ± 87	2.6 ± 0.5	[2]
	G. xylinus		20 × 1	35	0.5	13 ± 1.8‡	218 ± 40	2.4 ± 0.3	[22]
		0.72	35 × 2†	79	1	12 ± 1.1‡	123 ± 7	7.5 ± 0.6	[33]
		1.3	20 × 4		1	17.3 ± 1.2	185 ± 18	6.5 ± 1.0	[53]
	A. xylinus		50 × 5		50	17*	213*	1.6*	[54]
	A. aceti		20 × 5	40-60	2	9.3 ± 0.3	449 ± 22	10.3 ± 0.6	[55]
	G. xylinus	1.61	35 × 2†		1	9.5 ± 0.8‡	270 ± 10	6.2 ± 0.2	[23]
						16.9	260	2.1	[56]
	K. rhaeticus		35 × 15			7.4	100	1.5	[57]
	G. xylinus		15 × 5	20	0.6	9.4 ± 0.3	192 ± 14	3.1 ± 0.4	[58]
CNF	Kraft, Lodge pole pine	0.9	35 × 5		1	10*	140*		[52]
	Kraft, Silver birch	0.93	35 × 2†		1	12.8 ± 1.4‡	103 ± 13	4.2 ± 0.8	[33]
	Soda, Canola straw	1.3	20 × 4			13.6 ± 1.0	114 ± 8	5.7 ± 1.0	[53]
	Soda, Spruce	1.07	50 × 15	33		17.5 ± 1.0	154	8.6 ± 1.6	[59]
	Kraft, Douglas fir	1.53	20 × 3	60	1	13	223		[60]
	Sulfite, Softwood	1.14	60 × 5	200		13	180	2.1	[61]
	Sulfite, Softwood	1.34	60 × 6	70		14	104	2.6	[29]
	Sulfite, Softwood		40 × 5	60-80		13.2 ± 0.6¥	214 ± 7	10.1 ± 1.4	[16]
	Sulfite, Softwood		50 × 15	40	5	13.4 ± 0.3¥	232 ± 19	5 ± 1.1	[62]
	Sulfite, Softwood	1.28	60 × 5	60-80		9.9 ± 0.2	175 ± 2	8.5 ± 0.5	[63]
	Soda, Palm fruit	0.97	75 × 5	60	5	17.9 ± 1.2	137 ± 7	0.4 ± 0.1	[64]
			100 × 10	100	10	10*	135*		[65]
	Kraft, Bagasse				62.5	8.5 ± 0.9	131 ± 17		[66]
	Kraft, Hardwood		320 × 5	65	1	11.2 ± 2.3	230 ± 23	7.2 ± 2.1	[67]
	Kraft, Softwood		50 × 4†		2	8.5*	95*	4.3*	[44]
	Kraft, Softwood	1.47	30 × 4†		1	11.5 ± 0.7	158 ± 16	2.1 ± 0.5	[68]
			50 × 5	200	2	1.4 ± 0.2¥	23 ± 1.3	2.6 ± 0.3	[69]
	Kraft	1.15	35 × 5		1	14.9 ± 0.8¥	243 ± 16	6 ± 0.2	[70]
	Almond shell		38 × 5	70-90	3	5.3 ± 0.3	65 ± 3	4.2 ± 0.2	[71]
	Kraft, Spinifex		25 × 6		1	3.2 ± 0.2	84 ± 5	18 ± 0.2	[72]
	Kraft,		30 × 5			14.9 ± 0.8¥	243 ± 16	6 ± 0.2	[73]
	Soda, Canola straw		20 × 4		1	14.5*	132*	5.5*	[74]
	Kraft, Silver birch		50 × 15		5	18 ± 1.5	130 ± 12	4.5 ± 1	[75]
	Kraft, Peanut shell	1.39	40 × 5	60-90	1	7.1	182	8.5	[27]
	Kraft, Carrot		20 × 5	80-100	2	12.3 ± 1.3	243 ± 28	8.7 ± 0.7	[76]
	Kraft, Jack pinecone		10 × 3†			17*	273*		[77]
	Kraft, Poplar tree		35 × 5	60	1	18.3	147	0.9	[78]
	Kraft, Maize stalks		20 × *w*			8.8 ± 0.8	96 ± 3	2.3 ± 0.3	[79]

* Values estimated from figures.
† Dog bone shaped tensile test specimens.
§ Tensile modulus determined from engineering strain of the test specimen.
‡ Tensile modulus determined from compliance correction.
¥ Tensile modulus determined from strain monitored using a non-contact (optical) extensometer.

Cellulose network in the form of cellulose nanopapers represents a conceptually important material structure [16] for various applications, including filtration membranes [17], packaging [18], electronics [19] and as nano-reinforcement for polymers [15]. Therefore, an accurate method for determining the mechanical properties of cellulose nanopapers is of upmost importance. In this work, tensile tests were conducted on four different test specimen geometries for both BC and CNF nanopapers to elucidate the influence of specimen geometry on the measured tensile properties of cellulose nanopapers (at constant crosshead speed). The importance of an independent strain measurement of the test specimens is also discussed. An understanding of the influence of test specimen geometry on the measured tensile properties of cellulose nanopapers is not only important for the interpretation of the mechanical response but also for the design and optimisation of the mechanical properties of nanocellulose-reinforced polymer composites.

3.2 Experimental

3.2.1 Materials

CNF in the form of an aqueous gel with a consistency of 1.5 wt.-% was used in this work. To produce CNF, once-dried birch Kraft pulp containing approximately 23% amorphous xylan was soaked at 2.2% consistency overnight and dispersed using a high-shear mixer (Dispermix, Ystral GmbH) for 10 min at 2000 rpm. This pulp suspension was then fed into a Masuko supermasscolloider (Masuko Sangyo Co., Kawaguchi, Japan) and passed through the grinder five times. BC was extracted from commercially

available nata de coco cubes (Coconut gel in syrup, Xiangsun Ltd, Lugang Township, Changhua County, Taiwan). These nata de coco cubes contain 2.5 wt.-% BC (dry basis). Sodium hydroxide pellets (AnalaR NORMAPUR®, purity > 98.5%) were purchased from VWR International Ltd (Lutterworth, UK).

3.2.2 Extraction and purification of BC

For each batch of 150 g of nata de coco, the cubes were first soaked and dispersed in 3.5 L of de-ionised water using a magnetic stirrer and heated to 80 ºC. Once the desired temperature was achieved, 14 g of NaOH pellets were added into this dispersion to produce a 0.1 M NaOH solution. The suspension was left to stir for 2 h at 80 ºC to remove any remaining microorganism or soluble polysaccharides. After this purification step, the suspension containing nata de coco cubes was poured onto a metal sieve (mesh size = 300 μm) to drain away the NaOH solution. The nata de coco cubes were then rinsed with 5 L of de-ionised water to remove any residual NaOH on the surface of the cubes. After rinsing, the cubes were then blended in another 5 L of de-ionised water using a kitchen blender (Breville VBL065) operating at maximum power output of 800 W for 2 min to produce a homogeneous BC suspension. The BC suspension was then centrifuged at 7000 × *g* for 6 min to remove the excess water. The blending-centrifugation steps were repeated until a neutral pH was attained for the BC suspension.

3.2.3 Manufacturing of cellulose nanopapers

To produce BC and CNF nanopapers with grammage of 50 g m^{-2}, homogeneous nanocellulose suspensions were first produced by blending the nanocellulose for 3 min at consistency of 0.1 wt.-%, followed by vacuum filtration onto a 125 mm diameter filter paper (Grade 413, 5-13 μm particle retention, VWR International Ltd). The wet

nanocellulose filter cake was carefully removed from the wet and used filter paper, and sandwiched between two fresh filter papers, followed by two more blotting papers (Grade 3MM CHR, GE Healthcare, Buckinghamshire, UK) and wet pressed between two metal plates under a weight of 10 kg at room temperature for 10 min. This wet pressing step was repeated once more with fresh filter and blotting papers to further absorb water from the wet nanocellulose filter cake. Cellulose nanopapers were produced by sandwiching the partially dried nanocellulose filter cake from the 2nd wet pressing step between fresh filter and blotting papers, and heat consolidated at 120 °C overnight under a weight of 10 kg. The BC and CNF nanopapers produced were stored in sealed sample bags containing dried silica gel.

3.2.4 Morphology characterisation

- Porosity

The true density (ρ) of BC and CNF was obtained using He pycnometry (Accupyc II 1340, Micromeritics Ltd, Hexton, UK) measured on freeze-dried samples. Freeze-dried BC and CNF were produced by dispersing the previously prepared BC and CNF suspensions in Falcon tubes at a consistency of 0.05 wt.-% and flash frozen in liquid nitrogen prior to freeze-drying (Christ Alpha 1-2 LDplus, Newtown, UK). The envelope density (ρ_e) of BC and CNF nanopapers was determined using mercury intrusion porosimetry (Autopore IV 9500, Micromeritics Ltd, Hexton, UK) as it was found to be a suitable method to determine ρ_e of cellulose nanopapers [80]. Prior to the measurement, BC and CNF nanopapers were dried at 80 ºC overnight. With ρ and ρ_e known, the porosity (P) of the cellulose nanopapers can be calculated using the following equation:

$$P(\%) = \left(1 - \frac{\rho_e}{\rho}\right) \times 100 \quad (3.1)$$

❖ Air resistance

The air resistance of BC and CNF nanopapers was determined using a Gurley densometer equipped with an automated digital timer (Model 4150N & Model 4320, Gurley Precision Instruments, Troy, NY, USA). Circular test specimens of 1.5 inches in diameter were cut and clamped between two rubber gasket O-rings located in the measuring chamber with a cross-sectional area of 1 in^2. The air resistance of the cellulose nanopapers was determined by measuring the time taken for 2.5 cm^3 of air to pass through the nanopapers at a pressure differential of 12.2 inH_2O.

❖ SEM

The fracture surfaces of the test specimens from the fracture toughness test were characterised using a large chamber scanning electron microscope (S-3700N, Hitachi, Tokyo, Japan). An accelerating voltage of 15 kV was used. The samples were glued onto aluminium stubs and Au coated (Agar auto sputter coater, Agar Scientific, Stansted, UK) using a coating current of 40 mA for 1 min.

3.2.5 Mechanical properties characterisation

❖ Tensile properties

4 different tensile test specimens were studied in this work (Figure 8): (a) miniaturised dog bone, (b) miniaturised rectangular test specimen, (c) standard dog bone and (d) standard rectangular test specimen, respectively. The miniaturised dog bone shaped specimens (type 5B in BS ISO 527: 2012) possessed an overall length of 35 mm. The gauge length and width of this test specimen are 10 mm and 2 mm, respectively. The

standard dog bone shaped specimens (type 1BA in BS ISO 527: 2012) used in this study possessed an overall length of 75 mm, a gauge length of 25 mm and a width of 5 mm. Miniaturised rectangular test specimens were obtained by removing the ends of the standard dog bone shaped specimens to produce a rectangular dimension of 35 mm × 5 mm. The standard rectangular test specimen possessed dimensions of 70 mm × 15 mm.

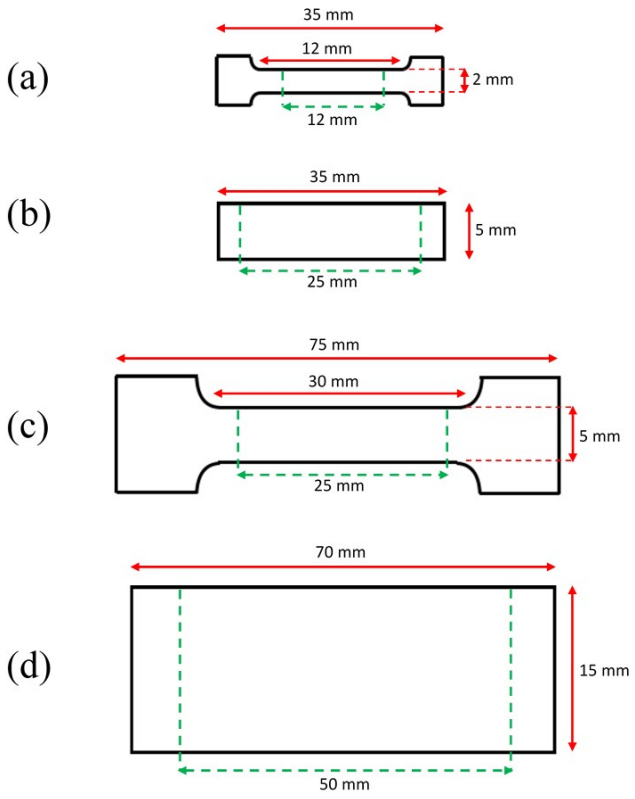

Figure 8: A schematic showing the 4 tensile test specimen geometries used in this study. (a) miniaturised dog bone shape, (b) miniaturised rectangular shape, (c) standard dog bone shape and (d) standard rectangular shape. The green dashed lines are the gauge length of the sample.

Preliminary results (data not presented here) showed that preparing the test specimens using a razor or scalpel blade could induce defects on the edges of the test specimens, leading to lower measured tensile properties of the samples. Therefore, all the

test specimens were cut using a manual cutting press (ZCP020, Zwick Testing Machines Ltd, Herefordshire, UK) equipped with the appropriate geometry of cutting die. Prior to the test, all the test specimens were secured onto paper testing cards (140 g m^{-2}) using a two-part cold curing epoxy resin (Araldite 2011, Huntsman Advanced Materials, UK). This was to avoid the clamps of the tensile tester from damaging the ends of the test specimens, potentially leading to earlier onset failure within the gripping zone of the test specimens. After securing the test specimens onto the testing cards, the exposed length of miniaturised test specimens and standard test specimens were 25 mm and 50 mm, respectively. Miniaturised tensile tests were carried out using a micro-tensile tester (Model MT-200, Deben UK Ltd, Woolpit, UK) equipped with a 200 N load cell. Tensile tests of the standard test specimens were performed using an Instron universal tester (Model 5969, Instron, High Wycombe, UK) equipped with a 1 kN load cell. Prior to the test, two points were marked in the axial and transverse directions on the surface of the test specimens, respectively. The strain of the test specimens was then monitored and recorded based on the movements of these marked points using a non-contacting video extensometer (iMetrum Ltd, Bristol, UK). The tensile tests were conducted at a crosshead displacement speed of 0.5 mm min^{-1}. Average results of 5 test specimens were reported for each type of sample geometry.

- Fracture toughness of the nanopapers

The fracture toughness (K_{1c}) of BC and CNF nanopapers was obtained from single edge-notched specimens with dimensions of 25 mm in overall length (L) and 15 mm in width (w). An initial crack was introduced at the centreline of the test specimen from the specimen's edge using a sharp scalpel. This initial crack length (a) was maintained

between 3.1 and 4.3 mm to ensure that the ratio between initial crack length and test specimen width ($\frac{a}{w}$) remained between 0.2 and 0.29. This was to maximise the efficiency of the function Y (equation 3.3) [81]. The single edge-notched cellulose nanopapers were then loaded in tension using a micro-tensile tester equipped with a 200 N load cell at a crosshead displacement of 0.5 mm min^{-1}. The distance between the grips were set to be 15 mm. The fracture toughness K_{1c} of the cellulose nanopapers was calculated from the maximum stress (σ_{max}) when crack propagation occurred using the following equation:

$$K_{1c} = Y\sigma_{max}a^{0.5} \tag{3.2}$$

where Y is [81]:

$$Y = 1.99 - 0.41\frac{a}{w} + 18.7\left(\frac{a}{w}\right)^2 - 38.48\left(\frac{a}{w}\right)^3 + 53.85\left(\frac{a}{w}\right)^4 \tag{3.3}$$

3.3 Results and Discussion

The morphology (see Figure 9) of BC and CNF nanopapers used in this work have been reported in another study [33]. Both types of nanocellulose possess rather uniform fibre diameters of approximately 50 nm. The uniformity of BC nanofibres is not surprising as the nanofibres are synthesised in a well-controlled manner by the cellulose-producing bacteria. As for CNF, passing the starting Kraft pulp through a high shear stone grinder (Masuko supermasscolloider) multiple times ensured that the resulting CNF possessed a uniform fibre diameter.

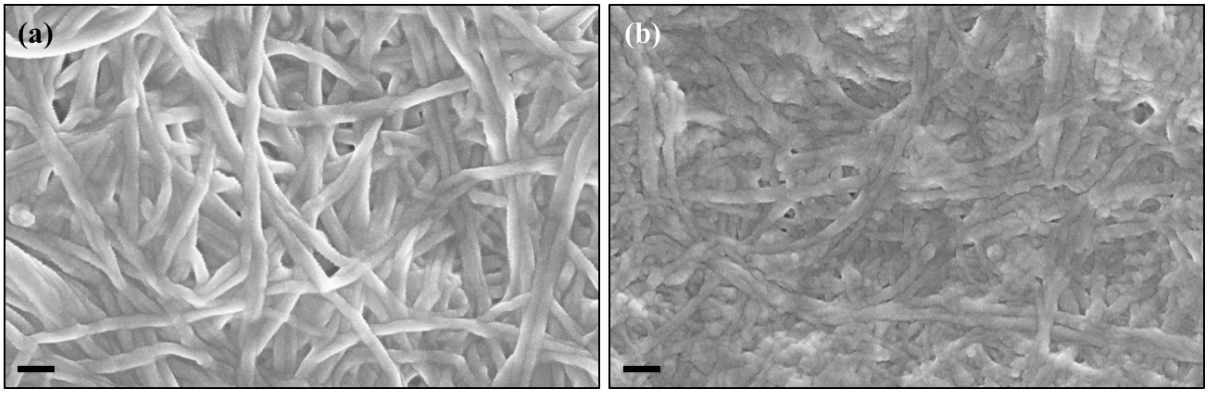

Figure 9: High resolution field emission scanning electron micrographs showing the morphology of (a) BC and (b) CNF nanofibres. Obtained from [33] with kind permission from ACS Publications. The scale bar represents 150 nm.

Table 4 summarises the density, porosity and air resistance of cellulose nanopapers manufactured in this work. The true density of CNF and BC was measured to be 1.51 g m^{-3}. BC nanopapers were also found to possess higher porosity compared to CNF nanopapers (Table 4). The higher porosity of BC nanopapers is postulated to be due to the inhomogeneous dispersion of BC in water prior to nanopaper production. Aggregates or bundles of BC can be observed in the BC suspension (Figure 10). This is a result of difficulties in disrupting the three-dimensional nano fibrous network of BC pellicles using a low energy blender. The CNF suspension, on the other hand, is more homogeneous. This leads to a more uniform formation of nanocellulose network within the CNF nanopaper compared to BC nanopaper (Figure 10), forming a more densely packed nanocellulose network in CNF nanopaper compared to BC nanopaper. Even though both the nanopapers were found to be porous, CNF nanopaper was found to be impermeable to air whilst 2.5 cm^3 of air passes through 1 in^2 of BC nanopaper in ~12000 s at a pressure differential of 12.2 inH_2O.

Table 4: A summary of the true density (ρ) of CNF and BC, bulk density (ρ_e), porosity (P) and air resistance of the CNF and BC nanopapers.

Nanopapers	ρ (g cm^{-3})	ρ_e (g cm^{-3})	*P* (%)	Air Resistance (s)
CNF	1.51 ± 0.01	1.37	9.2	> 172800
BC	1.51 ± 0.02	1.08	28.6	12368 ± 4955

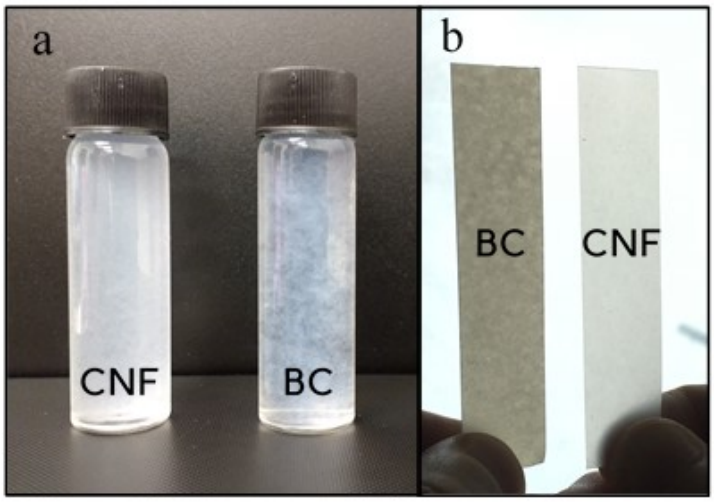

Figure 10: (a) 0.1 wt.% CNF and BC dispersed in water and (b) the homogeneity of produced BC and CNF nanopapers.

3.3.1 Influence of the sample geometry on the tensile modulus of nanopapers

Figure 11 shows the representative stress-strain curves of CNF and BC nanopapers for each test specimen geometry studied in this work. The stress-strain behaviour of CNF and BC nanopapers are similar. When a cellulose nanopaper is loaded under tension, it exhibits an initial elastic behaviour followed by inelastic deformation with a clear brittle and catastrophic failure.

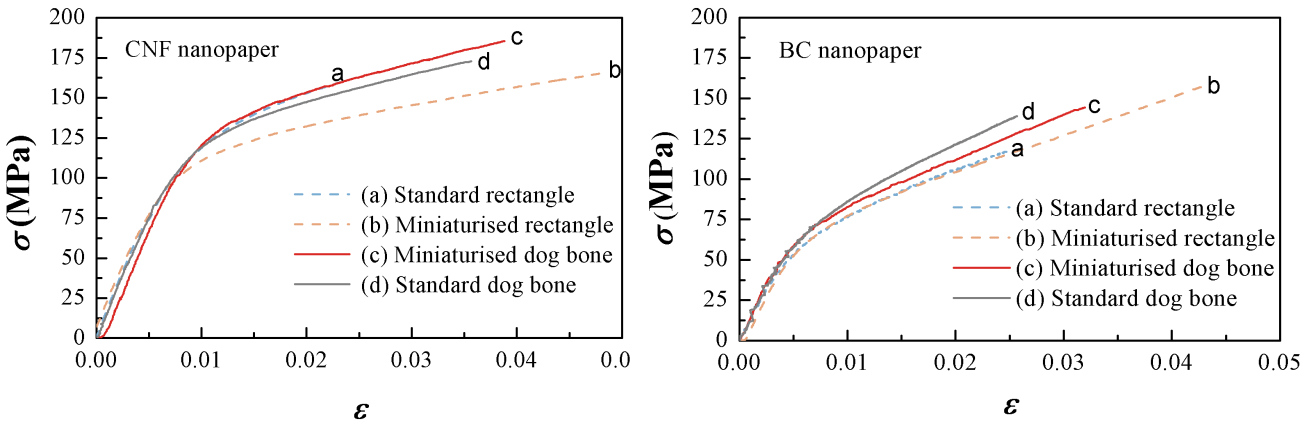

Figure 11: Representative stress-strain curves of CNF and BC nanopapers for 4 different test specimen geometries.

The measured tensile properties of the cellulose nanopapers are tabulated in

Table *5*. Overall, CNF nanopapers possessed slightly higher tensile moduli and strengths compared to BC nanopapers. Tensile moduli and strengths as high as 16.1 GPa and 182 MPa, respectively, were obtained for miniaturised dog bone test specimens of CNF nanopapers. For the same type of test specimen, the tensile modulus and strength of BC nanopapers was measured to be 15.2 GPa and 149 MPa, respectively. This slight difference in the measured tensile modulus and strength of CNF and BC nanopapers of the same test specimen geometry could be attributed to the higher porosity of BC nanopapers compared to CNF nanopapers. From Table 5, it can also be seen that the tensile moduli of both CNF and BC nanopapers do not differ much between different tensile test specimen geometries. The tensile moduli of CNF and BC nanopapers varied (within errors) between 14.5-16.1 GPa and 13.4-15.2 GPa, respectively, between different test specimen geometries. The elastic modulus of conventional paper is a function of pulp fibre modulus, degree of fibre-fibre bonding, fibre length and fibre dislocations [82]. Similar concepts can also be applied to cellulose nanopapers. Within

the same type of nanocellulose (either BC nanopapers or CNF nanopapers), the aforementioned attributes of the nanocellulose fibres and nanocellulose network are expected to be the same. As a result, the measured tensile moduli of cellulose nanopapers are not significantly affected by the different specimen geometries. It is worth mentioning at this point that the specific tensile moduli of BC nanopapers were found to be higher than CNF nanopapers. One possibility for this is that the intrinsic modulus of BC nanofibres could be higher than that of CNF [15].

In this chapter, the strain of the test specimens was determined from a non-contact video extensometer. Herein, the calculated tensile moduli of the cellulose nanopapers if an independent strain measurement was not used is also compared (Table 5). In this context, the strain of the test specimens was obtained from the crosshead displacement recorded by the test machine divided by the initial defined gauge length of the test specimens. A significant discreprancy can be observed between the tensile moduli determined from an independent strain measurement and strain calculated from the crosshead displacement of the test machine. The tensile moduli calculated from the crosshead displacement of the test machine is consistantly lower than that of the tensile moduli determined from an independent non-contact video extensometer. These values are also highly inconsistent, with tensile moduli values ranging between 6 and 13 GPa.

Table 5: Tensile properties of CNF and BC nanopapers for different specimen geometries. E, σ_{max} and ε denote the tensile modulus, tensile strength and strain-to-failure of the cellulose nanopapers, respectively.

	CNF nanopapers							
Test specimen geometry	$\boldsymbol{E}^{\S}$ (GPa)	$\frac{\boldsymbol{E}^{\S}}{\boldsymbol{\rho}}$ (GPa cm^3 g^{-1})	$\boldsymbol{E}^{\dagger}$ (GPa)	$\boldsymbol{\sigma_{max}}$ (MPa)	$\frac{\boldsymbol{\sigma_{max}}}{\boldsymbol{\rho}}$ (MPa cm^3 g^{-1})	$\boldsymbol{\sigma_w^T}$ (N m g^{-1})	$\boldsymbol{\varepsilon}$ (%)	$\boldsymbol{\nu_{12}}$
Miniaturised dogbone	16.1 ± 0.7	11.8 ± 0.7	7.1 ± 0.7	182 ± 21	133 ± 21	131 ± 7	4.4 ± 1.7	0.31 ± 0.12
Miniaturised rectangle	15.3 ± 2.8	11.2 ± 2.8	10.1 ± 1	162 ± 13	118 ± 13	122 ± 9	4.6 ± 1.7	0.36 ± 0.05
Standard dogbone	14.5 ± 0.5	10.6 ± 0.5	5.8 ± 0.8	168 ± 10	123 ± 10	129 ± 2	4.5 ± 0.3	0.29 ± 0.09
Standard rectangle	15.4 ± 0.5	11.2 ± 0.5	13.4 ± 1.4	157 ± 17	115 ± 17	110 ± 4	2.7 ± 0.6	0.25 ± 0.04
	BC nanopapers							
	$\boldsymbol{E}^{\S}$ (GPa)	$\frac{\boldsymbol{E}^{\S}}{\boldsymbol{\rho}}$ (GPa cm^3 g^{-1})	$\boldsymbol{E}^{\dagger}$ (GPa)	$\boldsymbol{\sigma_{max}}$ (MPa)	$\frac{\boldsymbol{\sigma_{max}}}{\boldsymbol{\rho}}$ (MPa cm^3 g^{-1})	$\boldsymbol{\sigma_w^T}$ (N m g^{-1})	$\boldsymbol{\varepsilon}$ (%)	$\boldsymbol{\nu_{12}}$
Miniaturised dogbone	15.2 ± 0.7	14.1 ± 0.7	7.2 ± 0.7	149 ± 13	138 ± 13	127± 3	3.5 ± 0.2	0.1 ± 0.06
Miniaturised rectangle	14.3 ± 1.1	13.2 ± 1.1	10.9 ± 0.7	147 ± 16	136 ± 16	116± 5	3.6 ± 0.9	0.11 ± 0.07
Standard dogbone	13.4 ± 1.5	12.4 ± 1.5	6.2 ± 0.6	138 ± 15	128 ± 15	111 ± 2	2.7 ± 0.4	0.14 ± 0.08
Standard rectangle	14.3 ± 1.4	13.2 ± 1.4	11.1 ± 3.4	120 ± 7	111 ± 7	99 ± 2	2.4 ± 0.4	0.11 ± 0.02

§ Tensile modulus determined using a non-contact video extensometer
† Tensile modulus determined from the cross-head displacement of the testing machine.

Any mechanical system will deform, however slightly, when subjected to an applied force. These could include the frame of the test equipment, the load cell, the grips used etc. These deformations are known as the system compliance and could potentially lead to significant error in calculating the deformation of the test specimen. The crosshead displacement output recorded by the system is the sum of the test equipment compliance and test specimen deformation:

$$\frac{1}{\left(\frac{\Delta P}{\Delta l}\right)} = \frac{1}{C_s} + \frac{1}{E} \times \frac{l_o}{A} \tag{3.4}$$

where $\frac{\Delta P}{\Delta l}$ is the slope of the recorded load-displacement curve, C_s is the compliance of the test equipment, l_o is the initial gauge length and A is the cross-sectional area of the test specimen, respectively. The derivation of this equation can be found in Appendix A. From this equation, it can be inferred that unless the test equipment is infinitely stiff ($C_s \to \infty$), the tensile modulus of a test specimen calculated from the crosshead displacement of the test equipment is prone to errors.

3.3.2 Influence of the sample geometry on the tensile strength of nanopapers

The tensile strength (σ_{max}) of the manufactured CNF and BC nanopapers are also summarised in Table 5. A tensile strength of 182 MPa was measured for CNF nanopaper on miniaturised dog bone test specimen. When miniaturised rectangular test specimens or standard dog bone test specimens were used, the measured tensile strength decreased to ~165 MPa. It should be noted that for both of these geometries, the width of the test specimens was the same (5 mm). When standard rectangular test specimens with a width

of 15 mm were used, the measured tensile strength decrease by 15% compared to the measured tensile strength using a miniaturised dog bone test specimens. Similar results were also observed for BC nanopapers. When the width of BC nanopaper test specimen was increased from 2 mm to 15 mm, the measured tensile strength decreased by 20% from 149 MPa to 120 MPa. The tensile indices of the CNF and BC nanopapers also followed the same trend as the tensile strengths of CNF and BC nanopapers. The observed decrease in tensile strength (and tensile index) of cellulose nanopaper when test specimen width was increased can be explained by the weakest link theory proposed by Freudenthal [83]. The tensile failure of cellulose nanopapers is a result of local deformation in a weak spot or an area with lower density within the cellulose nanopapers. An increase in test specimen width increases the probability of the presence of a defect, such as the presence of agglomerates of nanofibres or pores, responsible for lowering the tensile strength of cellulose nanopapers. This is consistant with the lower strain at failure of both CNF and BC nanopapers when the width of the test specimen was 15 mm. It should also be noted that decrease in the tensile strength of CNF nanopaper is within the standard deviation of the measurements but this is not the case for BC nanopaper. This is postulated to be due to CNF nanopapers possessing lower porosity and to the better formation of the nanocellulose network compared to BC nanopapers, which implies that the specimens are less prone to defects.

3.3.3 Influence of test specimen geometry on the Poisson's ratio of nanopapers

In Table 5, we also report the Poisson's ratios of cellulose nanopapers tested in tension. The Poisson's ratios of CNF and BC nanopapers were found to be ~0.30 and ~0.10, respectively. Poisson's ratio is a function of the packing of the structural elements

and is closely related to the ratio between bulk and shear moduli of the nanofibre network [84]. The higher the ratio between the bulk and shear moduli, the higher the Poisson's ratio of the resulting nanofibre network. As a result, the less porous CNF nanopapers possessed higher Poisson's ratio compared to the more porous BC nanopapers. In addition to this, the bulk and shear moduli of the nanofibre network are expected to be the same within the same type of nanocellulose fibres and nanofibre network. Therefore, the Poisson's ratio of the cellulose nanopapers is independent of test specimen geometry used.

3.3.4 Fracture resistance of cellulose nanopapers

Although defects within a cellulose nanopaper could be minimised, for example, by improving the processing parameters for nanonopaper manufacturing, it is highly unlikely that they could be completely eliminated. It is therefore desirable to quantify the fracture resistance of BC and CNF nanopapers. Single edge-notched BC and CNF nanopapers were tested in tension and the representative load-displacement curves are shown in Figure 12. The initial linear part of the load-displacement curves correspond to the strain potential energy stored in the cellulose nanopaper when a load was applied. When the applied load was high enough to create a new surface area, the introduced crack started to propagate and the test specimen failed catastrophically in a brittle manner.

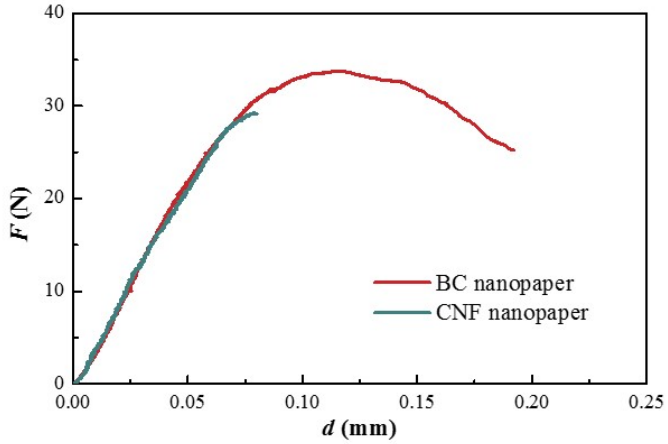

Figure 12: Representative load (F) – displacement (d) curves of the single edge notched BC and CNF nanopaper samples loaded under tension.

The critical stress intensity factors (K_{1c}) of CNF and BC nanopapers are tabulated in Table 6. The higher K_{1c} value of CNF nanopapers (7.3 MPa $m^{1/2}$) compared to BC nanopapers (6.6 MPa $m^{1/2}$) can be attributed to the lower intrinsic porosity of CNF nanopapers (~10%) compared to BC nanopapers (~30%). It is worth mentioning that the measured K_{1c} values of both BC and CNF nanopapers are comparable to that of the fracture toughness of single edge-notched aramid fibres [85].

Table 6: The stress intensity factor (K_{1C}) and time taken for complete fracture of test specimens when crack propagated (t) of CNF and BC nanopapers.

Sample	$\boldsymbol{K_{1C}}$ (MPa $m^{1/2}$)	$\boldsymbol{t}$ (s)
CNF nanopaper	7.3 ± 0.3	0.7 ± 0.2
BC nanopaper	6.6 ± 0.2	19.8 ± 5

The fracture surfaces of the single edge-notched cellulose nanopapers are shown in Figure 13. Two very different fracture morpholgies can be observed. Crack propagates along the path of the least resistance. In the case of CNF nanopaper, the crack is

hypothesised to propagate along the brittle hemicellulose [86]. The CNF used in this work contains approximately 23% hemicellulose. As BC nanopaper is pure nanocellulose without the presence of hemicellulose, crack can only propagate by the defibrillation of the nanocellulose network. As a result, the fracture surface of the single edge-notched BC nanopapers showed significant defibrillation, which suggests fibre-fibre debonding during crack propagation. This was not observed in the fracture surface of single edge-notched CNF nanopaper.

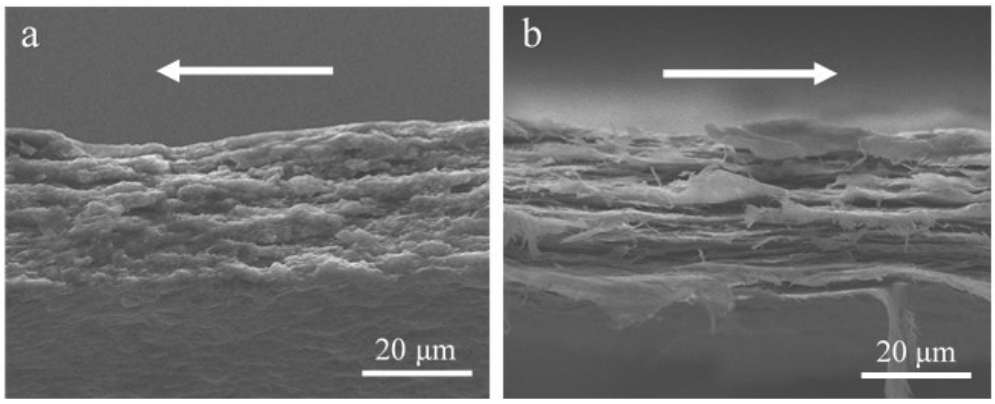

Figure 13: Fracture surface of single edge notched cellulose nanopapers. (a) CNF nanopaper and (b) BC nanopaper. The arrow denotes the direction of crack propagation.

In addition to this, single edge-notched CNF nanopapers failed catastrophically when maximum load was reached whilst the single edge-notched BC nanopapers showed a delayed catastrophic failure (see Figure 12). In fact, single edge-notched BC nanopapers took ~20 s for the complete fracture of the specimens when peak force was reached (Table 6). CNF nanopapers, on the other hand, fractured immediately when peak force was reached. This can be attributed to the differences in homogeneity of CNF and BC nanopapers. When the crack front encounter inhomogeneity in the areal density

nanocellulose across the through thickness of BC nanopapers locally, it propagates faster in the region of lower nanocellulose areal density as there are less fibre-fibre bonds in this region. As a result, the test specimen could still sustain load (albeit lower) as the displacement of the single edge-notched test specimen increased, delaying the catastrophic failure of the BC nanopaper. It is also postulated that BC possessed longer nanofibre length compared to CNF, leading to the observed difference in fracture behaviour of the cellulose nanopapers.

4 Low grammage BC nanopaper-reinforced polylactide composite laminates

4.1 Introduction

While it is evident that high performance cellulose nanopaper-reinforced polymer composites can be produced (as seen in Table 1), many of the reported tensile properties of cellulose nanopaper-reinforced polymer composites are still based on composites reinforced with only a single sheet of CNF or BC nanopaper. A previous study [33] has shown that cellulose nanopaper-reinforced epoxy composites containing 11 sheets of ~60 g m^{-2} reinforcing CNF or BC nanopapers possessed tensile moduli and strengths of ~8 GPa and ~100 MPa at nanocellulose loading fraction of 50-60 vol.-%. To the best of the author's knowledge, no studies have been conducted to investigate the reinforcing potential of cellulose nanopapers at different grammages for polymers.

Furthermore, the rate-limiting step towards the large-scale production of these composites is the time-consuming dewatering step to produce the cellulose nanopapers. Similar to conventional papermaking, cellulose nanopaper is typically produced by first creating a homogenous suspension of nanocellulose-in-water at low consistency (usually < 0.5 wt.-%), followed by dewatering using vacuum filtration onto a filter medium and heat consolidation. Dewatering time as high as 4 h have been previously reported to produce a 38 g m^{-2} CNF nanopaper from a 0.1 wt.-% consistency through a filter membrane with 0.1 μm pore size [60]. A new strategy towards reducing the de-watering time in the production of cellulose nanopapers is needed.

Therefore, in this work, for the first time, the use of (ultra-)low grammage BC nanopaper as reinforcement for polylactide is demonstrated. By reducing the grammage of the reinforcing cellulose nanopaper, the dewatering time to produce the cellulose

nanopaper can be significantly reduced, overcoming the rate-limiting step in the large-scale production of cellulose nanopaper-reinforced polymer composites. Model BC nanopapers with grammages of 5, 10, 25 and 50 g m^{-2} were produced and the influence of grammage on the mechanical properties of the resulting model BC nanopapers were investigated. Model polylactide laminated composites consisting a total BC nanopaper areal density of 50 g m^{-2} (e.g. laminated composites reinforced with 1 sheet of 50 g m^{-2}, 2 sheets of 25 g m^{-2}, 5 sheets of 10 g m^{-2}, 10 sheets of 50 g m^{-2} BC nanopaper(s), respectively) were also fabricated and characterised.

4.2 Experimental

Poly(L-lactic acid) (PLLA) (L9000, molecular weight ≥ 150 kDa, D-content ≈ 1.5%) was purchased from Biomer GmbH and used as the matrix for the production of BC-reinforced PLLA composites. Sodium hydroxide (pellets, purity > 98.5%) was purchased from VWR International (Lutterworth, UK). 1,4-Dioxane (ACS Reagent, purity ≥ 99%) was purchased from Sigma-Aldrich (Gillingham, UK). These materials were used as received without further purification. BC in the form of commercially available nata de coco (coconut gel in syrup) was purchased from a retailer (Xiangsun Ltd, Lugang Township, Changhua County, Taiwan).

To obtain purified BC, 150 g of nata de coco cubes were added to 3.5 L of de-ionised water and heated to 80 ºC under stirring. 14 g of NaOH pellets were then added into this dispersion to form a 0.1 N NaOH aqueous solution and left to stir at 80 ºC for 2 h. After this purification step, the dispersion was poured onto a metal sieve (mesh size = 300 μm) to recover the purified nata de coco cubes, followed by a rinsing step with 5 L of de-ionised water. The purified cubes were then blended (Breville VBL065) in another

5 L of de-ionised water for 2 min to create a homogeneous dispersion of BC-in-water, followed by centrifugation (SIGMA 4-16S, SciQuip ltd, Newton, UK) at 6800 × *g* to remove the excess water. This blending-centrifugation steps were repeated until neutral pH was attained for the BC-in-water dispersion. The final consistency of the BC-in-water was adjusted to 2 wt.-% prior to subsequent use.

4.2.1 BC nanopaper manufacturing

For this work, BC nanopapers with 4 different grammages (5 g m^{-2}, 10 g m^{-2}, 25 g m^{-2} and 50 g m^{-2}) were produced. To produce the BC nanopaper, the previously purified BC-in-water was first dispersed in 500 mL of de-ionised water using a blender (Breville VBL065) for 5 min, followed by filtration at a reduced pressure of 0.1 bar in a Büchner funnel onto a 12 cm diameter woven nylon fabric (PP180 Economy Peel Ply, Easy Composites Ltd, Staffordshire, UK) placed on top of a filter paper (Grade 413, 5-13 μm particle retention, VWR International Ltd, Lutterworth, UK). In conventional BC nanopaper production, the BC-in-water dispersion is filtered directly onto a filter paper. However, it was observed that the wet BC filter cakes to produce low grammage BC nanopapers were too fragile and difficult to remove directly from the used filter paper. Therefore, a nylon fabric was placed on top of the filter paper to aid the removal of the wet BC filter cake before subsequent processing.

After the filtration step, the wet BC filter cake along with the nylon fabric were carefully separated from the used filter paper and sandwiched between fresh filter and blotting papers (Grade 3MM CHR, VWR international Ltd, Lutterworth, UK), followed by a wet pressing step under a weight of 10 kg for 10 min to absorb the excess water from the wet BC filter cake and nylon fabric. This step was repeated twice, with fresh

filter and blotting papers used at every step. A final heat consolidation step was then performed in a hydraulic hot press (4122 CE, Carver Inc., Wabash, IN, USA) under a weight of 1 t at 120 °C for 30 min to further dry and consolidate the partially dried BC filter cake into a BC nanopaper. The dried and well-consolidated BC nanopaper was then carefully separated from the nylon fabric once the BC nanopaper had cooled to room temperature. All manufactured BC nanopapers were stored in a sealed environment containing silica gel pouches to keep the BC nanopapers dry.

4.2.2 BC nanopaper-reinforced PLLA laminates manufacturing

BC nanopaper-reinforced PLLA composite laminates were produced using film stacking method. The stacking sequences of BC nanopaper with different grammages and PLLA are shown in Figure 14. These stacking sequences were chosen such that the overall grammage of BC nanopaper within the composite laminates is kept constant at 50 g m^{-2}. Prior to producing the composite laminates, thin PLLA films were produced by solution casting. Briefly, PLLA pellets were dissolved in 1,4-dioxane at a mass ratio of 1:12 at 65 °C overnight under magnetic stirring. Once the polymer solution is cooled to room temperature, it was then casted onto a toughened glass plate using an automated film applicator (Elcometer 4340, Elcometer Ltd., Manchester, UK) and the solvent was evaporated to produce thin PLLA films. The speed of the casting knife was set to be 5 mm s^{-1}. The fabricated BC nanopapers and PLLA films were then stacked according to the stacking sequence shown in Figure 14 and sandwiched between two heat-resistant and non-stick polyimide films (UPILEX®, Goodfellow Cambridge Ltd, Huntingdon, UK). The lay-up was then pre-heated in a hydraulic hot press (4122 CE, Carver Inc.,

USA) to 180 °C for 3 min, followed by a consolidation step at the same temperature for 2 min under the weight of 1 t.

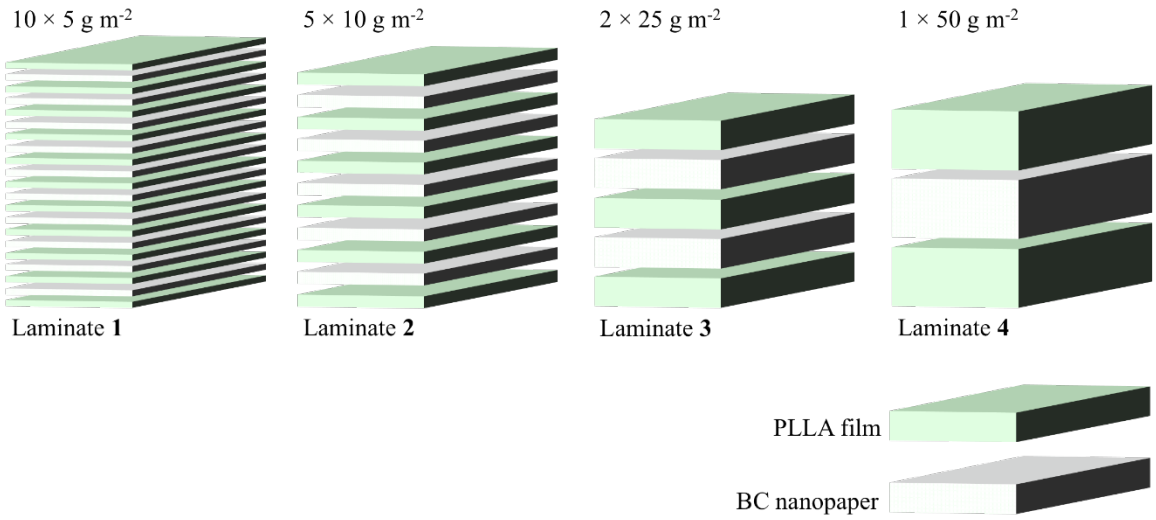

Figure 14: Stacking sequence of the 4 BC nanopaper-reinforced PLLA composite laminates.

BC nanopaper-reinforced PLLA laminates reinforced with 10 × 5 g m^{-2}, 5 × 10 g m^{-2}, 2 × 25 g m^{-2} and 1 × 50 g m^{-2} BC nanopaper(s) are herein termed Laminate **1**, Laminate **2**, Laminate **3** and Laminate **4**, respectively. All composite laminates were stored in a sealed environment containing silica gel pouches to keep the composite laminates dry prior to subsequent use. As a control, neat PLLA film was produced by hot pressing PLLA pellets directly at a temperature of 180 °C under the weight of 1 t for 2 min.

4.2.3 Characterisation of the nanopapers and composites

- Scanning electron microscopy (SEM)

The fracture surfaces of the BC nanopaper and BC nanopaper-reinforced PLLA composite laminates were investigated using a large chamber SEM (S-3700N, Hitachi, Tokyo, Japan) operated at an accelerating voltage of 10 kV. Prior to SEM, the tensile fractured samples were attached onto aluminium stubs using carbon tabs and Au coated (Agar auto sputter coater, Agar Scientific, Stansted, UK) at 40 mA for 20 s.

❖ Density and porosity of the nanopapers and their PLLA composites

The envelope density of the BC nanopapers and the manufactured composite laminates (ρ_e) was calculated by taking the ratio between the mass and the envelope volume of the specimen. The porosity of the BC nanopapers ($P_{\text{BC nanopaper}}$) was then calculated using:

$$P(\%) = \left(1 - \frac{\rho_e}{\rho}\right) \times 100 \tag{4.1}$$

where ρ_f is the absolute density of BC nanofibres, which was found to be 1.51 ± 0.02 g cm^{-3} using He pycnometry (see chapter 3). To calculate the porosity of the BC nanopaper-reinforced PLLA composite laminates ($P_{\text{composites}}$), the void free density of the composite laminates ($\rho_{c,\text{ void free}}$) was first calculated from the measured weight fraction of BC ($w_{f,\text{ BC}}$) within the composite laminates:

$$\rho_{c,\text{ void free}} = \frac{1}{\frac{1-w_{f,\text{ BC}}}{\rho_m} + \frac{w_{f,\text{ BC}}}{\rho_f}} \tag{4.2}$$

where ρ_m is the absolute density of neat PLLA, which was measured to be 1.26 ± 0.01 g cm^{-3} using He pycnometry. The porosity of the BC nanopaper-reinforced PLLA composite laminates was then calculated from:

$$P_{\text{composites}}(\%) = \left(1 - \frac{\rho_e}{\rho_c}\right) \times 100 \quad (4.3)$$

- ❖ Tensile properties of the different grammage nanopapers and their respective PLLA laminated composites

Tensile tests of BC nanopapers with different grammages and BC nanopaper-reinforced PLLA laminates reinforced with different BC nanopaper grammages were conducted in accordance to BS EN ISO 527: 2012. Prior to the test, dog bone shape test specimens were cut using a manual cutting press (ZCP020, Zwick Testing Machines Ltd., Leominster, UK). The test specimens possessed an overall length of 35 mm, a gauge length of 10 mm and the narrowest part of the dog bone shape specimen has a width of 2 mm, respectively. To avoid damaging the gripping zone of the test specimens, which could potentially lead to earlier onset failure of the specimens, all test specimens were secured onto 140 g m^{-2} paper testing cards using a two-part cold curing epoxy resin (Araldite 2011).

Tensile tests were carried out using a micro-tensile tester (Model MT-200, Deben UK Ltd., Woolpit, UK) equipped with a 200 N load cell. A pair of dots were marked on the surface of each test specimen in the direction of load. The strain of the test specimen was evaluated by monitoring the movement of these two dots using a non-contact optical extensometer (iMetrum Ltd., Bristol, UK). Tensile tests were conducted using a crosshead displacement speed of 0.2 mm min^{-1} (correspond to a strain rate of 0.01 s^{-1}). The reported tensile properties were averaged over 5 test specimens.

4.3 Results and discussion

4.3.1 Dewatering time of the BC-in-water suspensions

The dewatering time of BC-in-water suspensions to produce BC nanopapers with grammages of 5, 10, 25 and 50 g m^{-2} are shown in Figure 15. At the start of the dewatering process, BC nanofibres are deposited on the filter medium as a thin layer of BC network. As the dewatering progresses, the nanofibres deposit one over the other on top of this thin layer of BC network, forming a layered structure (see Figure 16 for the SEM images showing the internal morphology of fabricated BC nanopapers). Similar layered structure has also been observed by numerous researchers [54,56,87].

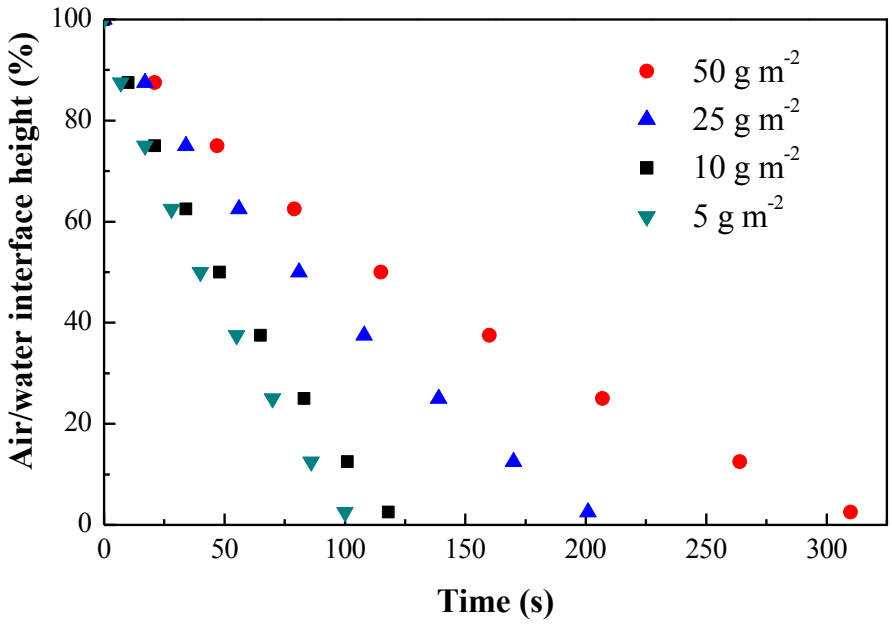

Figure 15: Dewatering time of the BC-in-water suspensions to produce BC nanopaper with different grammages.

The build-up of the BC filter cake leads to an increase in the flow resistance (e.g. a reduction in the permeability) of water through the filter cake. As a result, the dewatering time of producing 5 g m^{-2} nanopaper, which possessed thinner filter cake, is

significantly lower than the dewatering time to produce 50 g m^{-2} BC nanopaper, which has a thicker filter cake.

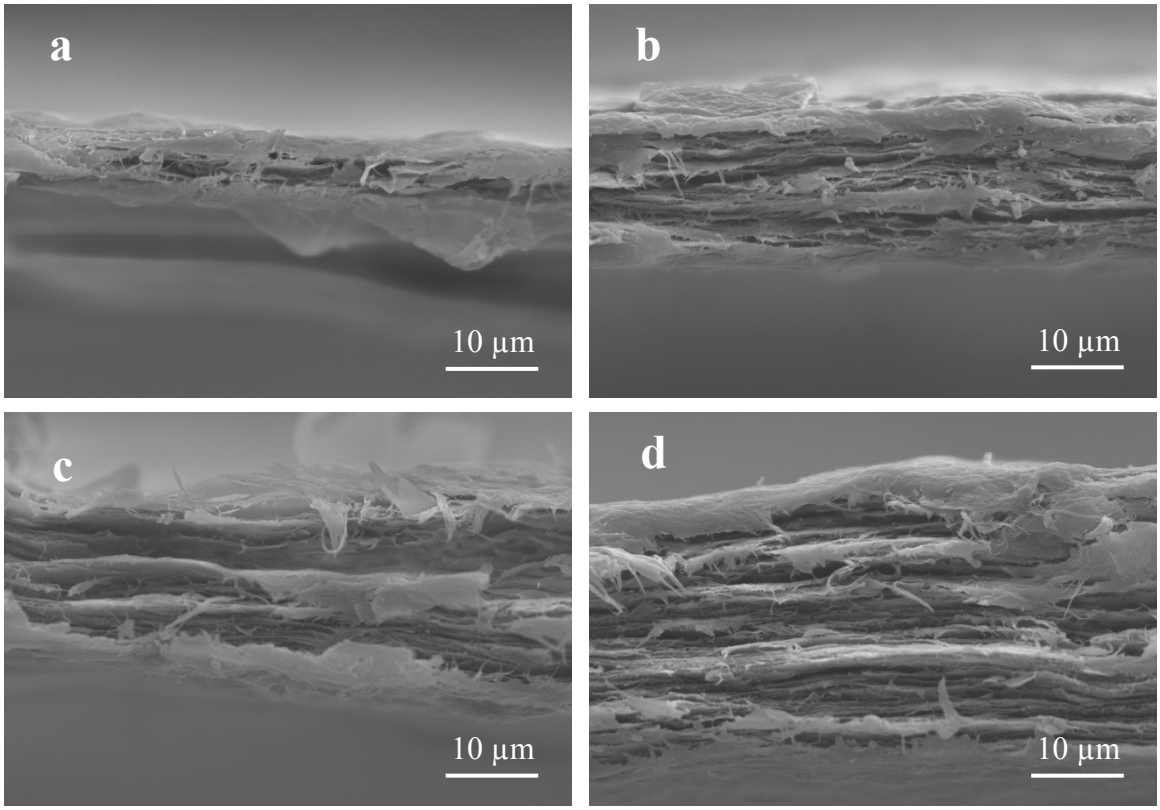

Figure 16: Fractured surfaces of (a) 5 g m^{-2}, (b) 10 g m^{-2}, (c) 25 g m^{-2} and (d) 50 g m^{-2} nanopapers.

It is also worth mentioning that the dewatering time of BC-in-water suspension reported in this work is significantly lower than the dewatering time of CNF-in-water suspensions reported by various authors. Nogi et al. [60] reported a dewatering time of 3-4 h to produce a 38 g m^{-2} CNF nanopaper from a CNF-in-water suspension with a consistency of 0.1 wt.-% through a hydrophilic polytetrafluoroethylene membrane filter with a pore size of 0.1 µm. A dewatering time of 45 min have been reported [62] to

produce a ~50 g m^{-2} CNF nanopaper from a suspension with a consistency of 0.2 wt.-%, filtered through a nitrocellulose filter membrane with a pore size of 0.65 μm. In contrast, the longest dewatering time in this chapter was approximately 5 min, which was to produce a 50 g m^{-2} BC nanopaper from 0.1 wt.-% BC-in-water suspension. This was attributed to the homogeneity of the nanocellulose suspensions. It has been previously reported that CNF forms a homogeneous suspension in water whilst aggregates or bundles of BC is often observed, due to difficulties in disrupting the three-dimensional nano fibrous network of BC pellicles using a low energy blender [88]. A combination of inhomogeneous BC dispersion in water and larger pore size of the hydrophilic filter medium used in this work (e.g. a filter paper with particle retention of 5-13 μm compared to filter membranes with pore size < 1 μm) led to the observed significant discrepancy between the dewatering time of BC- and CNF-in-water suspension at similar consistency.

4.3.2 Porosity of the BC nanopapers at different grammages

The thickness and porosity of the fabricated BC nanopapers as a function of grammage are shown in Figure 17. A 5 g m^{-2} BC nanopaper possessed a porosity of 78%. However, increasing the BC nanopaper grammage to 50 g m^{-2} led to a progressive reduction in the porosity of the BC nanopaper to 48%. This reduction in BC nanopaper porosity with increasing BC nanopaper grammage, which suggests better packing efficiency of BC nano fibrous network as the grammage increases, leads to the non-linearity of the thickness versus grammage plot (Figure 17).

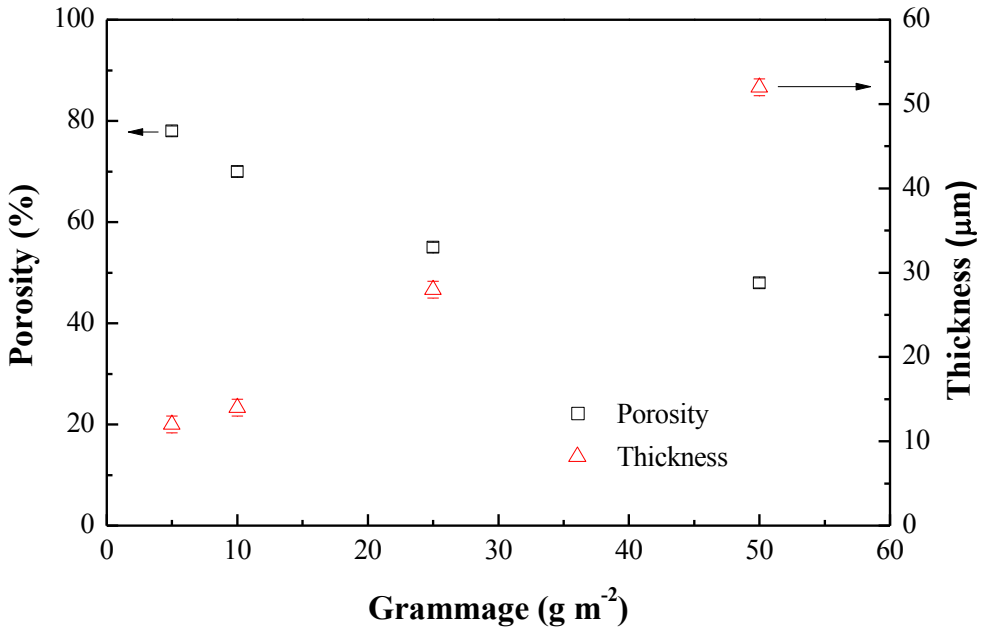

Figure 17: Porosity and thickness of BC nanopapers as a function of grammage.

In addition to the dewatering of BC-in-water suspension, another important step in the production of high load bearing capacity BC nanopaper is the prevention of wet BC filter cake shrinkage during drying. If a cellulose fibre network is restrained from shrinkage, the slacks of the free fibre segments (e.g. exposed fibres within two fibre contact points) in the cellulose fibre network are removed, thereby improving the mechanical properties of the resulting dried cellulose fibre network [89]. This is also known as fibre segment activation.

In this chapter, wet BC filter cake was restrained from shrinkage by applying a weight of 1 t during the heat consolidation step. It is postulated that the application of such high compaction load led to the slippage and repositioning of BC nanofibres within the wet BC filter cake. The BC nanofibres could fill the voids within the wet filter cake,

improving the packing efficiency and leading to a reduction in the porosity of the resulting dried and well-consolidated BC nanopaper. This also corroborates with the moisture content of the wet BC filter cakes to produce BC nanopapers with different grammage at various stages of the nanopaper production (see Table 7).

Table 7: Water content of the wet and partially dried BC filter cake for different nanopaper grammage after each processing step.

	Water content [wt.-%]			
	50 g m^{-2}	25 g m^{-2}	10 g m^{-2}	5 g m^{-2}
Wet BC filter cake prior to 1st wet pressing step	88	86	85	78
Partially dried BC filter cake after the 1st wet pressing step prior to the 2nd wet pressing step	79	69	27	0
Partially dried BC filter cake after the 2nd wet pressing step prior to the heat consolidation step	66	24	0	0

The wet BC filter cake was found to possess a moisture content of ~80 wt.-% after the dewatering step, independent of the grammage of nanopapers to be produced. However, the wet filter cakes to produce 5 g m^{-2} and 10 g m^{-2} BC nanopapers dried after the first and second wet pressing step, respectively, which use an applied compaction load of only 10 kg. The application of a compaction load of 1 t onto an already-dried 5 g m^{-2} and 10 g m^{-2} BC nanopaper during the heat consolidation step no longer leads to nanofibre slippage as the BC nanofibre network has dried, leading to the observed high porosity for these BC nanopapers. The wet filter cakes to produce 25 g m^{-2} and 50 g m^{-2}

BC nanopapers, on the other hand, were found to possess significant higher moisture content prior to the heat consolidation step. Due to the higher moisture content of filter cake to produce 50 g m^{-2} BC nanopaper compared to 25 g m^{-2} nanopaper, the effect of BC nanofibre slippage and hence, "void-filling", is more pronounced. As a result, 50 g m^{-2} BC nanopaper possessed lower porosity compared to 25 g m^{-2} BC nanopaper.

4.3.3 Tensile properties of BC nanopapers at different grammages

The representative stress-strain curves of the fabricated BC nanopapers at different grammages tested in uniaxial tension exhibited an initial elastic deformation, followed by inelastic deformation prior to catastrophic failure (see Figure 18).

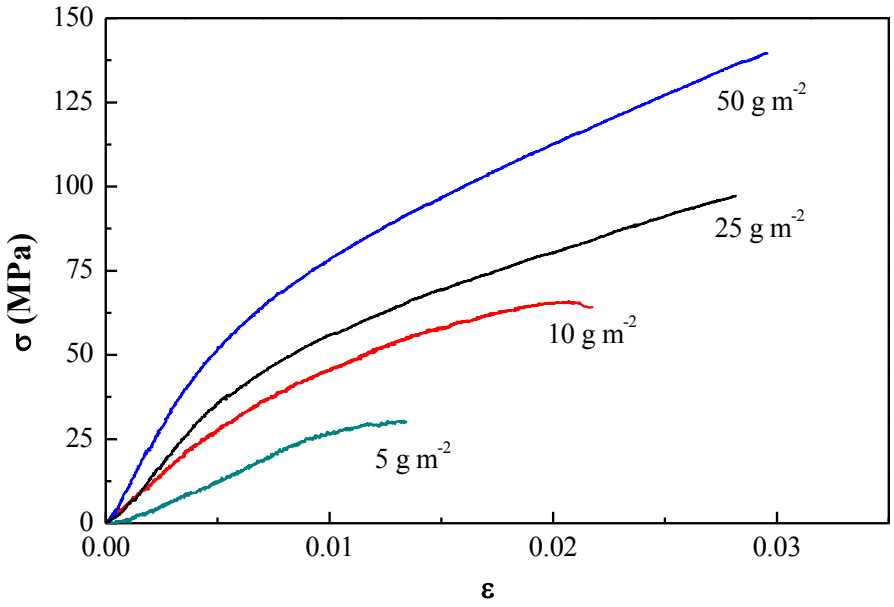

Figure 18: Representative stress-strain curves of the BC nanopapers under uniaxial loading.

The tensile modulus and strength of 5 g m^{-2} BC nanopaper were measured to be 2.4 GPa and 31 MPa, respectively (see Table 8). Increasing the grammage of BC

nanopaper led to a progressive increase in tensile modulus and strength of up to 12.2 GPa and 134 MPa, respectively, for 50 g m^{-2} BC nanopaper. Similar trends have been observed for conventional paper made from micrometre-sized pulp fibres, whereby the tensile properties of paper increase with increasing grammage [90,91]. It can also be seen from Table 8 that both the specific tensile modulus and strength of BC nanopapers increase with increasing nanopaper grammage, suggesting that difference in the porosity of the nanopapers, is not the sole reason for the observed tensile properties variation.

Table 8: Tensile modulus (E), strength (σ_{max}), strain at break (ε), specific modulus (E/ρ_e), specific strength (σ/ρ_e) and toughness (U_T) of the BC nanopapers.

Sample	E [GPa]	σ_{max} [MPa]	ε [%]	E/ρ_e [GPa cm^3 g^{-1}]	σ/ρ_e [MPa cm^3 g^{-1}]	U_T [J m^{-3}]
5 g m^{-2}	2.4 ± 0.2	31 ± 3	1.9 ±0.1	7.3 ±1.2	91 ±18	0.3 ±0.1
10 g m^{-2}	5.0 ± 0.2	59 ± 2	2.3 ±0.2	10.9 ±1.8	128 ±26	0.7±0.1
25 g m^{-2}	8.9 ± 0.6	104 ±3	3.2 ±0.2	13.1 ±2.2	153 ±31	2.1±0.1
50 g m^{-2}	12.2 ± 0.5	134 ±3	3.0 ±0.1	15.6 ±2.6	172 ±35	2.5±0.1

The stress transfer efficiency of a random fibre network [92] is related to the mean coverage of a fibre network, ($\bar{c}$), defined as the expected number of fibres covering a point in the plane of support of the fibre network [93]. Mathematically, $\bar{c}$ is expressed as:

$$\bar{c} = \frac{\bar{\beta}\omega}{\delta} \tag{4.4}$$

where $\bar{\beta}$ denotes the grammage, ω denotes the fibre width and δ represents the linear density of the fibre. The higher the value of $\bar{c}$, the better the stress transfer efficiency between the fibres of in the random fibre network. It can therefore be inferred from equation 4.4 that the higher grammage of BC nanopaper, the higher the value of $\bar{c}$ and hence, better stress transfer between BC nanofibres within the nanopaper as both ω and δ are the same for all fabricated BC nanopapers. Furthermore, a reduction in BC nanopaper grammage also leads to an increase in the relative amount of BC fibres between the surface and the bulk of the nanopapers. As the nanofibres on the surface are less efficient at transferring load [92], the (specific) tensile properties of the BC nanopapers decreases with decreasing nanopaper grammage.

4.3.4 Tensile properties and internal morphology of the BC nanopaper-reinforced PLLA composite laminates

Table 9 summarises the tensile properties of BC nanopaper-reinforced PLLA composite laminates reinforced with 10 sheets of 5 g m^{-2} (Laminate **1**), 5 sheets of 10 g m^{-2} (Laminate **2**), 2 sheets of 25 g m^{-2} (Laminate **3**) and 1 sheet of 50 g m^{-2} (Laminate **4**) BC nanopaper(s), respectively. It can be seen from Table 9 that all BC nanopapers possessed excellent reinforcing ability for PLLA to produce high performance BC nanopaper-reinforced PLLA composite laminates. Tensile moduli of between 10.5 and 11.8 GPa were obtained for the BC nanopaper-reinforced PLLA composite laminates at $v_{f,\,BC}$ = 39 – 53 vol.-%. The tensile strengths of the BC nanopaper-reinforced PLLA composite laminates were measured to be between 95 and 111 MPa. The slight variation

of tensile properties between the composite laminates can be attributed to the variation in $v_{f,BC}$ and porosity of the composites. By contrast, the tensile modulus and strength of neat PLLA were measured to be only 3.6 GPa and 57.5 MPa, respectively.

Table 9: Fibre volume fraction ($v_{f\,fibre}$), tensile modulus (E), tensile strength (σ_{max}) and strain at break (ε) Envelop density (ρ_e), theoretical density ($\rho_{c,\,void\,free}$) and porosity ($P_{composites}$) the composites and neat PLLA.

Sample	$v_{f\,fibre}$ [%]	E [GPa]	σ_{max} [MPa]	ε [%]	ρ_e [g cm^{-3}]	$\rho_{c,\,void\,free}$ [g cm^{-3}]	$P_{composites}$ [%]
PLLA	0	3.6 ± 0.1	57.5 ± 1.0	3.5 ± 0.4	1.26 ± 0.01	1.26 ± 0.01	0 ± 0
Laminate **1**	39 ± 3	10.7 ± 0.4	95.0 ± 0.9	2.2 ± 0.1	1.25 ± 0.07	1.36 ± 0.01	8 ± 1
Laminate **2**	48 ± 2	11.2 ± 0.4	102.4 ± 1.8	2.5 ± 0.1	1.23 ± 0.02	1.38 ± 0.01	11 ± 1
Laminate **3**	50 ± 3	10.5 ± 0.2	100.7 ± 1.9	3.0 ± 0.1	1.16 ± 0.01	1.39 ± 0.01	16 ± 1
Laminate **4**	53 ± 2	11.8 ± 0.2	111.4 ± 2.2	2.4 ± 0.1	1.28 ± 0.07	1.39 ± 0.01	8 ± 1

The fracture surfaces of the BC nanopaper-reinforced PLLA composite laminates loaded under uniaxial tension are shown in Figure 19. The observed internal morphology of the composite laminates is consistent with the stacking sequence shown in Figure 19, suggesting minimal bulk impregnation of the BC nanopapers by molten PLLA even when the grammage of the BC nanopaper is as low as 5 g m^{-2}.

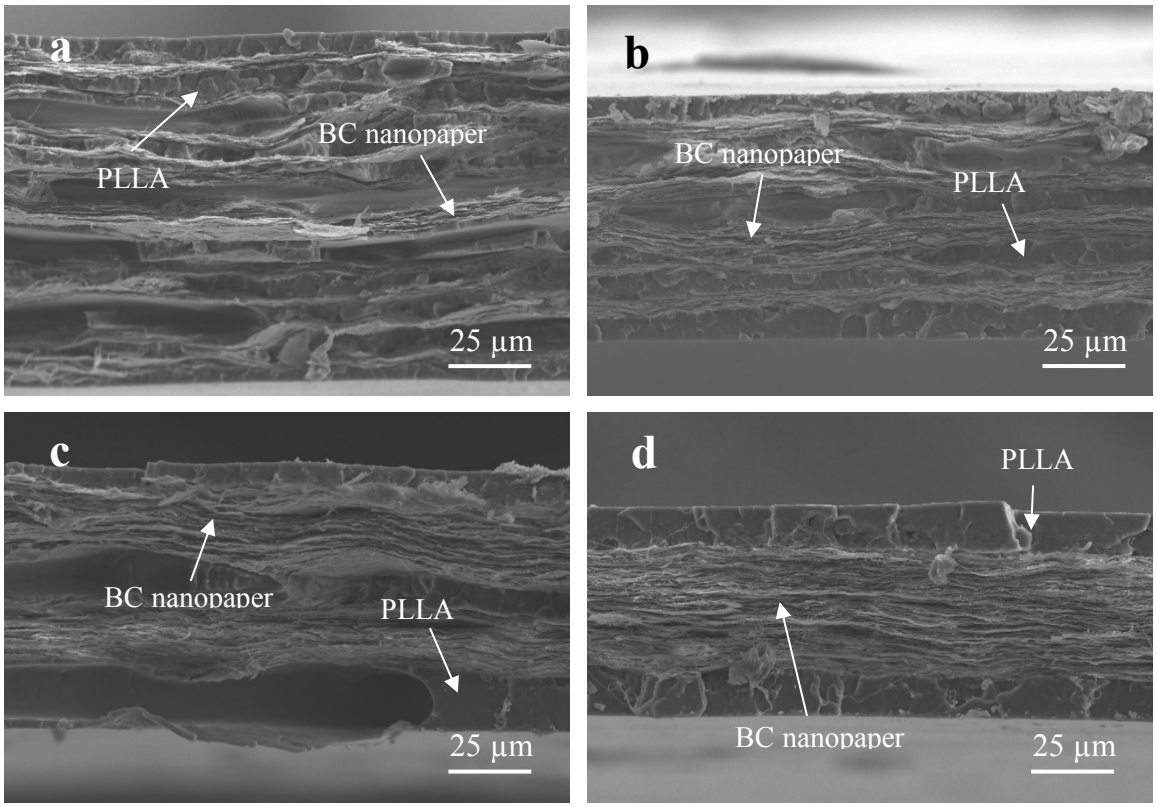

*Figure 19: Fractured surfaces of (a) Laminate **1**, consisting of 10 × 5 g m^{-2} BC nanopapers, (b) Laminate **2**, consisting of 5 × 10 g m^{-2} BC nanopapers (c) Laminate **3**, consisting of 2 × 25 g m^{-2} BC nanopapers and (d) Laminate **4**, consisting of 1 × 50 g m^{-2} BC nanopaper.*

It has been previously shown that the tensile modulus and strength of a cellulose nanopaper-reinforced polymer composites follow closely the prediction of the volume weighted average between the tensile properties of the cellulose nanopaper and the polymer matrix (equation 2.1 and equation 2.2). BC nanopaper-reinforced PLLA composites reinforced with 5 g m^{-2} BC nanopaper should possess a measured tensile modulus of 3.1 GPa and 47.5 MPa, respectively (see Figure 20).

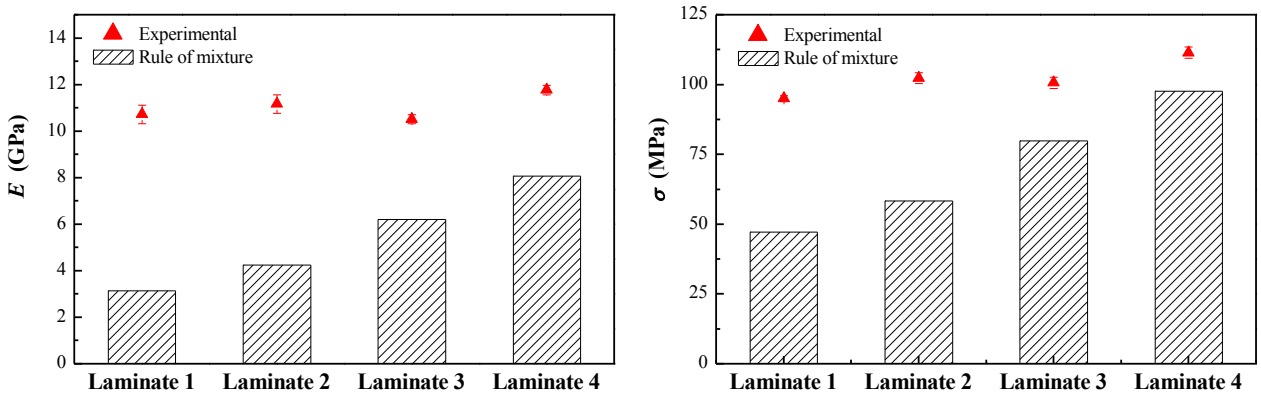

Figure 20: Tensile modulus and strength obtained experimentally and using the rule of mixture prediction for the manufactured composite laminates.

However, the experimentally determined tensile modulus and strength of BC nanopaper-reinforced PLLA composite laminates reinforced with 10 sheets of 5 g m-2 BC nanopapers were 10.7 GPa and 95 MPa, respectively. Significant positive deviation can be observed between the experimentally measured and the "rule-of-mixture" predicted tensile properties of all BC nanopaper-reinforced PLLA composite laminates fabricated in this work. This discrepancy between the experimentally determined and "rule-of-mixture" predicted tensile properties can be ascribed to the porosity of the resulting composite laminates.

The porosity of Laminates **1** – **4** was found to be ~8-16%. However, the BC nanopapers fabricated in this work possessed measured porosities of between 48% and 78% (Figure 17). Assuming that BC nanopapers are uniform rectangular slabs that are incompressible and impermeable to molten PLLA, the theoretical porosity of the composite laminates ($P_{\text{theoretical}}$) is estimated to be between 33% and 58%. These values are significantly higher than the experimentally determined porosity values for the BC nanopaper-reinforced PLLA composite laminates fabricated (see Table 9). Since

cellulose nanopapers possess a rough surface [94], the porosity of a BC nanopaper can be categorised into surface porosity (due to roughness) and bulk porosity (due to bubbles, cracks, etc.). It is postulated that the heat consolidation of molten thin PLLA films and BC nanopapers led to impregnation of the surface porosity of the BC nanopapers, leading to composites with porosity lower than $P_{\text{theoretical}}$.

5 Mechanical response of multi-layer BC nanopaper-reinforced polylactide laminated composites

5.1 Introduction

The mechanical response of BC pellicle- or BC nanopaper-reinforced polymer composites has been studied on composites consisting of only a single sheet of BC network embedded within a polymer matrix [22,23]. Very few studies have utilised more than a single sheet of BC network to produce BC nanopaper-reinforced polymer composites. Lee et al. [33] have previously reported the properties of BC nanopaper-reinforced epoxy laminated composites consisting of 11 sheets of BC nanopaper but the focus of that study was to compare the reinforcing effect of BC with wood-derived cellulose nanofibres. The mechanical response of BC composites with more than one sheet of BC network embedded within the polymer matrix is still not well understood. Furthermore, manufacturing process of a composite is a scale-dependent process [95]. It is hypothesised that scaling up the number of reinforcing BC networks in the composites might present new challenges to the manufacturing process. Therefore, in this work, laminated composites consisting of more than a single sheet of BC network in the form of BC nanopaper are studied to identify limitations in our understanding of the manufacturing process and mechanical response of BC composites.

5.2 Experimental

5.2.1 Materials

Poly(L-lactic acid) (PLLA) (L9000, molecular weight ≥ 150 kDa, D-content ≈ 1.5%) was purchased from Biomer GmbH and used as the matrix for the production of BC nanopaper-reinforced PLLA laminated composites. 1,4-Dioxane (ACS Reagent, purity ≥ 99%) was purchased from Sigma-Aldrich (Gillingham, UK) and used as the

solvent for PLLA. Sodium hydroxide (pellets, purity ≥ 98.5%) was purchased from VWR International (Lutterworth, UK). BC was extracted from commercially available nata de coco (Coconut gel in syrup, Xiangsun Ltd, Lugang Township, Changhua Country, Taiwan).

❖ Extraction and purification of BC from nata de coco

Briefly, 150 g of nata de coco cubes were first dispersed in 3.5 L of de-ionised water using a magnetic stirrer and heated to 80 °C. 14 g of NaOH pellets were added into this dispersion to form a 0.1 M NaOH solution, which was then left to stir at 80 °C for 2 h. After this step, the suspension containing the nata de coco cubes was poured onto a metal sieve (mesh size = 300 μm) to recover the purified nata de coco cubes. The cubes were rinsed with 5 L of de-ionised water to remove excess NaOH solution on the surface of the cubes prior to blending in another 5 L of de-ionised water using a blender (Breville BVL065) operating at maximum power output of 800 W for 2 min to create a homogenous BC-in-water suspension. This BC suspension was then centrifuged at 6800 × *g* for 7 min and the resulting supernatant decanted. The blending-centrifugation step was repeated until a BC suspension with neutral pH was obtained. The final BC-in-water suspension has a consistency of 2 wt.-% and it was stored at 5 °C prior to use.

5.2.2 BC nanopapers manufacturing

BC nanopaper with a grammage of 50 g m^{-2} was prepared in this work. The previously purified BC was dispersed in water using a blender (Breville BVL065) to produce a BC-in-water suspension of 0.1 wt.-% consistency. The suspension was then vacuum filtered onto a 125 mm diameter filter paper (Grade 413, 5-13 μm particle retention, VWR International Ltd, Lutterworth, UK). The wet BC filter cake was

carefully removed from the filter paper and sandwiched between two fresh filter papers and six blotting papers (Grade 3MM CHR, GE Healthcare, Buckinghamshire, UK), followed by wet pressing under a weight of 10 kg for 10 min at room temperature to absorb the excess water. This operation was repeated once more with fresh filter papers and blotting papers to further absorb the water from the BC filter cake. A final pressing step was then performed under a weight of 1 t at an elevated temperature of 120 °C for 30 min to dry and consolidate the partially dried BC filter cake into BC nanopaper. The BC nanopapers fabricated possessed a thickness of 46 ± 3 μm.

5.2.3 Laminated composite manufacturing

In this work, film stacking followed compression moulding of PLLA and BC nanopaper(s) was used to manufacture composites. BC nanopaper-reinforced PLLA laminated composites consisting of (i) 1 sheet, (ii) 3 sheets, (iii) 6 sheets and (iv) 12 sheets of BC nanopaper(s), respectively, were fabricated in this work. In order to attain high volume fraction of BC nanopaper(s) in the laminated composites, it is essential to use thin PLLA films [23]. To produce these, PLLA pellets were first dissolved in 1,4-dioxane at a mass ratio of 1:12 at 65 °C overnight under magnetic stirring. The polymer solution was then left to cool to room temperature prior to solution casting onto a glass plate using an automatic film applicator (Model 4340, Elcometer Ltd, Manchester, UK). After casting, 1,4-dioxane was then left to evaporate for at least 24 h prior to subsequent use. The average thickness of the PLLA films produced was 10 ± 3 μm.

BC nanopaper-reinforced PLLA laminated composites were fabricated by sandwiching the previously prepared BC nanopaper(s) with the thin PLLA films following the stacking sequence shown in Figure 21. A ceramic seam roller was used

remove any air bubbles trapped between the layers of BC nanopaper(s) and thin PLLA films. The BC nanopaper(s)-PLLA lay-up was sandwiched between two non-stick 125 μm thick polyester release films (Mylar® A, Lohmann Adhesive Tape System, Milton Keynes, UK) secured onto steel plates using heat-resistant tape (Easy composites, Staffordshire, UK). The whole set up was then pre-heated without pressing force to 180 °C for 3 min in a hydraulic press (4122CE, Carver Inc., Wabach, IN, USA). The pressing force of the hydraulic press was then increased to 0.5 t at the same temperature for another 3 min to consolidate the BC nanopaper(s) and PLLA films into BC nanopaper-reinforced PLLA laminated composites. BC nanopaper-reinforced PLLA laminated composites consisting of 1, 3, 6 and 12 sheet(s) of BC nanopaper(s) are herein termed composite **1**, composite **2**, composite **3** and composite **4**, respectively, with measured thickness of 60 ± 5, 177 ± 8, 382 ± 21 and 683 ± 12 μm, respectively. These BC nanopaper-reinforced PLLA laminated composites possessed BC weight fraction (w_f) of 69-75 wt.-% based on simple mass gain measurements. All samples produced were annealed at 120 °C for 30 min prior to characterisation.

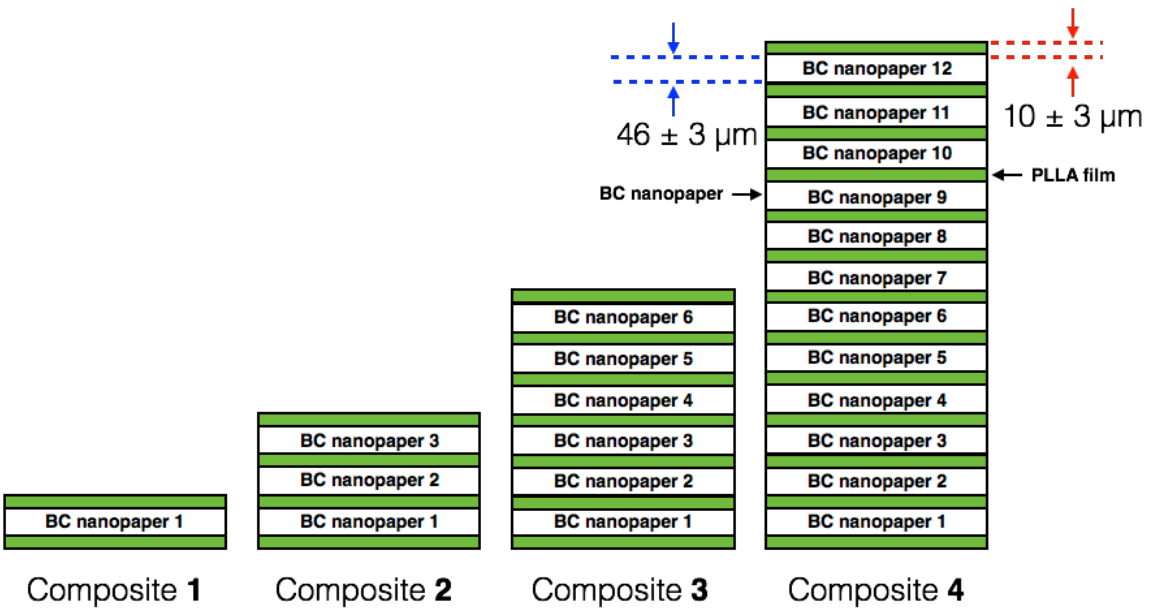

Figure 21: Stacking sequence of BC nanopaper-reinforced PLLA laminated composites fabricated in this work.

5.2.4 Composite characterisation

- ❖ Porosity of the BC nanopapers and laminated composites

He pycnometry (Accupyc II 1340, Micromeritics Ltd, Hexton, UK) was used to determine the true density of BC nanofibres (ρ_f) and neat PLLA (ρ_m). To determine the envelope density (ρ_e) of BC nanopapers and BC nanopaper-reinforced PLLA laminated composites, the thickness of the BC nanopapers and BC nanopaper-reinforced PLLA laminated composites was first measured using a digital micrometre (Mitutoyo MDC Lite, RS Components Ltd., Northants, UK) and ρ_e was calculated by taking the ratio between mass and envelop volume of the specimen. The porosity of the BC nanopapers ($P_{\text{BC nanopaper}}$) was then calculated using:

$$P(\%) = \left(1 - \frac{\rho_e}{\rho}\right) \times 100 \qquad (5.1)$$

To evaluate the porosity of the BC nanopaper-reinforced PLLA laminated composites, the theoretical (e.g. void free) density of the laminated composites (ρ_c) was first calculated from the weight fraction of BC ($w_{f,\,BC}$) within the laminated composites:

$$\rho_{c,\,\text{void free}} = \frac{1}{\frac{1-w_{f,\,BC}}{\rho_m}+\frac{w_{f,\,BC}}{\rho_f}} \tag{5.2}$$

The porosity of the BC nanopaper-reinforced PLLA laminated composites ($P_{\text{composite}}$) was then calculated using:

$$P_{\text{composites}}(\%) = \left(1-\frac{\rho_e}{\rho_c}\right)\times 100 \tag{5.3}$$

❖ Tensile properties of the BC nanopapers and laminated composites

Tensile testing was conducted in accordance to BS EN ISO 527: 2012. Prior to the test, neat PLLA film, BC nanopapers and BC nanopaper-reinforced PLLA laminated composites were cut into miniaturised dog-bone shaped test specimens using a punch die (ZCP 020, Zwick Testing Machines Ltd, Herefordshire, UK). These miniaturised dog-bone shaped specimens possessed an overall length of 35 mm, a gauge length of 10 mm and the narrowest part of the specimen has a width of 2 mm. All test specimens were secured onto 140 g m^{-2} paper testing cards using a two-part cold curing epoxy resin (Araldite 2011, Huntsman Advanced Materials, UK) to avoid damages to the gripping area of the test specimens by the clamps of the tensile tester, potentially leading to an earlier onset failure within the gripping zone of the test specimens. Tensile testing was performed using a micro-tensile tester (Model MT-200, Deben UK Ltd, Woolpit, UK) equipped with a 200 N load cell. Prior to the test, two points were marked on the surface of the test specimens in the direction of the applied load. The strain of the test specimens

was evaluated by monitoring the movement of these two marked points using a non-contact video extensometer (iMetrum Ltd., Bristol, UK). All test specimens were loaded with a crosshead displacement speed of 0.5 mm min^{-1} (corresponding to a strain rate of 0.05 s^{-1}). Average results of 5 test specimens were reported for each sample.

- Scanning electron microscopy

The internal morphology and microstructure of the non-fractured BC nanopaper-reinforced PLLA laminated composites were investigated using SEM. The laminated composites were first embedded in a two-part polyester resin (KLEER-SET, MetPrep Ltd., Coventry, UK) and polished (Saphir 550, Advanced Materialography, UK) using progressively finer sandpapers (P600 and P1200), followed by polishing cloth (first with polishing suspensions containing 0.3 μm alumina, followed by 0.06 μm silica suspensions). The polished polyester resin blocks containing the laminated composites were then mounted onto SEM stubs using carbon tabs, followed by Au coated (Agar Auto Sputter Coater, Essex, UK) at 40 mA for 40 s prior to SEM (Hitachi S-3700N, Tokyo, Japan). The fracture surfaces of the BC nanopaper-reinforced PLLA laminated composites were also investigated using SEM. Prior to SEM, the specimens were mounted onto aluminium stubs using carbon tabs, followed by Au coating using the previously described coating current for 20 s.

5.3 Results and discussion

5.3.1 Porosity of the laminated composites

Table 10 summarises the porosity of BC nanopaper-PLLA laminated composites reinforced with 1, 3, 6 and 12 sheet(s) of BC nanopaper(s), along with the porosity of neat PLLA and BC nanopapers. The porosity of BC nanopaper fabricated in this work

was found to be 33%. This is consistent with the values obtained in chapter 3. A trend could also be observed for the porosity of BC-reinforced PLLA laminated composites (table 1, composites **1** to **4**). When PLLA was reinforced with one sheet of BC nanopaper, a laminated composite porosity of ~17% was obtained. Increasing the number of reinforcing BC nanopapers to 3 sheets led to an increase in the porosity of the resulting laminated composites to 24%. A further increase in the number of reinforcing BC nanopapers to 6 and 12 sheets, respectively, increased the porosity of the resulting laminated composites to ~30%. The theoretical porosity of the laminated composites ($P_{\text{theoretical}}$) was also estimated based on the porosity attained for BC nanopapers. Assuming that BC nanopapers are uniform rectangular slabs that are not compressible and not permeable to molten PLLA, $P_{\text{theoretical}}$ can be estimated using:

$$P_{\text{theoretical}} = 1 - \frac{\rho_{\text{BC nanopaper}}}{\rho_{\text{f}}}\left[\frac{(1-w_{\text{f}})\rho_{\text{f}}+w_{\text{f}}\rho_{\text{m}}}{(1-w_{\text{f}})\rho_{\text{BC nanopaper}}+w_{\text{f}}\rho_{\text{m}}}\right] \quad (5.4)$$

The $P_{\text{theoretical}}$ of laminated composites **1** to **4** was estimated to be ~25% (see Table 10). Composites **1** and **2** possess porosities lower than, or similar to $P_{\text{theoretical}}$ while composites **3** and **4** possessed porosity values higher than $P_{\text{theoretical}}$. The lower than $P_{\text{theoretical}}$ for composite 1 could be attributed to the degree of consolidation of a single sheet of BC nanopaper with PLLA. The higher than $P_{\text{theoretical}}$ for composites **3** and **4**, on the other hand, could be attributed to the presence of scale-induced defects as the number of sheets of BC nanopapers increases to 6 and 12 sheets, respectively. To further elucidate this deviation of porosity values of the laminated composites from theoretical values, the internal morphology of the fabricated BC nanopaper-reinforced PLLA laminated composites was further investigated (see next section).

Table 10: The density and porosity of neat PLLA, BC nanopaper and laminated composites. ρ_e, ρ and P denote the envelope density, true/theoretical density and porosity, respectively.

Sample	ρ_e (g cm^{-3})	$\rho^{\S}$ (g cm^{-3})	P (%)	$P_{theoretical}$ (%)
PLLA	1.26 ± 0.01	1.26 ± 0.01	0	
Composite **1**	1.17 ± 0.09	1.42 ± 0.01	17 ± 1	25 ± 1
Composite **2**	1.09 ± 0.05	1.43 ± 0.01	24 ± 1	26 ± 1
Composite **3**	0.98 ± 0.05	1.42 ± 0.01	31 ± 2	25 ± 1
Composite **4**	1.00 ± 0.02	1.44 ± 0.01	30 ± 1	26 ± 1
BC nanopaper	1.00 ± 0.07	1.51 ± 0.01	33 ± 1	

§ ρ obtained using He pycnometry for neat PLLA and BC nanopaper, and calculated using equation 5.2 for the laminated composites.

5.3.2 Internal morphology of the laminated composites

The polished cross-sections revealing the internal structure of the BC nanopaper-reinforced PLLA laminated composites are shown in Figure 22a-d. A multi-layer structure consisting of alternating layers of PLLA and BC nanopaper that are consistent with the stacking sequence used (see Figure 21) can be observed, suggesting little or no impregnation of the BC nanopaper(s). This is attributed to the high viscosity of molten PLLA (>5000 Pa s at 180 °C) [96] and the small pore size of the nanocellulose network [80]. In this context, the reinforcing effect of the laminated composites stems from BC nanopapers instead of individual BC nanofibres [15].

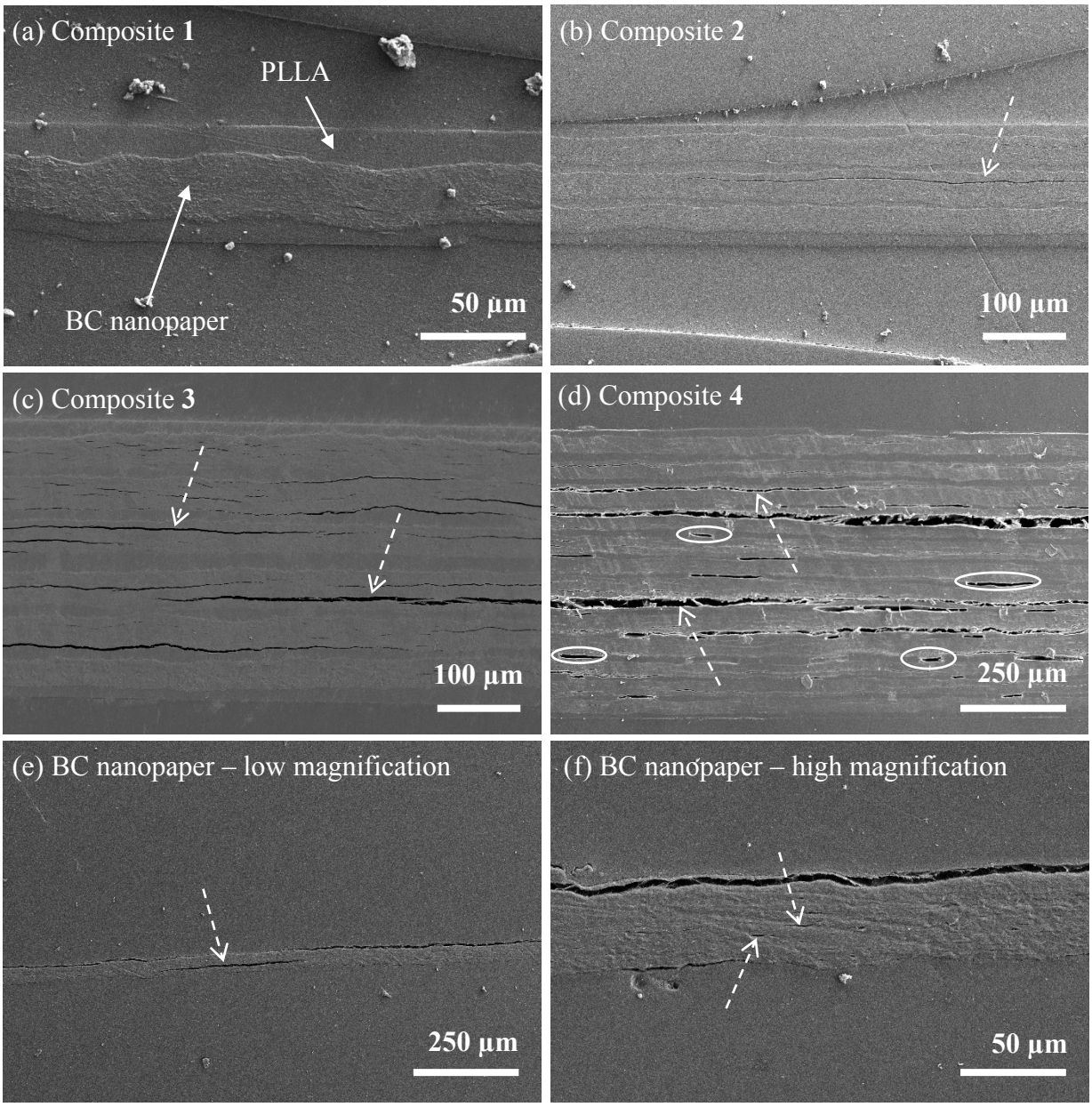

*Figure 22: Polished cross-sections of the BC nanopaper-reinforced PLLA laminated composites and BC nanopaper. (a) Composite **1**, (b) Composite **2**, (c) Composite **3**, (d) Composite **4**, (e, f) BC nanopaper. The dotted arrows show the presence of micro-cracks in the reinforcing BC nanopaper. The circles show the voids in composite **4**.*

Figure 22a-d also show the presence of various defects in the laminated composites. Three types of defects were observed; thickness inhomogeneity and out-of-

plane waviness of BC nanopaper(s) in the laminated composites, voids between adjacent layers of BC nanopapers (see ellipses in Figure 22d) and micro-cracks within the BC nanopapers (see dotted arrows). The thickness inhomogeneity and out-of-plane waviness of BC nanopaper can be ascribed to the formation of aggregates/bundles of BC in the starting BC-in-water suspension, which was due to difficulties in disrupting the 3-dimensional network of BC pellicles with low energy blending (as described in chapter 3). As a result of the BC aggregates in the suspension, the formation of BC network within the BC nanopaper is non-uniform, leading to the observed thickness inhomogeneity and waviness of BC nanopaper.

Voids between adjacent BC nanopapers are also observed in composite **4**, which consists of 12 sheets of reinforcing BC nanopapers. The origin of these voids can be attributed to air bubbles trapped during the lay-up of composite **4**. The large number of layers in composite **4** (12 sheets of BC nanopaper and 13 layers of PLLA) and the short consolidation time (to avoid degradation of PLLA) led to difficulties in removing the trapped air bubbles between the layers of PLLA and BC nanopaper.

To ascertain whether micro-cracks are present in the starting BC nanopapers, the internal morphology of neat BC nanopaper (Figure 22e-f) was investigated. Micro-crack could also be observed in the nanopaper (see arrow, Figure 22e and Figure 22e). The formation of micro-cracks in neat BC nanopaper is hypothesised to be due to the residual stress formed during the drying of wet BC filter cake to produce BC nanopaper. When conventional paper dries, the surface layers contract and the material in the centre complies. This difference in the response of the neighbouring materials during this contraction would lead to the formation of residual stress in conventional paper [97]. It is

postulated a similar effect occurred in the BC nanopaper. In the heat consolidation step, the partially dried BC filter cake was sandwiched between two filter papers and heat pressed. This was to prevent the lateral contraction of the filter cake by restraining the BC filter cake onto filter papers during drying. While lateral contraction of the BC filter cake was prevented, the contraction and shrinking in the through-thickness direction still occurred as the moisture ratio of the filter cake decreased. Since the outer layers of the BC filter cake were restrained onto the filter papers during drying, it is anticipated the drier outer layers compared to the swollen wet core, coupled with the non-uniform formation of BC network in the nanopaper led to the formation of micro-cracks in the BC nanopaper.

It could also be observed from Figure 22a to Figure 22d that the presence and severity of micro-cracks in the reinforcing BC nanopapers increased with increasing sheets of BC nanopaper in the laminated composites. As the BC nanopaper-PLLA laminate consolidates under heat and an external pressing force, the molten PLLA in between adjacent layers of BC nanopapers or between BC nanopaper and non-stick release film will start to flow. If the resistance to flow is low (e.g. adjacent to the surface of non-stick release film), the molten PLLA will flow and conform to the waviness of BC nanopaper, as observed in composite **1**. As a result, the severity and presence of defects are low for BC nanopaper-PLLA laminate reinforced with one sheet of BC nanopaper. This is also consistent with the absence of severe micro-cracks in the BC nanopapers at the top and bottom layers of composites **2** to **4**. However, if the resistance to the flow of molten PLLA is too high (e.g. between two adjacent BC nanopapers, due to surface roughness and waviness of BC nanopaper), the flow of molten PLLA will lead

to the delamination of the BC nanopaper. This situation is further accentuated by the inhomogeneity and waviness of BC nanopaper, with regions of non-uniform areal density of BC in the nanopaper. As a result, the severity and presence of micro-cracks in the BC nanopaper at the mid-plane of the laminated composites with ≥ 3 sheets of BC nanopapers were high and increased with the number of sheets of BC nanopapers in the laminated composites. Similar effects have also been observed in the consolidation of carbon fibre-reinforced polymer laminates [98].

5.3.3 Tensile properties of the laminated composites

The tensile properties of neat PLLA, BC nanopaper and their laminated composites are summarised in Table 11. BC nanopapers was found to possess tensile modulus (E) and strength ($\sigma_{\max}$) of ~15 GPa and ~140 MPa, respectively. These values are consistent with values obtained by various researchers [88]. By reinforcing PLLA with BC nanopaper at BC volume fraction ($v_{\mathrm{f,\,BC}}$) of 65 – 72 vol.-%, tensile moduli of 12.4 – 13.6 GPa were obtained. The slight variation in the measured tensile modulus of the laminated composites is attributed to the slight variations of $v_{\mathrm{f,\,BC}}$. Higher $v_{\mathrm{f,\,BC}}$ leads to higher measured E. The results also suggest that the measured E is relatively independent of porosity and the number of reinforcing BC nanopapers in the laminated composites. This could be due to the fact that for elastic modulus, the point-to-point variations at small scales will be averaged out over the volume of the specimens tested and the porosity of the composites in this chapter do not differ significantly from each other [99].

Table 11: The tensile properties of neat PLLA, BC nanopaper and their laminated composites. $v_{f,BC}$, E, σ_{max} and ε denote the fibre volume fraction of BC within the laminated composites, tensile modulus, tensile strength and strain-to-failure, respectively.

Sample	$v_{f,BC}$ (%)	E (GPa)	σ_{max} (MPa)	ε (%)
PLLA	0	4.4 ± 0.2	62 ± 5	1.7 ± 0.1
Composite **1**	65 ± 2	12.4 ± 1.5	121 ± 8	3.4 ± 0.3
Composite **2**	70 ± 3	13.4 ± 0.8	121 ± 5	2.3 ± 0.2
Composite **3**	66 ± 2	12.7 ± 0.9	105 ± 3	2.5 ± 0.1
Composite **4**	72 ± 3	13.6 ± 0.2	95 ± 11	1.6 ± 0.3
BC nanopaper	1	14.9 ± 1.4	142 ± 13	2.9 ± 0.7

Unlike the measured E of the BC nanopaper-reinforced PLLA laminated composites, a knockdown effect can be observed for the measured σ_{max} of the laminated composites. The tensile strength decreases consistently from 121 MPa for laminated composites reinforced with 1 sheet of BC nanopaper (composite **1**) to only 95 MPa for laminated composites reinforced with 12 sheets of BC nanopapers (composite **4**). This decrease in tensile strength of the laminated composites could be explained by the weakest link theory: failure initiate from a flaw within the material [83]. As observed in Figure 22, the severity of the micro-cracks increases with increasing number of sheets of BC nanopapers in the laminated composites. These micro-cracks acted as flaws, leading to early onset failure of the laminated composites. As a result, composite **4** possessed the lowest σ_{max} due to the presence of a large number of micro-cracks.

The representative stress-strain curves for PLLA, BC nanopaper and each type of laminated composite fabricated in this work are shown in Figure 23. The stress-strain curve of BC nanopaper comprised of an initial elastic behaviour, followed by an inelastic deformation prior to catastrophic fracture at a strain-to-failure (ε) of ~3%. PLLA, on the other hand, failed in a brittle manner at $\varepsilon = 2\%$. The stress-strain curves of composites **1** to **3** showed a catastrophic failure when peak loads were reached while composite **4,** which contained 12 sheets of BC nanopapers, showed a progressive failure.

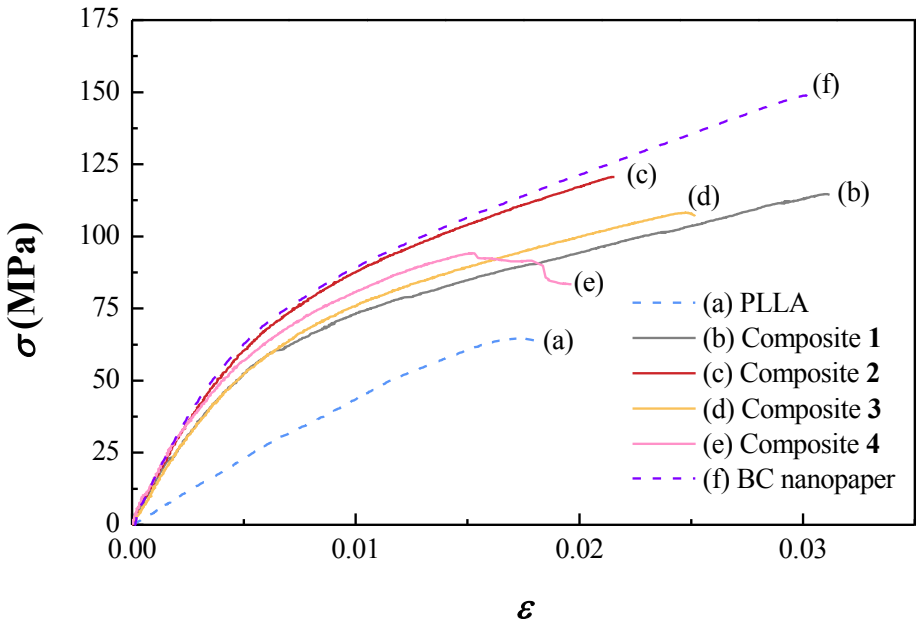

Figure 23: Representative stress-strain curves obtained for the neat PLLA, BC nanopaper and the fabricated laminated composites

When peak load was reached for composite **4**, one (or more) BC nanopaper(s) fractured from the micro-cracks present. The load (which was lower than loads sustained by composites **1** to **3** at the point of fracture) was then transferred locally to surrounding BC

nanopapers that could still sustain the load exerted on the specimen, leading to the observed progressive failure of the specimens.

5.3.4 Fracture surfaces of the laminated composites

The fracture surfaces of composites **1** to **4**, which provides further information on the influence of number of sheet(s) of BC nanopaper(s) in the laminated composites, are shown in Figure 24. In all cases, significant defibrillation was observed for BC nanopapers and the presence of ribbons and scarps on the fracture surface of the PLLA is indicative of a brittle fracture [100], which also corroborate with the stress-strain curve of PLLA. Composite **1** exhibited a localised fracture surface while composites **2** to **4** showed more extensive fracturing throughout the specimen. Such extensive fracturing process is consistent with the presence of micro-cracks in the reinforcing BC nanopapers.

When peak load is reached, micro-cracks within the BC nanopaper will start to propagate and coalesce forming larger cracks [101], which ultimately led to the fracture of the BC nanopaper. Composite **1** was reinforced only with one sheet of BC nanopaper. The fracture of BC nanopaper in composite **1** will lead to the fracture of the composite, leading to a more localised fracture. Composites **2** to **4** were reinforced with more than one sheet of BC nanopaper. When a BC nanopaper fractures, the load is transferred to surrounding intact BC nanopapers, and caused the micro-cracks (which might not be on the same plane) in the nearby BC nanopapers to start propagating, leading to the observed extensive fracturing process.

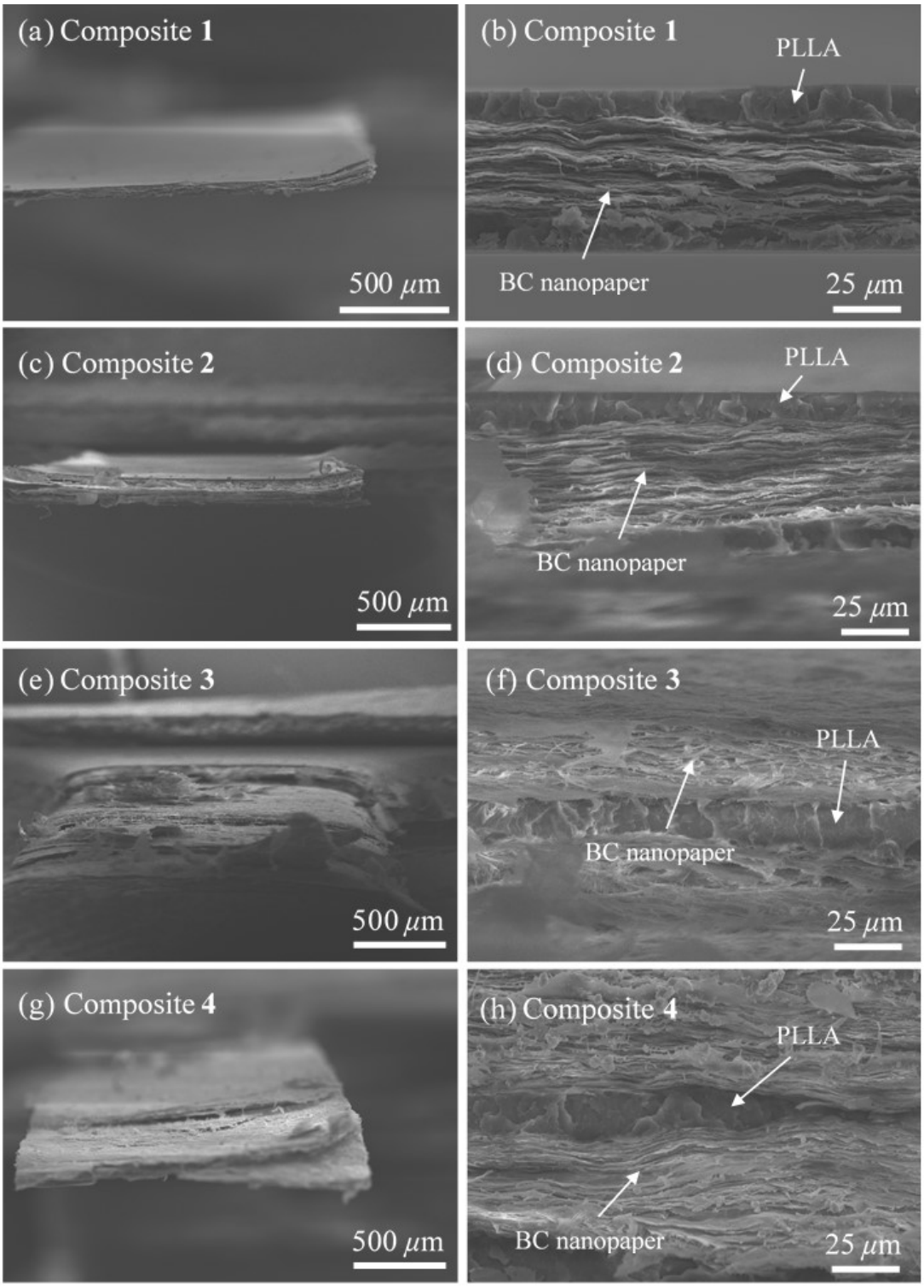

Figure 24: Fracture surfaces of the laminated composites at low magnification (a, c, e, g) and high magnification (b, d, f, g), respectively.

It is also worth noting that the de-bonding of BC nanopaper/PLLA interface was not observed. Similar observation was also obtained for BC sheet (in the form of pellicle)-reinforced PLLA composites [36]. Direct wetting measurements showed that the contact angle of PLLA droplet on a single BC nanofibre was found to be 35.4 ± 0.8°. This results suggest good thermodynamic adhesion between BC and PLLA [102]. Therefore, the fracture process of BC nanopaper-reinforced PLLA laminated composites is governed by the fracture process of BC nanopaper within the laminated composites instead of the BC nanopaper/PLLA interface.

6 LCA of nanocellulose-reinforced polymer composites

6.1 Introduction

It is evident that high performance BC- and CNF-reinforced polymer composites can be produced. However, one major question remains: "*Are nanocellulose-reinforced polymer composites truly environmentally friendly compared to commercially available renewable polymers and engineering materials?*" With increasing demand for environmental friendlier materials, it is timely to investigate the environmental impact associated with the manufacturing of nanocellulose-reinforced polymer composites. Therefore, in this chapter, the environmental impacts associated with the manufacturing of BC- and CNF-reinforced polymer composites is quantified through a life cycle assessment approach, starting from the production of nanocellulose (i.e. the cradle) to the end-of-life (i.e. the grave) of the nanocellulose-reinforced polymer composites.

6.2 Methodology

6.2.1 Goal and scope definition

The aim of this chapter is to evaluate the environmental impacts of high performance BC- and CNF-reinforced epoxy composites through a cradle-to-grave LCA including their manufacturing, use phase and end-of-life. Two commercially available benchmark materials were chosen for comparison: (i) 30 wt.-% randomly oriented glass fibre-reinforced polypropylene (GF/PP) composites and (ii) polylactide, which is considered the best performing bio-derived polymer [15]. Both materials were chosen because of their extensive industrial usage as well as relatively similar mechanical properties. This translates in their production being done with a process optimised for large production volumes. The system boundary for the nanocellulose-reinforced epoxy

composites and the benchmark materials is shown schematically in Figure 25. A distinction is made between the foreground system, which is defined as the processes of main importance in regards to the study (direct measurements can often be taken), and the background system, which is defined as the processes used to support the foreground system (supply of energy and materials) [103].

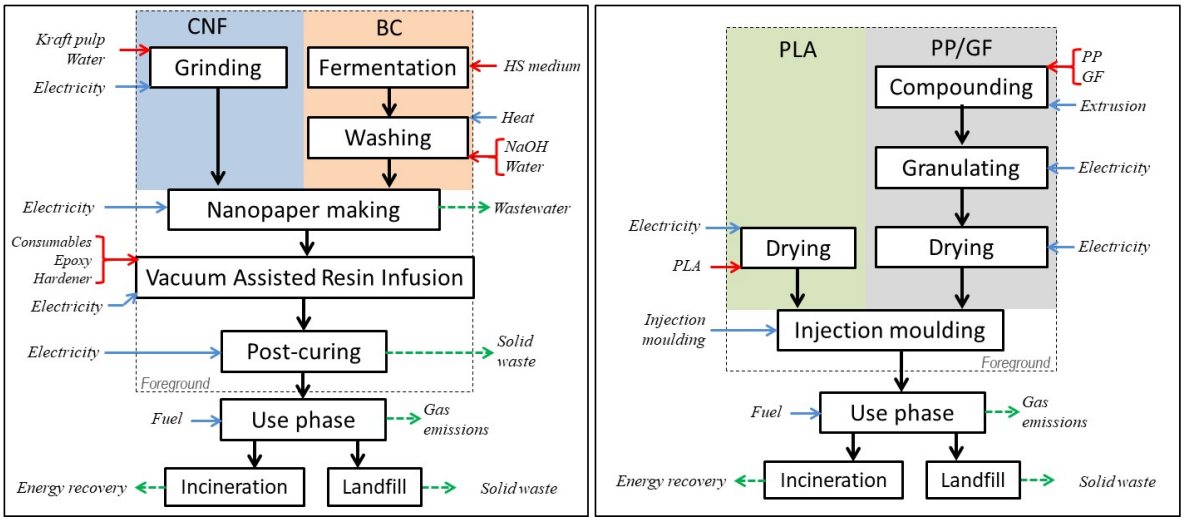

Figure 25: Schematic diagram showing the system boundaries of the model representing the life cycle of BC- and CNF-reinforced polymer composites (left), and PLA and GF/PP composite (right). The red, blue and green arrows represent consumables or raw materials required, energy input and waste (materials and energy), respectively.

6.2.2 Polymer and composite manufacturing processes

The manufacturing of BC- and CNF-reinforced epoxy composites assumed in this system is based on another study [33]. This study was chosen as high loading of nanocellulose, which is a pre-requisite to producing high performance nanocellulose-reinforced polymer composites [15], was achieved using conventional vacuum assisted resin infusion, a widely used composite manufacturing technique. Briefly, never-dried

bleached birch Kraft pulp (*Betula pendula*) was passed through a Supermass Colloider (Masuko Sangyo Co., Kawaguchi, Japan) seven times and the final obtained consistency of CNF in water was approximately 2 wt.-%. The CNF suspension was diluted to 0.4 wt.-% prior to nanopaper manufacturing. Similarly, BC pellicles were first cut into small pieces and blended (Breville BL18 glass jug blender, Pulse Home Products Ltd., Oldham, UK) for 2 min at a consistency of 0.1 wt.-%. The manufacturing of both BC and CNF nanopaper closely resembles that of conventional paper manufacturing process, whereby the BC and CNF suspension were vacuum filtered, wet pressing under a 10 kg weight, followed by drying at 55 °C to obtain BC and CNF nanopapers. To manufacture BC- and CNF-reinforced epoxy composites, 11 nanopapers were sandwiched between two PTFE coated glass fabrics (FF03PM, Aerovac, West Yorkshire, UK) and placed on top of a polyester porous flow medium (15087B, Newbury Engineer Textile, Berkshire, UK). Another polyester porous flow medium was placed on top of the PTFE coated glass fabric. A heat stabilised Nylon 6 vacuum bag (Capran 519, Aerovac, West Yorkshire, UK) was then used to cover the whole set up and vacuum sealant tape (SM5127, Aerovac, West Yorkshire, UK) was used to seal the set up. A vacuum was then applied (~15 mmHg) and the liquid epoxy resin (PRIME 20ULV, Gurit Ltd, Isle of Wight and Hamble, UK) was fed at room temperature from the bottom of the flow medium (tooling side) through the stack of nanopapers and exit through non-tooling side. The resin was left to cure at room temperature for 24 h, followed by a post-curing step at 50 °C for 16 h. The resulting BC- and CNF-reinforced epoxy composite panels were ~1 mm thick, containing 49 vol.-% and 58 vol.-% of BC and CNF loadings, respectively. In this LCA model, a commercially available randomly oriented GF/PP composite consisting of 30

wt.-% glass fibres (which is equal to 13 vol.-%), known under the trade name of Eurostar Starpylen MX06050[†] was modelled. To manufacture the GF/PP composites, the glass fibres were assumed to be compounded with polypropylene in an extruder prior to palletisation and injection moulded into the final composite parts. To manufacture neat PLA parts, the model assumed that dried PLA pellets were injection moulded to produce the final PLA part.

6.2.3 A comparison criterion: the functional unit

A functional unit (f.u.) quantifies the function provided by the analysed system and provides a base for comparison with alternative systems. In order to compare the four different materials with different mechanical performances, a performance indicator found using Ashby's method [39] based on the specific tensile stiffness of the materials is used to calculate the equivalent mass of the material required to reach the same level of performance. The equivalent mass of material required is expressed as:

$$\frac{m - m_{ref}}{m_{ref}} = \frac{E_{ref}/\rho_{ref}}{E/\rho} - 1 \tag{6.1}$$

where m, E, ρ are the mass, tensile modulus and density of BC-reinforced epoxy composites, GF/PP model composites and neat PLA, respectively. m_{ref}, E_{ref} and ρ_{ref} are the mass, tensile stiffness and density of a reference material. In this LCA model, m_{ref} = 1 kg of CNF-reinforced epoxy composite is arbitrarily chosen as reference. The derivation of equation 6.1 can be found in Appendix B. The mass of materials compared in this LCA model along with materials properties are summarised in Table 12.

[†] Mechanical data obtained from http://www.matweb.com/

Table 12: The functional unit used in this LCA. E, ρ and m denote the tensile modulus, density and equivalent mass of the materials required. E and ρ of BC- and CNF-reinforced epoxy composites, as well as neat PLA were obtained from Lee et al. [33] and Montrikittiphant et al. [23], respectively.

Material	E (GPa)	ρ (kg m^{-3})	E/ρ (GPa m^3 kg^{-1})	m_{total} (kg)	$m_{reinforcement}$ (kg)
PLA	3.9 ± 0.2	1210	3.22	1.96	0
GF/PP*	5.7	1120	5.09	1.24	0.392
CNF/epoxy	8.5 ± 0.2	1350	6.30	1.00	0.650
BC/epoxy	7.1 ± 0.1	1320	5.38	1.17	0.653

*The properties used in this chapter are based on commercially available randomly oriented GF/PP composites under the trade name of Eurostar Starpylen MX06050.

6.2.4 Calculation method and impact categories

This LCA model uses the CML 2001 impact assessment method (April 2013 version) developed by the Centre for Environmental Science in Leiden University [104] using a life cycle engineering software, GaBi (version 6, PE International, Leinfelden-Echterdingen, Germany). This method uses midpoint indicators to model at an early stage the effects of substances on the environment at an early stage (also known as problem-oriented approach) which minimises uncertainties [105]. The chosen impact indicators for this LCA along with their brief description are summarised in 2.2.1.These impact categories have been chosen based on their significance to this LCA model and their link to distinct environmental mechanisms.

6.3 Life cycle inventory

All the data used in this chapter was obtained from: (i) the GaBi databases, (ii) Ecoinvent version 2.2, (iii) literature values and (iv) the author's own estimations.

❖ Foreground data

All the input and output data were scaled to the equivalent of manufacturing the previously calculated mass of materials to be compared. The electricity usage of the vacuum pump was measured using P4400 Kill-A-Watt power usage meter (P3 International, New York, USA).

❖ Background data

The electricity production was assumed to be supplied from the electricity grid mix for Great Britain (45.9% from natural gas, 28.3% from hard coal, 16.3% from nuclear, 1.3% from heavy fuel oil, 0.3% from coal gases and 8% from renewable energies). Global and European data averages were used in absence of data from Great Britain. If data was not available from both Great Britain and Global/European averages, the data from Switzerland or Germany was then used.

❖ Energy balance

To estimate the energy required in any process steps, the following equation was used:

$$Q = \int_{T_1}^{T_2} \left(\sum_i m_i \times C_{P,i} \right) dT \qquad (6.2)$$

where Q is the energy required, m_i and $C_{P,i}$ are the mass and the heat capacity of compound i, respectively. For the estimation of the energy required to post cure BC- and CNF-reinforced epoxy composites, the heat capacity of cellulose and epoxy resin were taken as 1.55 J g^{-1} K^{-1} [106], and 1 J g^{-1} K^{-1} [107], respectively. The energy required to heat the water for the purification of BC pellicles was also calculated using equation 6.2.

6.3.1 Key assumptions

The following assumptions were made in this LCA model:

(i) The yield of BC is highly dependent on the strain of cellulose-producing bacteria used, the carbon source, supplement supplied and the culture time [13]. In this LCA model, BC is assumed to be produced by *A. xylinum* (ATCC 53582) using Hestrin-Schramm medium [108] consisting of 2% (w/v) glucose, 0.5% (w/v) yeast extract and peptone, 0.27% (w/v) disodium hydrogen phosphate and 0.115% (w/v) citric acid. The BC yield used in this study was 3.2 g L^{-1} based on an in-house preliminary study.

(ii) BC is purified by heating the BC pellicles in 0.1 M NaOH solution to 80 °C for 20 min. In this LCA model, it was assumed that 36 L of 0.1 M NaOH solution is needed to purify 653 g (dry weight) of BC pellicles.

(iii) The manufacturing of nanocellulose-reinforced composite panels will no doubt require more epoxy resin than what was needed by the final BC- and CNF-reinforced composite panels as additional epoxy resin was needed to fill the gap in the vacuum bag and infusion tubes. Nevertheless, it was assumed in this LCA model that the additional epoxy resin needed exert no significant influence on the LCA results.

(iv) Material losses during Kraft pulp grinding, nanopaper manufacturing, polymer and glass fibres compounding, injection moulding and (composite) parts finishing were assumed to be negligible. Heat loss during the post curing of the BC- and CNF-reinforced epoxy composites was assumed to be insignificant.

(v) A recent study by Josset et al. [44] showed that an energy requirement of 5.25 kWh kg^{-1} was needed to fibrillate Kraft pulp to CNF using a Masuko grinder. This value was used in this LCA model for the production of CNF from Kraft pulp.

(vi) An industrial paper manufacturing process was modelled in the life cycle engineering software, GaBi, to model the manufacturing of BC and CNF nanopapers. The paper making data associated with paper production from bleached Kraft pulp was used. The longer water drainage time required by nanocellulose was omitted.

(vii) The environmental impacts associated with the transportation of materials were neglected as glass fibres are extremely well industrialised whereas nanocellulose is only starting to be produced industrially. Including material transportation would thus masks the environmental differences linked only to the materials.

(viii) The efficiency of all electrical appliances (vacuum oven, resin infusion plates, vacuum pumps etc.) was assumed to be 100%.

(ix) BC- and CNF-reinforced epoxy composites, GF/PP and PLA were assumed to be equally durable in this LCA model.

6.3.2 Use phase and end-of-life

A cradle-to-grave LCA was performed in this chapter, whereby the use phase of the polymer and composite parts in a car (a highly researched application for green composites) [109] and their end-of-life were considered.

- ❖ Use phase impact

To evaluate the environmental impact associated with the use phase of the polymer and composite parts in a car, the fuel consumption was allocated in function of the weight of the parts in the car using [110]:

$$\text{Fuel economy}_{\text{panel}} = \frac{\text{Weight}_{\text{panel}}}{\text{Weight}_{\text{car}}} \times \text{Fuel economy}_{\text{car}} \times c \quad (6.3)$$

A factor "*c*" was introduced to account for aerodynamics, as the reduction in fuel consumption of the polymer and composite parts is not only directly proportional to the weight reduction of the car [110]. A *c* value of 0.5, which signifies that a 10% weight reduction of the car lowers the fuel consumption by 5%, was chosen according to a study conducted on Peugeot - Citroën cars [111]. The equivalent distance used to model the use phase of each part was calculated based on an average car weighting 1500 kg driven for 200,000 km with a fuel consumption of 7.3 L km^{-1}. This fuel consumption also corroborates the average fuel consumption of a car in the EcoInvent database.

- ❖ End-of-life (EOL)

In 2011, it was estimated that 50% of the plastic waste generated in Switzerland went into landfills, 30% of the plastic waste were incinerated to recover energy whilst the remainder were recycled [112]. The process of recycling depends on numerous factors such as waste flow and the type of plastic. Due to the uncertainty associated with the recycling process, it was assumed that 60% of composite panels would go into landfill and 40% of the composite panels were incinerated to recover energy. The process of recycling was not considered. All the glass fibres in GF/PP were assumed to be incombustible and sent to landfill as part of the combined ash from the incinerator. Furthermore, a recent report published by the European Plastics Recyclers Association showed that less than 15% of polymer waste from the automotive industry is recycled [113], with approximately 60% of these waste disposed in landfill or incinerated without energy recovery. Therefore, it was assumed that 60% of PLA was sent to landfill and 40% incinerated to recover energy. A recent study on the anaerobic digestion of PLA in

landfills showed that no statistically significant biogas (CH_4 and CO_2) was generated [114]. Therefore, this LCA model further assumed that there was no significant biogas contribution when PLA was landfilled compared to the other materials.

6.4 Results and discussion

6.4.1 Cradle-to-gate analysis

A cradle–to-gate LCA model includes all steps from raw materials extraction to the finished product at the factory gate. The cradle-to-gate GWP and ADf associated with the production of PLA, GF/PP, BC- and CNF-reinforced epoxy composites are shown in Figure 26.

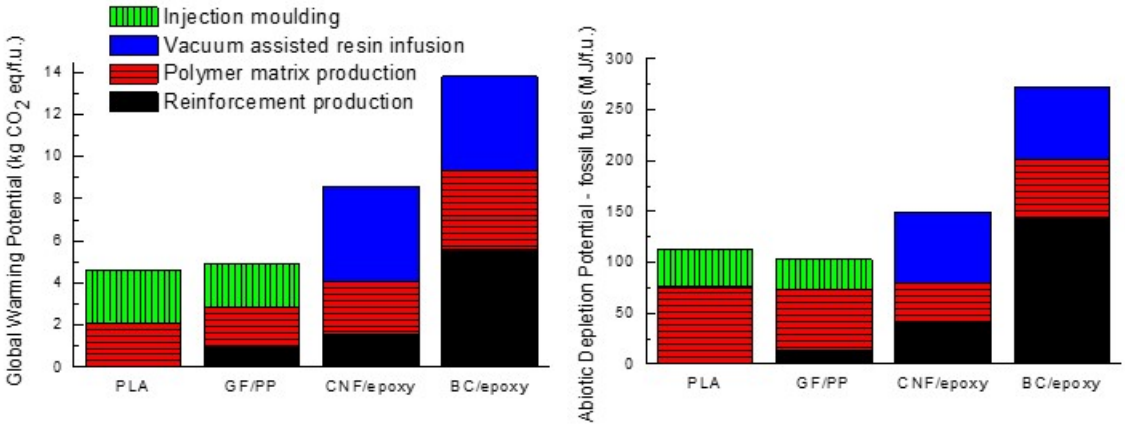

Figure 26: Global warming potential and fossil energy consumption for the production (from cradle-to-gate) of the two benchmark materials and two nanocellulose-reinforced composites.

Even though the equivalent mass of neat PLA is larger, the GWP of neat PLA is lower than GF/PP. This could be attributed to the 1.9 kg CO_2 eq kg^{-1} of environmental credits of PLA as a result of carbon sequestration associated with corn production [50],

whereby for 1 kg of PLA, 2.5 kg of corn is needed[‡]. The ADf for PLA however, is higher than that of GF/PP. As GF/PP possess higher tensile modulus compared to PLA (5.7 GPa *vs* 3.9 GPa), the equivalent mass of GF/PP required would be much smaller than that of PLA to sustain the same tensile load, leading to the observed lower environmental impact of GF/PP in other impact categories (see Appendix C for a comprehensive environmental impact of all modelled materials). Nevertheless, both BC- and CNF-reinforced epoxy composites have higher environmental impacts compared to the benchmark PLA and GF/PP. The results showed that the GWP of both BC- and CNF-reinforced epoxy composites are higher than that of PLA and GF/PP. Furthermore, the ADf of the production of BC-reinforced epoxy composites was found to be 2.4 and 2.6 times higher than neat PLA and GF/PP (see Figure 26), respectively, even though BC-reinforced epoxy composites possess higher tensile modulus compared to neat PLA and GF/PP, implying that less BC-reinforced epoxy composites is needed to comply with the functional unit. Similar observations could also be made for CNF-reinforced epoxy composite, whereby higher ADf is observed for the manufacturing of these composites compared to neat PLA and GF/PP. The higher GWP and ADf associated with the manufacturing of BC- and CNF-reinforced epoxy composites suggest that nanocellulose-reinforced polymer composites might not be environmental friendlier than commercially available bio-derived polymer, such as PLA or engineering materials, such as GF/PP composites.

[‡] Value given by NatureWorks on its website: http://www.natureworksllc.com/

Table 13: Detailed impacts associated with the production of the BC- and CNF-reinforced epoxy composites.

Consumables used	GWP (kg CO_2 eq/f.u.)	ADf (MJ/f.u.)
Resin feed tube	0.07	1.96
Porous medium	1.30	33.66
Sealants	0.41	11.38
Vacuum bag	0.55	6.29
Consumables end-of-life	0.30	-4.48

From Figure 26, it can be seen that one of the major contributors to the environment is the manufacturing of BC- and CNF-reinforced epoxy composites based on the VARI. This is due to the consumables used in the manufacturing processes, many of which are not eco-friendly. Table 13 further shows the contributions of the consumables used in the VARI process to the environment. These consumables constitute to approximately 24% and 45% of the total ADf associated with the VARI process of BC- and CNF-reinforced epoxy composites, respectively. The production of the porous flow medium used in the VARI, for example, has almost as high ADf as the production of the epoxy resin used. Overall, it is the use of fibrous networks that limits the manufacturing method choices and is thus accountable for these impacts. Furthermore, it can also be seen from Figure 26 that the GWP and ADf for the production of BC- and CNF-reinforced epoxy composites stems from the production of the reinforcing phase, i.e. the production of CNF from wood pulp and the biosynthesis of BC from low molecular weight sugar. It should also be noted that the equivalent mass of glass fibres, CNF and BC considered in this chapter are different (see Table 12).

Therefore, the higher GWP and ADf for the production of CNF can be attributed to the larger amount of CNF required to reinforce the epoxy matrix (versus the amount of GF required in the PP). Nonetheless, it is clear that the production process of BC is much more energy intensive, leading to higher ADf compared to the production of CNF and GF, even when the differences in the mass of CNF and GF are considered. This is due to the energy required to produce the chemicals used for the HS medium.

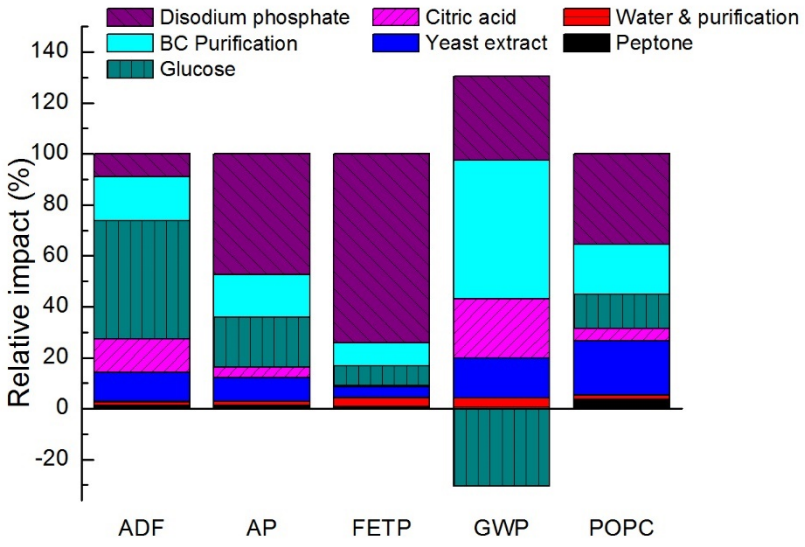

Figure 27: Detailed hot spot analysis of the production of bacterial cellulose

To further elucidate this, a detailed hot spot analysis of the relative environmental impacts associated with the synthesis of BC is shown Figure 27. The production of the glucose used for the HS medium (4.08 kg per functional unit) contributes 61 MJ in the ADf category. This accounts for half of the ADf in the production of 0.653 kg of BC (131 MJ) and accounts for 25% of the ADf in production of 1.17 kg of BC-reinforced epoxy composites (272 MJ). Nevertheless, the production of glucose also provides an environmental credit in the GWP indicator as glucose is produced from starch, which is

in turn obtained from corn cultivation where carbon dioxide can be sequestered. In addition to this, the use of disodium phosphate in HS medium is also a major contributor to the acidification potential and freshwater ecotoxicity potential of the BC-reinforced epoxy composite (see appendix C for detailed breakdown in every impact indicator) accounting for respectively 21% and 37% of these impacts. The environmental burden associated with BC production also originates from the purification of BC after culturing in HS medium. The cultured BC pellicles have to be washed and purified to remove any chemicals and bacteria used in HS medium as highly purified BC pellicles possess better thermal stability, thermo-mechanical and mechanical properties [115–117]. The LCA model results show that this purification step, equivalent to 2.6 kg CO_2 eq, contributes 54% and 19% of the GWP of the BC production (see Figure 27) and the BC-reinforced epoxy composite manufacturing respectively. In terms of ADf, the 22.7 MJ required for the purification corresponds to 17% of the BC production.

6.4.2 Cradle-to-grave analysis

A major contributor to the life cycle global warming potential is the use phase associated with the composite automotive part [118,119]. The heavier the part, the higher the fuel consumption allocated to the part and thus, more exhaust gas is produced. As aforementioned, the motivation of using nanocellulose as reinforcement for polymers is the possibility of exploiting the high tensile stiffness and strength of cellulose crystals [120], thereby producing high performance lightweight structures, reducing fuel consumption of the vehicle. The GWP and ADf associated with the manufacturing, use phase and end of life of PLA and the other composites in the cradle-to-grave scenario is shown in Figure 27.

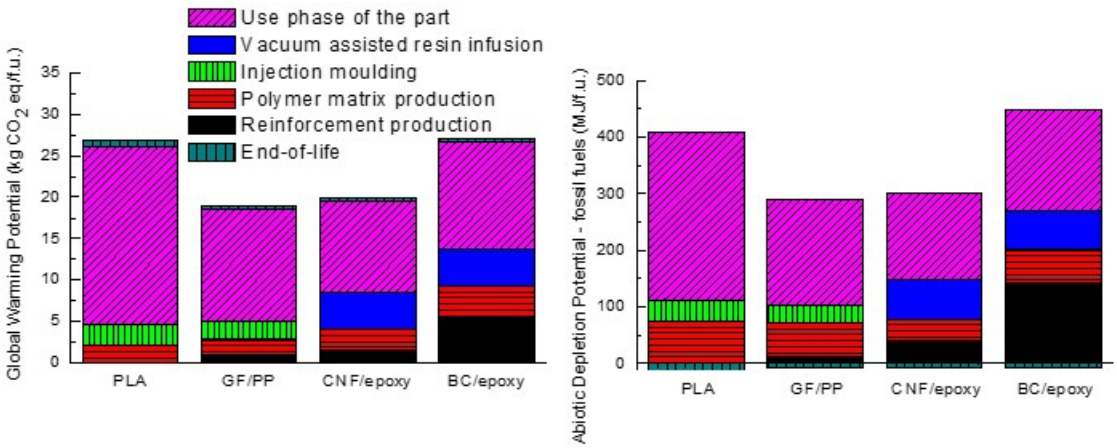

Figure 28: GWP and ADf (from cradle-to-grave) of the two benchmark materials and two nanocellulose-reinforced composites.

Contrary to the cradle-to-gate results, which show that the environmental burden associated with the manufacturing of BC- and CNF-reinforced epoxy composites are higher compared to the production of GF/PP and neat PLA, the cradle-to-grave LCA showed otherwise. When the use phase of the polymer/composite parts is considered, neat PLA contributes the highest cradle-to-grave GWP and ADf. On the other hand, GF/PP composites contribute the lowest cradle-to-grave GWP and ADf compared to the neat PLA. This can be attributed to the differences in the mass required between the two materials to reach the same performance (see Table 12). Conversely, even though the equivalent mass of GF/PP is higher than that of BC- and CNF-reinforced epoxy composites, the GWP and ADf for the manufacturing of GF/PP composites are lower than that of the nanocellulose-reinforced epoxy composites, leading to lower cradle-to-grave GWP and ADf compared to the nanocellulose-reinforced epoxy composites. This LCA model suggests that whilst the manufacturing of nanocellulose-reinforced epoxy

composites might not be as environmentally friendly as neat PLA and GF/PP, the "green credentials" of nanocellulose-reinforced epoxy composites are comparable to that of neat PLA and GF/PP composites when the use phase and end-of-life of the composites were considered.

A recent study by Pietrini et al. [121] showed that the non-renewable energy use for the manufacturing of nanoclay-reinforced polymer composites was a function of the tensile modulus of the nanocomposites. Lee et al. [4] have also recently showed that the tensile modulus ($E_{\text{nanocomposite}}$) of cellulose nanopaper-reinforced polymer composites can be predicted using simple rule-of-mixture (equation 2.1). In order to identify the v_f at which BC- and CNF-reinforced epoxy composites will perform environmentally better compared to neat PLA and GF/PP, the cradle-to-grave GWP and ADf of BC- and CNF-reinforced epoxy composites as a function of v_f was plotted using $E_{\text{composites}}$ calculated[§] from equation 2.1 (see Figure 29). As a comparison, the cradle-to-grave GWP of and ADf for neat PLA and 30 wt.-% randomly oriented GF/PP composites are also shown on the same figure. The dotted line shown in Figure 29 represents an imaginary state whereby cellulose nanopapers can be used to reinforce polymer matrices at such extreme loadings. It should be mentioned than while reaching v_f > 60 vol.-% is possible, it is extremely difficult because of the high density and low permeability of nanopapers. Such loading fractions will lead to longer resin impregnation times that will increase in return the environmental impact of the composite. Nevertheless, the analysis of the results showed that with increasing v_f, whereby the production of both CNF and BC will place

[§] The input parameters for equation 4 are E_{matrix} = 3.0 ± 0.1 GPa, $E_{\text{f, BC nanopaper}}$ = 12.0 ± 1.1 GPa and $E_{\text{f, CNF nanopaper}}$ = 12.8 ± 1.4 GPa, respectively.

heavier environmental burden, the cradle-to-grave GWP and ADf decrease. This is due to the increase of the tensile moduli of BC- and CNF-reinforced epoxy composites, thereby lowering the amount of materials required to comply with the functional unit and reducing the impacts of the use phase significantly. Whilst both the cradle-to-grave GWP and ADf for BC- and CNF-reinforced epoxy composites can be lower than that of neat PLA when v_f > 60 vol.-%, both the cradle-to-grave impacts of BC-reinforced epoxy composites are always higher than the cradle-to-grave impacts of GF/PP, even at high BC loadings. This can be attributed to the production of BC, whereby the heavy environmental burden associated with the production of BC is not offset by the weight reduction of BC-reinforced epoxy composite.

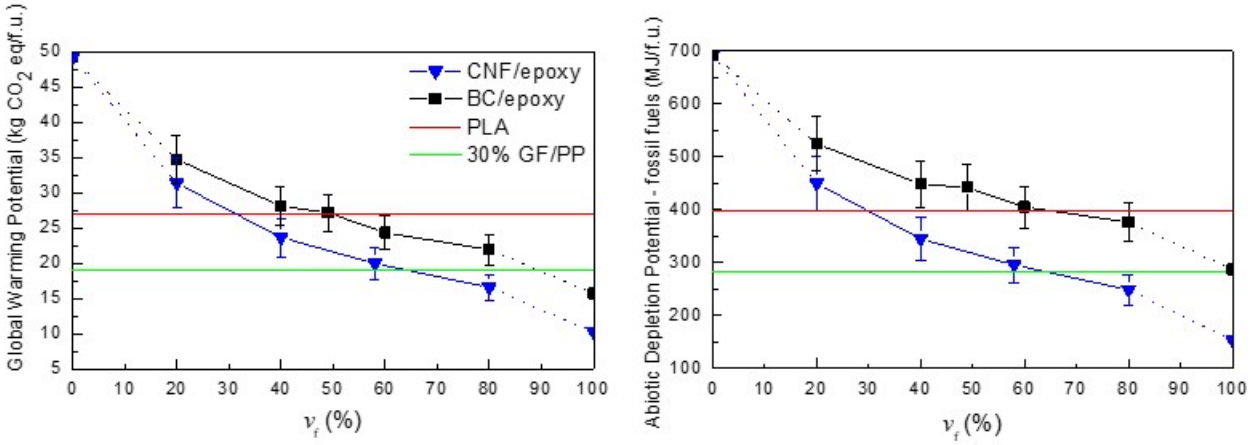

Figure 29: GWP and ADf of the nanocellulose-reinforced polymer composites for different nanocellulose loading. The dotted lines represent the hypothetical cases of a neat epoxy, BC or CNF part.

It is worth noting that the modulus of the nanocellulose sheets considered here match expectations when considering the lowest tensile modulus (around 30 GPa) predictions for nanocellulose fibres [122]. However, succeeding in producing nanocellulose

networks that fully utilise the tensile properties of cellulose crystals could lead to higher properties. Hence, more research should be conducted on improving the manufacturing of nanocellulose sheets.

7 Concluding remarks

7.1 Sample geometry dependency on the measured tensile properties of cellulose nanopapers

In chapter 3, the influence of test specimen geometries on the measured tensile properties of CNF and BC nanopapers was studied. Overall, the tensile moduli (E) and strengths (σ) of CNF nanopapers were found to be higher than that of BC nanopapers (CNF nanopaper: E = 16.1-14.5 GPa, σ = 182-157 MPa and BC nanopaper: E = 15.2-13.4 GPa, σ = 149-120 MPa). This is attributed to the lower porosity of CNF nanopaper (~10%) compared to BC nanopapers (~30%) manufactured in this work. The tensile moduli (calculated from the strain of the test specimens determined from a non-contact video extensometer) of both CNF and BC nanopapers were not strongly dependent on the geometry of the tensile test specimen used. However, if test specimen strain was calculated from the crosshead displacement of the test machine divided by the initial gauge length of the test specimen, the tensile moduli was found to be consistantly lower than that determined from the non-contact video extensometer. This difference is a result of the compliance of the test equipment and emphasises the importance of using an independent strain measurment when performing tensile testing of cellulose nanopapers.

The measured tensile strength of cellulose nanopapers was the highest when the test was conducted on miniaturised dog bone test specimens with 2 mm (CNF nanopaper: σ = 182 MPa, BC nanopaper: σ = 149 MPa). The measured tensile strength of CNF and BC nanopapers decreased by 20% when the tensile test specimen width increased to 15 mm. This is due to wider test specimens being more prone to defects or flaws. CNF nanopapers was also found to possess higher Poisson's ratio compared to BC nanopapers (~0.3 for CNF nanopapers vs ~0.1 for BC nanopapers). This is a result of the lower

porosity of CNF nanopapers compared to BC nanopapers. Furthermore, it was observed that the Poisson's ratio of CNF and BC nanopapers was independent of test specimen geometries used. Fracture resistance of single edge notched cellulose nanopapers were conducted. CNF nanopaper possessed higher critical stress intensity factor (K_{1c}) compared to BC nanopapers (CNF nanopaper: K_{1c} = 7.3 MPa $m^{1/2}$, BC nanopaper: K_{1c} = 6.6 MPa $m^{1/2}$). CNF nanopapers fractured catastrophically when peak force was achieved. The crack on single edge notched BC nanopapers, on the other hand, propagated for ~20 s before catastrophic fracture. This is due to inhomogeneity in the aeral density of BC across the through thickness of the BC nanopapers.

7.2 Low grammage BC nanopaper-reinforced PLLA laminated composites

In chapter 4, low grammage BC nanopapers were manufactured and used as reinforcing phase in BC nanopaper / PLLA composite laminates. It was found a 5 g m^{-2} BC nanopaper was 3 times faster to filter than a 50 g m^{-2} nanopaper and was fully dried before the hot-pressing/consolidation step. Due to the slower drying of higher grammage nanopapers, fibre movement occurred under 1 t pressure leading to better packing while fibre movement could only occur under 10 kg (before the wet cake was fully dry) pressure which lead to high porosities. The porosity of the neat BC nanopapers increased from 48% to 78% for the 50 g m^{-2} and 5 g m^{-2} nanopapers, respectively, due to the slower drying of higher grammage nanopapers which allowed fibre movement under 1 t pressure. The tensile modulus and strength of the 50 g m^{-2} nanopapers was found to be 11.8 GPa and 111 MPa, respectively. Both properties decreased roughly linearly with decreasing grammage with the 5 g m^{-2} BC nanopaper possessing a tensile modulus and strength of 2.4 GPa and 31 MPa, respectively. This was ascribed to the lower coverage $\bar{c}$

of the lower grammage nanopapers which translates in lower stress transfer efficiency between fibres.

Laminated composites containing 10, 5, 2 and 1 layer(s) of 5, 10, 25 and 50 g m^{-2} nanopapers were fabricated. The 4 produced composites possessed comparable tensile properties with a tensile modulus and strength around 10 GPa and 100 MPa, respectively. It is postulated that measured properties of the composites remained the same because of similar porosities of the composite despite large variations of porosities between different nanopaper grammages. SEM images of the fractures composites revealed a layered structure with no or little impregnation occurring.

7.3 Mechanical response of multi-layer BC nanopaper-reinforced PLLA composite laminates

In chapter 5, the mechanical response of BC nanopaper-reinforced PLLA laminated composites as a function of number of sheets of reinforcing BC nanopaper was studied. It was found that by scaling up the number of reinforcing BC nanopapers from 1 sheet to 12 sheets, the porosity of the resulting BC nanopaper-reinforced PLLA laminated composites increased from 17% (laminated composites reinforced with 1 sheet of BC nanopaper) to ~30% (laminated composites reinforced with 12 sheets of BC nanopapers). The tensile moduli of the laminated composites were found to be ~12.4 – 13.6 GPa (at $v_{f,BC}$ = 65 – 72 vol.-%), insensitive to the number of sheets of reinforcing BC nanopaper in the laminated composites. However, the tensile strength of the laminated composites decreased by up to 25% from 121 MPa for PLLA laminated composites reinforced with 1 and 3 sheets of BC nanopaper(s) to only 95 MPa for laminated composites reinforced with 12 sheets of BC nanopapers. Fractographic

analysis also showed that laminated composites reinforced with more than ≥ 3 sheets of BC nanopapers exhibited an extensive fracture of the test specimens while composites reinforced with only 1 sheet of BC nanopaper showed a localised fracture.

These observations were attributed to the presence of scale-induced defects as the number of sheets of reinforcing BC nanopapers increases. As the number of sheets of reinforcing BC nanopaper increased, it was also observed that the presence and severity of these defects increased. Three types of defects have been observed in the BC nanopaper-PLLA laminated composites; (i) thickness inhomogeneity and out-of-plane waviness of BC nanopaper(s) in the laminated composites, which is a result of the formation of aggregates/bundles in the starting BC-in-water suspension prior to nanopaper manufacturing, (ii) voids between adjacent layers of BC nanopapers, which originated from air bubbles trapped during the lay-up of large number of sheets of BC nanopapers and difficulties in removing them as the lay-up was too thick, and (iii) micro-cracks within the BC nanopapers, which is attributed to the formation of residual stress during the drying of BC nanopapers. The presence and severity of these micro-cracks in the BC nanopapers were hypothesised to be accentuated during the consolidation step to produce PLLA laminated composites reinforced with multi-layers of BC nanopapers.

7.4 LCA of nanocellulose-reinforced polymer composites

In chapter 6, a cradle-to-grave LCA of BC- and CNF-reinforced epoxy composites was performed to evaluate their environmental impacts starting from the production of CNF or BC to the end-of-life of the nanocellulose-reinforced epoxy composites. Neat PLA and 30% randomly oriented GF/PP were used as benchmark materials for comparison. To compare the environmental performance of materials with

different mechanical performance, specific tensile moduli of the materials were used to evaluate the equivalent mass of the material required to achieve the same uniaxial tensile load.

For the manufacturing phase, this study showed that amongst the four materials compared, BC- and CNF-reinforced epoxy composites have higher GWP (13.8 kg CO_2 eq for BC-reinforced epoxy and 8.6 kg CO_2 eq for CNF-reinforced epoxy) and ADf (271.6 MJ for BC-reinforced epoxy and 149.6 MJ for CNF-reinforced epoxy) compared to neat PLA and GF/PP even though the specific tensile moduli of the nanocellulose-reinforced epoxy composites are higher than neat PLA and GF/PP, implying that smaller equivalent mass for nanocellulose-reinforce epoxy composites is required. In addition to the production of CNF from Kraft pulp (0.76 kg CO_2 eq and 28 MJ) and the biosynthesis of BC (4.8 kg CO_2 eq and 131 MJ), the composite manufacturing process, whereby numerous environmental unfriendly consumables are required for VARI, also contributes to the poor environmental performance of nanocellulose-reinforced epoxy composites.

When the use phase and end-of-life of the nanocellulose-reinforced epoxy composites were taken into account, it was found that neat PLA contributes to a high cradle-to-grave GWP (26.9 kg CO_2 eq) and ADf (398 MJ). GF/PP composites has the lowest cradle-to-grave GWP (18.9 kg CO_2 eq) and ADf (283.5 MJ) compared to the neat PLA. This can be attributed to the differences in the equivalent mass required between the two materials. This LCA model further showed that when the use phase and the end-of-life of nanocellulose-reinforced epoxy composites were considered, the "green credentials" of nanocellulose-reinforced epoxy composites are comparable to that of neat PLA and GF/PP composites. Life cycle scenario analysis also showed that both the

cradle-to-grave GWP and ADf of BC- and CNF-reinforced epoxy composites can be lower than that of neat PLA when v_f > 60 vol.-%, indicating that high nanocellulose loading fraction of composites is desired to produce materials with "greener credentials" than neat PLA.

However, the GWP and ADf of BC-reinforced epoxy composites were found to be always higher than that of GF/PP, even at high BC loadings. This can be attributed to the production of BC, whereby the heavy environmental burden associated with the production of BC is not offset by the weight reduction of BC-reinforced epoxy composite. To produce "truly green" nanocellulose-reinforced polymer composites, it is therefore desirable to reduce the energy necessary to produce CNF, synthesise BC at much higher yields and employ composite manufacturing processes with lower environmental impact.

8 Future work

The work conducted in this thesis opens new path of research to further improve the use of cellulose nanopapers as polymer reinforcement.

8.1 On cellulose nanopapers

The use of a wet-end additives (cationic starch), like in the paper industry, was investigated as part of this PhD. The work showed promising results with important increase in tensile properties of both BC and CNF nanopapers. Further work remains to be done to understand why this is the case. Another simple step should be the optimisation of the amount and nature of the additive(s). Korhonen et al. [123] for example demonstrated that a combination of cationic starch and polyacrylamide (PAM) was the most effective to increase paper strength. The method of addition can also be investigated. In the preliminary work previously mentioned, the starch was cooked "manually" and added in the suspension. However, industrially, it is added by spraying after jet-cooking which could lead to higher increase in tensile properties of the nanopapers.

Chapter 4 also briefly identifies dewatering as one of the major area where progress can be made for the production of cellulose nanopapers. In the present thesis, only filtration under vacuum was used to produce nanopapers but this technique has limitations, e.g. the necessity for vacuum that is both complex and energy intensive. Other nanopaper manufacturing process have already been used to quicken nanopaper making [62,75] but progress remains to be done, particularly for industrial scaling.

8.2 On cellulose nanopaper-reinforced polymer composites

It was observed that cellulose nanopapers retained the pattern of the filtration membrane that was used to manufacture them. For example, the weaved pattern of a nylon cloth can be imprinted on the nanopaper as seen in Figure 30. This capacity of the cellulose nanopaper to possess a shaped surface opens many new possibilities. The simple creation of a surface roughness could favour adhesion with a polymer and thus increase the mechanical properties of a laminated composite.

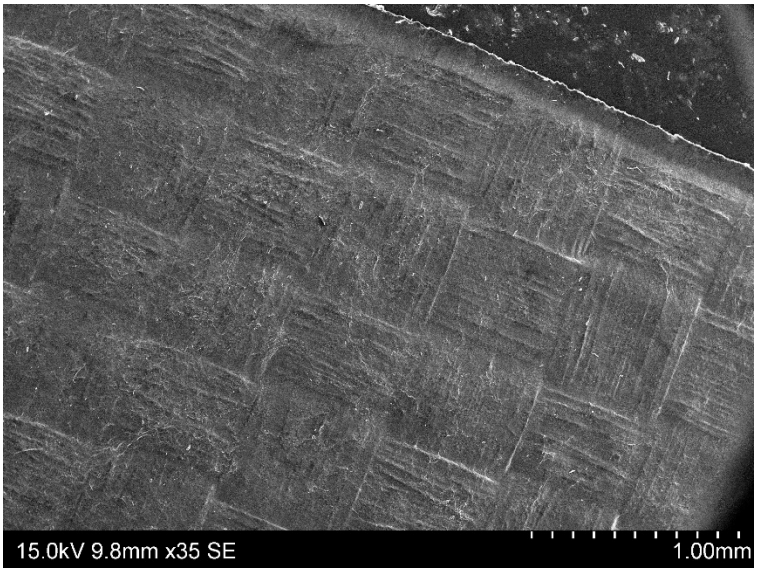

Figure 30: Weaved pattern of a nylon cloth imprinted on a cellulose nanopaper

The creation of a specific pattern could also have potential to be used in microfluidics for medical applications. The ability of nanocellulose to be shaped on a substrate and the work of Beneventi et al. also demonstrate the existing possibility of producing a 3D shaped cellulose nanopaper already adopting a finalised product form [75].

In many studies, cellulose nanopapers are used as relatively cheap and environmental friendly substrate material [19,124]. However, the claims of inexpensiveness are not verified and are often claimed based on the origin (wood) of the

nanocellulose. An exhaustive cost study could reveal these claims to be false due to each application requiring different complex manufacturing processes. Similarly, the environmental friendly credits given to the cellulose nanopapers as a substrate should be investigated. The end-of-life of cellulose nanopapers and their composites also needs to be examined in detail as some questions are left unanswered. It is for example not known how long would a cellulose nanopaper-reinforced composite need to fully biodegrade and in which conditions. We also need to acquire knowledge on the possibilities and advantages of recycling these materials as opposed to recovering energy when incinerating them.

The optimisation of cellulose nanopaper-reinforced polymer composites should be continued bearing in mind real applications. This is to better target groups of features such composites must possess in order to become valid and replace current materials. The literature review in this work revealed the possibility to produce transparent cellulose nanopaper-reinforced polymer composites [24,25,35]. Transparent polymers such as polymethyl methacrylate and polycarbonate are often used in impact resistance applications. Their reinforcement with nanocellulose could help increase their energy dissipation ability (due to the high specific surface area of nanocellulose) while maintaining their transparency.

References

[1] S.J. Eichhorn, C. Baillie, N. Zafeiropoulos, L.Y. Mwaikambo, M.P. Ansell, A. Dufresne, K.M. Entwistle, P.J. Herrera-Franco, G.C. Escamilla, L. Groom, M. Hughes, C. Hill, T.G. Rials, P.. Wild, Review: Current international research into cellulosic fibres and composites, Journal of Materials Science. 36 (2001) 2107–2131.

[2] Y.C. Hsieh, H. Yano, M. Nogi, S.J. Eichhorn, An estimation of the Young's modulus of bacterial cellulose filaments, Cellulose. 15 (2008) 507–513.

[3] I. Sakurada, Y. Nukushina, T. Ito, Experimental determination of elastic modulus of crystalline regions in oriented polymers, J Polym Sci. 57 (1962) 651–660.

[4] M. Matsuo, C. Sawatari, Y. Iwai, F. Ozaki, Effect of orientation distribution and crystallinity on the measurement by X-ray-diffraction of the crystal-lattice moduli of cellulose-I and cellulose-II, Macromolecules. 23 (1990) 3266–3275.

[5] R. Rusli, S.J. Eichhorn, Determination of the stiffness of cellulose nanowhiskers and the fiber-matrix interface in a nanocomposite using Raman spectroscopy, Appl Phys Lett. 93 (2008).

[6] S.A. Wainwright, W.D. Biggs, J.D. Currey, J.M. Gosline, Mechanical design in organisms, Princeton University Press, 1982.

[7] T. Saito, R. Kuramae, J. Wohlert, L.A. Berglund, A. Isogai, An ultrastrong nanofibrillar biomaterial: the strength of single cellulose nanofibrils revealed via sonication-induced fragmentation, Biomacromolecules. 14 (2013) 248–253.

[8] K. Wuhrmann, A. Heuberger, K. Mühlethaler, Elektronenmikroskopische Untersuchungen an Zellulosefasern nach Behandlung mit Ultraschall., Experientia. 2 (1946) 105–107.

[9] T. Taniguchi, K. Okamura, New films produced from microfibrillated natural fibres, Polym Int. 47 (1998) 291–294.

[10] P. Lahtinen, S. Liukkonen, J. Pere, A. Sneck, H. Kangas, A comparative study of fibrillated fibers from different mechanical and chemical pulps, BioResources. 9 (2014) 2115–2127.

[11] F.W. Herrick, R.L. Casebier, J.K. Hamilton, K.R. Sandberg, Microfibrillated cellulose: morphology and accessibility, in: A. Sarko (Ed.), Wiley, 1983: pp. 797–813.

[12] A.F. Turbak, F.W. Snyder, K.R. Sandberg, Microfibrillated cellulose, a new cellulose product: properties, uses, and commercial potential, Applied Polymer Symposium. 37 (1983) 815–827.

[13] K.Y. Lee, G. Buldum, A. Mantalaris, A. Bismarck, More than meets the eye in bacterial cellulose: biosynthesis, bioprocessing, and applications in advanced fiber composites, Macromol Biosci. 14 (2014) 10–32.

[14] D. Klemm, F. Kramer, S. Moritz, T. Lindstrom, M. Ankerfors, D. Gray, A. Dorris, Nanocelluloses: a new family of nature-based materials, Angew. Chem. Int. Ed. Engl. 50 (2011) 5438–5466.

[15] K.-Y. Lee, Y. Aitomäki, L.A. Berglund, K. Oksman, A. Bismarck, On the use of nanocellulose as reinforcement in polymer matrix composites, Composites Science and Technology. 105 (2014) 15–27.

[16] M. Henriksson, L.A. Berglund, P. Isaksson, T. Lindström, T. Nishino, Cellulose nanopaper structures of high toughness, Biomacromolecules. 9 (2008) 1579–1585.

[17] A.W. Carpenter, C.-F. de Lannoy, M.R. Wiesner, Cellulose nanomaterials in water treatment technologies, Environ. Sci. Technol. 49 (2015) 5277–5287.

[18] C. Aulin, M. Gallstedt, T. Lindstrom, Oxygen and oil barrier properties of microfibrillated cellulose films and coatings, Cellulose. 17 (2010) 559–574.

[19] T. Hassinen, A. Alastalo, K. Eiroma, T.-M. Tenhunen, V. Kunnari, T. Kaljunen, U. Forsström, T. Tammelin, All-printed transistors on nano cellulose substrate, MRS Advances. 1 (2016) 645–650.

[20] A. Boldizar, C. Klason, J. Kubat, P. Naslund, P. Saha, Prehydrolyzed cellulose as reinforcing filler for thermoplastics, International Journal of Polymeric Materials. 11 (1987) 229–262.

[21] H. Yano, J. Sugiyama, A.N. Nakagaito, M. Nogi, T. Matsuura, M. Hikita, K. Handa, Optically Transparent Composites Reinforced with Networks of Bacterial Nanofibers, Adv. Mater. 17 (2005) 153–155.

[22] F. Quero, M. Nogi, H. Yano, K. Abdulsalami, S.M. Holmes, B.H. Sakakini, S.J. Eichhorn, Optimization of the mechanical performance of bacterial cellulose/poly(L-lactic) acid composites, ACS Applied Materials & Interfaces. 2 (2010) 321–330.

[23] T. Montrikittiphant, M. Tang, K.Y. Lee, C.K. Williams, A. Bismarck, Bacterial cellulose nanopaper as reinforcement for polylactide composites: renewable thermoplastic nanopapreg, Macromolecular Rapid Communications. 35 (2014) 1640–1645.

[24] S. Kunjalukkal Padmanabhan, C. Esposito Corcione, R. Nisi, A. Maffezzoli, A. Licciulli, PolyDiethyleneglycol–bisallyl carbonate matrix transparent nanocomposites reinforced with bacterial cellulose microfibrils, European Polymer Journal. 93 (2017) 192–199.

[25] E.R.P. Pinto, H.S. Barud, R.R. Silva, M. Palmieri, W.L. Polito, V.L. Calil, M. Cremona, S.J.L. Ribeiro, Y. Messaddeq, Transparent composites prepared from bacterial cellulose and castor oil based polyurethane as substrates for flexible OLEDs, J. Mater. Chem. C. 3 (2015) 11581–11588.

[26] J. Juntaro, S. Ummartyotin, M. Sain, H. Manuspiya, Bacterial cellulose reinforced polyurethane-based resin nanocomposite: A study of how ethanol and processing pressure affect physical, mechanical and dielectric properties, Carbohydrate Polymers. 87 (2012) 2464–2469.

[27] B. Wang, D. Li, Strong and optically transparent biocomposites reinforced with cellulose nanofibers isolated from peanut shell, Composites Part A: Applied Science and Manufacturing. (2015).

[28] S. Iwamoto, A.N. Nakagaito, H. Yano, Nano-fibrillation of pulp fibers for the processing of transparent nanocomposites, Applied Physics a-Materials Science & Processing. 89 (2007) 461–466.

[29] M. Henriksson, L.A. Berglund, Structure and properties of cellulose nanocomposite films containing melamine formaldehyde, J. Appl. Polym. Sci. 106 (2007) 2817–2824.

[30] P.-Y. Kuo, L. de A. Barros, N. Yan, M. Sain, Y. Qing, Y. Wu, Nanocellulose Composites with Enhanced Interfacial Compatibility and Mechanical Properties Using a Hybrid-Toughened Epoxy Matrix, Carbohydrate Polymers. (2017).

[31] Y. Aitomäki, S. Moreno-Rodriguez, T.S. Lundström, K. Oksman, Vacuum infusion of cellulose nanofibre network composites: Influence of porosity on permeability and impregnation, Materials & Design. 95 (2016) 204–211.

[32] A. Mautner, J. Lucenius, M. Österberg, A. Bismarck, Multi-layer nanopaper based composites, Cellulose. (2017) 1–15.

[33] K.-Y. Lee, T. Tammelin, K. Schulfter, H. Kiiskinen, J. Samela, A. Bismarck, High performance cellulose nanocomposites: comparing the reinforcing ability of bacterial cellulose and nanofibrillated cellulose, ACS Appl. Mater. Interfaces. 4 (2012) 4078–86.

[34] A.N. Nakagaito, S. Iwamoto, H. Yano, Bacterial cellulose: the ultimate nano-scalar cellulose morphology for the production of high-strength composites, Applied Physics a-Materials Science & Processing. 80 (2005) 93–97.

[35] H. Yano, J. Sugiyama, A.N. Nakagaito, M. Nogi, T. Matsuura, M. Hikita, K. Handa, Optically transparent composites reinforced with networks of bacterial nanofibers, Adv Mater. 17 (2005) 153–155.

[36] F. Quero, M. Nogi, H. Yano, K. Abdulsalami, S.M. Holmes, B.H. Sakakini, S.J. Eichhorn, Optimization of the Mechanical Performance of Bacterial Cellulose/Poly(l-lactic) Acid Composites, ACS Appl. Mater. Interfaces. 2 (2010) 321–330.

[37] H. Baumann, A.-M. Tillman, The Hitch Hiker's guide to LCA. An orientation in life cycle assessment methodlogy and application, USA, 2004.

[38] R. Clift, A. Doig, G. Finnveden, The application of Life Cycle Assessment to Integrated Solid Waste Management - Part 1 - Methodology, Process Saf Environ. 78 (2000) 279–287.

[39] M.F. Ashby, Materials Selection in Mechanical Design, Third Edition, Elsevier Butterworth-Heinemann, Burlington, 2005.

[40] C.L. Simoes, S.M. Xara, C.A. Bernardo, Influence of the impact assessment method on the conclusions of a LCA study. Application to the case of a part made with virgin and recycled HDPE, Waste Manag Res. 29 (2011) 1018–1026.

[41] D. Lazarevic, E. Aoustin, N. Buclet, N. Brandt, Plastic waste management in the context of a European recycling society: Comparing results and uncertainties in a life cycle perspective, Resources, Conservation and Recycling. 55 (2010) 246–259.

[42] A. Azapagic, Sustainable chemical engineering, Green Chem. 6 (2004) 394–394.

[43] K.L. Spence, R.A. Venditti, O.J. Rojas, Y. Habibi, J.J. Pawlak, A comparative study of energy consumption and physical properties of microfibrillated cellulose produced by different processing methods, Cellulose. 18 (2011) 1097–1111.

[44] S. Josset, P. Orsolini, G. Siqueira, A. Tejado, P. Tingaut, T. Zimmermann, Energy consumption of the nanofibrillation of bleached pulp, wheat straw and recycled newspaper through a grinding process, Nordic Pulp & Paper Research Journal. 29 (2014) 167–175.

[45] H. Lee, S. Mani, Mechanical pretreatment of cellulose pulp to produce cellulose nanofibrils using a dry grinding method, Ind. Crop. Prod. 104 (2017) 179–187.

[46] Q. Li, S. McGinnis, C. Sydnor, A. Wong, S. Renneckar, Nanocellulose Life Cycle Assessment, ACS Sustainable Chemistry & Engineering. 1 (2013) 919–928.

[47] F. Piccinno, R. Hischier, S. Seeger, C. Som, Life Cycle Assessment of a New Technology To Extract, Functionalize and Orient Cellulose Nanofibers from Food Waste, ACS Sustainable Chem. Eng. 3 (2015) 1047–1055.

[48] R. Arvidsson, D. Nguyen, M. Svanström, Life cycle assessment of cellulose nanofibrils production by mechanical treatment and two different pretreatment processes, Environ. Sci. Technol. 49 (2015) 6881–6890.

[49] C. Hohenthal, M. Ovaskainen, D. Bussini, P. Sadocco, T. Pajula, H. Lehtinen, J. Kautto, K. Salmenkivi, Final Assessment of Nano Enhanced New Products, SUNPAP, 2012.

[50] E.T.H. Vink, S. Davies, J. Kolstad, The eco-profile for current Ingeo polylactide production, Industrial Biotechnology. (2010) 212–224.

[51] S. Yamanaka, K. Watanabe, N. Kitamura, M. Iguchi, S. Mitsuhashi, Y. Nishi, M. Uryu, The structure and mechanical properties of sheets prepared from bacterial cellulose, Journal of Materials Science. 24 (1989) 3141–3145.

[52] A.N. Nakagaito, S. Iwamoto, H. Yano, Bacterial cellulose: the ultimate nano-scalar cellulose morphology for the production of high-strength composites, Appl Phys A. 80 (2005) 93–97.

[53] H. Yousefi, M. Faezipour, S. Hedjazi, M.M. Mousavi, Y. Azusa, A.H. Heidari, Comparative study of paper and nanopaper properties prepared from bacterial cellulose nanofibers and fibers/ground cellulose nanofibers of canola straw, Industrial Crops and Products. 43 (2013) 732–737.

[54] S. Gea, F.G. Torres, O.P. Troncoso, C.T. Reynolds, F. Vilasecca, M. Iguchi, T. Peijs, Biocomposites based on bacterial cellulose and apple and radish pulp, IPP. 22 (2007) 497–501.

[55] N. Butchosa, C. Brown, P.T. Larsson, L.A. Berglund, V. Bulone, Q. Zhou, Nanocomposites of bacterial cellulose nanofibers and chitin nanocrystals: fabrication, characterization and bactericidal activity, Green Chem. 15 (2013) 3404–3413.

[56] M. Iguchi, S. Yamanaka, A. Budhiono, Bacterial cellulose—a masterpiece of nature's arts, Journal of Materials Science. 35 (2000) 261–270.

[57] L. Rozenberga, M. Skute, L. Belkova, I. Sable, L. Vikele, P. Semjonovs, M. Saka, M. Ruklisha, L. Paegle, Characterisation of films and nanopaper obtained from cellulose synthesised by acetic acid bacteria, Carbohydrate Polymers. 144 (2016) 33–40.

[58] H. Shim, M. Karina, R. Yudianti, L. Indrarti, J. Azuma, H. Uyama, One-sided surface modification of bacterial cellulose sheet as 2,3-dialdehyde, Polymer-Plastics Technology and Engineering. 54 (2015) 305–309.

[59] K. Syverud, P. Stenius, Strength and barrier properties of MFC films, Cellulose. 16 (2008) 75–85.

[60] M. Nogi, S. Iwamoto, A.N. Nakagaito, H. Yano, Optically transparent nanofiber paper, Adv Mater. 21 (2009) 1595–1598.

[61] A.J. Svagan, M.A.S. Azizi Samir, L.A. Berglund, Biomimetic polysaccharide nanocomposites of high cellulose content and high toughness, Biomacromolecules. 8 (2007) 2556–2563.

[62] H. Sehaqui, A. Liu, Q. Zhou, L.A. Berglund, Fast preparation procedure for large, flat cellulose and cellulose/inorganic nanopaper structures, Biomacromolecules. 11 (2010) 2195–2198.

[63] H. Sehaqui, Q. Zhou, L.A. Berglund, Nanostructured biocomposites of high toughness—a wood cellulose nanofiber network in ductile hydroxyethylcellulose matrix, Soft Matter. 7 (2011) 7342–7350.

[64] A. Ferrer, I. Filpponen, A. Rodriguez, J. Laine, O.J. Rojas, Valorization of residual Empty Palm Fruit Bunch Fibers (EPFBF) by microfluidization: Production of nanofibrillated cellulose and EPFBF nanopaper, Bioresource Technol. 125 (2012) 249–255.

[65] S.-J. Chun, S.-Y. Lee, G.-H. Doh, S. Lee, J.H. Kim, Preparation of ultrastrength nanopapers using cellulose nanofibrils, Journal of Industrial and Engineering Chemistry. 17 (2011) 521–526.

[66] M.L. Hassan, A.P. Mathew, E.A. Hassan, N.A. El-Wakil, K. Oksman, Nanofibers from bagasse and rice straw: process optimization and properties, Wood Sci Technol. 46 (2010) 193–205.

[67] M. Osterberg, J. Vartiainen, J. Lucenius, U. Hippi, J. Seppala, R. Serimaa, J. Laine, A fast method to produce strong NFC films as a platform for barrier and functional materials, ACS Applied Materials & Interfaces. 5 (2013) 4640–4647.

[68] V. Kumar, R. Bollström, A. Yang, Q. Chen, G. Chen, P. Salminen, D. Bousfield, M. Toivakka, Comparison of nano- and microfibrillated cellulose films, Cellulose. 21 (2014) 3443–3456.

[69] M. Jonoobi, Y. Aitomäki, A.P. Mathew, K. Oksman, Thermoplastic polymer impregnation of cellulose nanofibre networks: Morphology, mechanical and optical properties, Composites Part A-Appl. S. 58 (2014) 30–35.

[70] F. Ansari, S. Galland, M. Johansson, C.J.G. Plummer, L.A. Berglund, Cellulose nanofiber network for moisture stable, strong and ductile biocomposites and increased epoxy curing rate, Composites Part A-Appl. S. 63 (2014) 35–44.

[71] I. Urruzola, E. Robles, L. Serrano, J. Labidi, Nanopaper from almond (Prunus dulcis) shell, Cellulose. 21 (2014) 1619–1629.

[72] N. Amiralian, P.K. Annamalai, P. Memmott, E. Taran, S. Schmidt, D.J. Martin, Easily deconstructed, high aspect ratio cellulose nanofibres from Triodia pungens; an abundant grass of Australia's arid zone, RSC Adv. 5 (2015) 32124–32132.

[73] F. Ansari, M. Skrifvars, L. Berglund, Nanostructured biocomposites based on unsaturated polyester resin and a cellulose nanofiber network, Composites Science and Technology. 117 (2015) 298–306.

[74] H. Yousefi, M. Mashkour, R. Yousefi, Direct solvent nanowelding of cellulose fibers to make all-cellulose nanocomposite, Cellulose. 22 (2015) 1189–1200.

[75] D. Beneventi, E. Zeno, D. Chaussy, Rapid nanopaper production by spray deposition of concentrated microfibrillated cellulose slurries, Industrial Crops and Products. 72 (2015) 200–205.

[76] G. Siqueira, K. Oksman, S.K. Tadokoro, A.P. Mathew, Re-dispersible carrot nanofibers with high mechanical properties and reinforcing capacity for use in composite materials, Composites Science and Technology. 123 (2016) 49–56.

[77] N. Rambabu, S. Panthapulakkal, M. Sain, A.K. Dalai, Production of nanocellulose fibers from pinecone biomass: Evaluation and optimization of chemical and mechanical treatment conditions on mechanical properties of nanocellulose films, Industrial Crops and Products. 83 (2016) 746–754.

[78] Q. Li, W. Chen, Y. Li, X. Guo, S. Song, Q. Wang, Y. Liu, J. Li, H. Yu, J. Zeng, Comparative study of the structure, mechanical and thermomechanical properties of cellulose nanopapers with different thickness, Cellulose. 23 (2016) 1375–1382.

[79] A. Mtibe, L.Z. Linganiso, A.P. Mathew, K. Oksman, M.J. John, R.D. Anandjiwala, A comparative study on properties of micro and nanopapers produced from cellulose and cellulose nanofibres, Carbohydrate Polymers. 118 (2015) 1–8.

[80] P. Orsolini, B. Michen, A. Huch, P. Tingaut, W.R. Caseri, T. Zimmermann, Characterization of pores in dense nanopapers and nanofibrillated cellulose membranes: a critical assessment of established methods, ACS Appl. Mater. Interfaces. 7 (2015) 25884–25897.

[81] W. F Brown Jr., J. E Srawley, Plane strain crack toughness testing of high strength metallic materials., American society for testing and materials, Philadelphia, 1966.

[82] D.H. Page, A theory for the elastic modulus of paper, Br. J. Appl. Phys. 16 (1965) 253–258.

[83] A.M. Freudenthal, Fatigue and fracture mechanics, Institute for the Study of Fatigue, Fracture and Structural Reliability, George Washington Univ., 1972.

[84] G.N. Greaves, A.L. Greer, R.S. Lakes, T. Rouxel, Poisson's ratio and modern materials, Nat Mater. 10 (2011) 823–837.

[85] M. Herráez, A. Fernández, C.S. Lopes, C. González, Strength and toughness of structural fibres for composite material reinforcement, Phil. Trans. R. Soc. A. 374 (2016).

[86] M. Gröndahl, L. Eriksson, P. Gatenholm, Material properties of plasticized hardwood xylanx for potential application as oxygen barrier films, Biomacromolecules. 5 (2004) 1528–1535.

[87] F. Quero, S.J. Eichhorn, M. Nogi, H. Yano, K.-Y. Lee, A. Bismarck, Interfaces in Cross-Linked and Grafted Bacterial Cellulose/Poly(Lactic Acid) Resin Composites, J Polym Environ. 20 (2012) 916–925.

[88] M. Hervy, A. Santmarti, P. Lahtinen, T. Tammelin, K.-Y. Lee, Sample geometry dependency on the measured tensile properties of cellulose nanopapers, Materials & Design. (n.d.).

[89] A. Vainio, H. Paulapuro, Interfiber Bonding and Fiber Segment Aactivation in Paper, BioResources. 2 (2007) 442–458.

[90] W.H. Burgess, Effect of Basis Weight on Tensile Strength, 53 (1970) 1680–1682.

[91] R.S. Seth, J.T. Jantunen, C.S. Moss, The Effect of Grammage on Sheet Properties, Appita. 42 (1989) 42–48.

[92] S.J. I'Anson, W. Sampson, S. Savani, Density Dependent Influence of Grammage on Tensile Properties of Handsheets, Journal of Pulp and Paper Science. 34 (2008) 182–189.

[93] S.J. Eichhorn, W.W. Sampson, Statistical geometry of pores and statistics of porous nanofibrous assemblies, J R Soc Interface. 2 (2005) 309–318.

[94] X. Xu, J. Zhou, L. Jiang, G. Lubineau, T. Ng, B.S. Ooi, H.-Y. Liao, C. Shen, L. Chen, J.Y. Zhu, Highly transparent, low-haze, hybrid cellulose nanopaper as electrodes for flexible electronics, Nanoscale. 8 (2016) 12294–12306.

[95] R. Amacher, J. Cugnoni, J. Botsis, L. Sorensen, W. Smith, C. Dransfeld, Thin ply composites: Experimental characterization and modeling of size-effects, Composites Science and Technology. 101 (2014) 121–132.

[96] H.J. Lehermeier, J.R. Dorgan, Melt rheology of poly(lactic acid): Consequences of blending chain architectures, Polym Eng Sci. 41 (2001) 2172–2184.

[97] M. Östlund, S. Östlund, L. Carlsson, C. Fellers, The influence of drying restraints and beating degree on residual stress build-up in paperboard, Journal of Pulp and Paper Science (JPPS). 30 (2004) 289–293.

[98] T.J. Dodwell, R. Butler, G.W. Hunt, Out-of-plane ply wrinkling defects during consolidation over an external radius, Composites Science and Technology. 105 (2014) 151–159.

[99] M.R. Wisnom, Size effects in the testing of fibre-composite materials, Composites Science and Technology. 59 (1999) 1937–1957.

[100] E.S. Greenhalgh, Failure Analysis and Fractography of Polymer Composites, Woodhead Publishing Ltd, 2009.

[101] W.G. Perkins, Polymer toughness and impact resistance, Polym Eng Sci. 39 (1999) 2445–2460.

[102] K.-Y. Lee, J.J. Blaker, A. Bismarck, Surface functionalisation of bacterial cellulose as the route to produce green polylactide nanocomposites with improved properties, Composites Science and Technology. 69 (2009) 2724–2733.

[103] S. Evangelisti, P. Lettieri, D. Borello, R. Clift, Life cycle assessment of energy from waste via anaerobic digestion: a UK case study, Waste Management. 34 (2014) 226–37.

[104] J. Guinee, Handbook on Life Cycle Assessment - Operational Guide to the ISO Standards, 2002. http://www.springer.com/gp/book/9781402002281 (accessed March 15, 2017).

[105] J.C. Bare, P. Hofstetter, D.W. Pennington, H.A.U. de Haes, Midpoints versus endpoints: The sacrifices and benefits, Int. J. LCA. 5 (2000) 319.

[106] A.V. Marchenko, Thermo-mechanical properties of materials, in: E. of L.S. System (Ed.), Cold Regions Science and Marine Technology, Oxford, UK, 2010.

[107] W. Martienssen, Polymers, in: H. Warlimont (Ed.), Springer Handbook of Condensed Matter and Materials Data, Springer, 2005: pp. 511–512.

[108] S. Hestrin, M. Schramm, Synthesis of Cellulose by Acetobacter-Xylinum .2. Preparation of Freeze-Dried Cells Capable of Polymerizing Glucose to Cellulose, Biochem J. 58 (1954) 345–352.

[109] G. Koronis, A. Silva, M. Fontul, Green composites: A review of adequate materials for automotive applications, Composites Part B: Engineering. 44 (2013) 120–127.

[110] R. Le Borgne, P. Feillard, Analyse du cycle de vie - Application dans l'industrie automobile, (2000).

[111] A. Bignonnet, Approche globale d'allégement des véhicules, Mécanique & Industries. 2 (2001) 173–180.

[112] S. Mudgal, L. Lyons, Plastic Waste In The Environment, European Commission DG ENV, 2011.

[113] How to boost plastics recycling and increase resource efficiency?, Plastic Recyclers Europe, 2012.

[114] J.J. Kolstad, E.T.H. Vink, B. De Wilde, L. Debeer, Assessment of anaerobic degradation of Ingeo™ polylactides under accelerated landfill conditions, Polymer Degradation and Stability. 97 (2012) 1131–1141.

[115] S. Gea, C.T. Reynolds, N. Roohpour, B. Wirjosentono, N. Soykeabkaew, E. Bilotti, T. Peijs, Investigation into the structural, morphological, mechanical and thermal behaviour of bacterial cellulose after a two-step purification process, Bioresource Technol. 102 (2011) 9105–9110.

[116] J. George, K. Ramana, S. Sabapathy, A. Bawa, Physico-mechanical properties of chemically treated bacterial (Acetobacter xylinum) cellulose membrane, World J Microb Biot. 21 (2005) 1323–1327.

[117] J. George, V.A. Sajeevkumar, R. Kumar, K.V. Ramana, S.N. Sabapathy, A.S. Bawa, Enhancement of thermal stability associated with the chemical treatment of

bacterial (Gluconacetobacter xylinus) cellulose, J Appl Polym Sci. 108 (2008) 1845–1851.

[118] A.L. Roes, E. Marsili, E. Nieuwlaar, M.K. Patel, Environmental and Cost Assessment of a Polypropylene Nanocomposite, Journal of Polymers and the Environment. 15 (2007) 212–226.

[119] S.M. Lloyd, L.B. Lave, Life cycle economic and environmental implications of using nanocomposites in automobiles, Environ Sci Technol. 37 (2003) 3458–3466.

[120] S.J. Eichhorn, G.R. Davies, Modelling the crystalline deformation of native and regenerated cellulose, Cellulose. 13 (2006) 291–307.

[121] M. Pietrini, L. Roes, M. Patel, E. Chiellini, Comparative Life Cycle Studies on Poly(3-hydroxybutyrate)-Based Composites as Potential Replacement for Conventional Petrochemical Plastics, Biomacromolecules. 8 (2007) 2210–2218.

[122] S. Tanpichai, F. Quero, M. Nogi, H. Yano, R.J. Young, T. Lindström, W.W. Sampson, S.J. Eichhorn, Effective Young's Modulus of Bacterial and Microfibrillated Cellulose Fibrils in Fibrous Networks, Biomacromolecules. 13 (2012) 1340–1349.

[123] M.H.J. Korhonen, A. Sorvari, T. Saarinen, J. Seppälä, J. Laine, Deflocculation of Cellulosic Suspensions with Anionic High Molecular Weight Polyelectrolytes, BioResources. 9 (2014) 3550–3570.

[124] A. Razaq, L. Nyholm, M. Sjödin, M. Strømme, A. Mihranyan, Paper-Based Energy-Storage Devices Comprising Carbon Fiber-Reinforced Polypyrrole-Cladophora Nanocellulose Composite Electrodes, Adv. Energy Mater. 2 (2012) 445–454.

Appendix A: derivation of the compliance equation

The total elongation (Δl) recorded during tensile test can be expressed as:

$$\Delta l = \Delta l_{\text{test specimen}} + \Delta l_{\text{test equipment}} = \Delta l_{\text{test specimen}} + \frac{\Delta P}{C_s} \quad \text{(S1)}$$

$\Delta l_{\text{test specimen}}$ and $\Delta l_{\text{test equipment}}$ represent the recorded elongation of test tensile test speciment and test equipment, respectively. ΔP and C_s denote the measured load and compliance of the test equipment (Hooke's spring constant).

The tensile modulus (E) of the test specimen be written as:

$$E = \frac{\Delta\sigma}{\Delta\varepsilon} = \frac{\Delta P}{A} \times \frac{l_0}{\Delta l_{\text{test specimen}}} \quad \text{(S2)}$$

$\Delta\sigma$, $\Delta\varepsilon$, l_0 and A are the tensile stress, specimen strain, initial gauge length and cross sectional area of the test specimen, respectively.

Combining equations (S1) and (S2):

$$\frac{1}{\left(\frac{\Delta P}{\Delta l}\right)} = \frac{1}{C_s} + \frac{1}{E} \times \frac{l_o}{A} \quad \text{(S3)}$$

Appendix B: performance indicator and weight variation calculation

In tension:

$$\sigma = \frac{F}{S} \rightarrow E_1 = \frac{\Delta F}{S_1 \Delta \varepsilon} \; or \; S_1 = \frac{\Delta F}{E_1 \Delta \varepsilon_1}$$

Where ε is the elongation ($\varepsilon = \frac{\Delta l}{l}$), F the force (tension applied), S the section of the part and σ and E the tensile strength and modulus, respectively.

$$\rho_1 = \frac{m_1}{S_1 l}$$

$$m_1 = \rho_1 \left(\frac{\Delta F . l}{E_1 . \Delta \varepsilon} \right)$$

$$m_{ref} = \rho_{ref} \left(\frac{\Delta F . l}{E_1 . \Delta \varepsilon} \right)$$

Because the length l, the force and the elongation are constraints:

$$\frac{m_1 - m_{ref}}{m_{ref}} = \frac{\frac{\rho_1}{E_1} - \frac{\rho_{ref}}{E_{ref}}}{\frac{\rho_{ref}}{E_{ref}}}$$

The performance indicator PI is defined as the specific tensile modulus such as:

$$PI = \frac{E}{\rho}$$

Thus:

$$\frac{m_1 - m_{ref}}{m_{ref}} = \frac{\frac{\rho_1}{E_1}}{\frac{\rho_{ref}}{E_{ref}}} - 1 = \frac{\frac{1}{PI_1} - \frac{1}{PI_{ref}}}{\frac{1}{PI_{ref}}} = \left(\frac{1}{PI_1} - \frac{1}{PI_{ref}} \right) . PI_{ref}$$

This gives us:

$$\frac{m_1 - m_{ref}}{m_{ref}} = \frac{PI_{ref}}{PI_1} - 1$$

Appendix C: detailed LCA results in all impact categories

Cradle-to-gate:

Material	ADF (MJ/f.u.)	AP (kg SO2 eq/f.u.)	FETP (kg DCB eq/f.u.)	GWP (kg CO2 eq/f.u.)	POPC (kg ethene eq/f.u.)
PLA	112.6	0.03	2.9	4.6	0.004
GF/PP	102.9	0.02	1.1	4.9	0.003
CNF/epoxy	149.6	0.03	0.7	8.6	0.004
BC/epoxy	271.6	0.07	2.8	13.8	0.007

Detailed production of the CNF/epoxy composite:

	ADF (MJ/f.u.)	AP (kg SO2 eq/f.u.)	FETP (kg DCB eq/f.u.)	GWP (kg CO2 eq/f.u.)	POPC (kg ethene eq/f.u.)
Porous medium	33.66	0.0045	0.200	1.30	0.00091
Other consumables	32.79	0.0062	0.194	2.89	0.00125
CNF Paper (no grinding)	14.62	0.0056	0.256	-0.39	0.00057
Epoxy Resin	34.13	0.0060	0.001	2.34	0.00064
Epoxy hardener	5.72	0.0003	0.001	0.21	0.00007
Fibrillation by grinding	24.69	0.0062	0.002	1.93	0.00037
Electricity	3.95	0.001	0.0004	0.3	0.00005

Detailed production of BC:

	ADF (MJ/f.u.)	AP (kg SO2 eq/f.u.)	FETP (kg DCB eq/f.u.)	GWP (kg CO2 eq/f.u.)	POPC (kg ethene eq/f.u.)
Peptone	1.81	0.001	0.01	-0.017	0.0001
Water	1.76	0.001	0.087	0.2	0.0001
Yeast extract	15.19	0.005	0.092	0.757	0.0007
Citric acid	17.15	0.002	0.013	1.113	0.0002
Glucose	60.86	0.01	0.175	-1.443	0.0004
Pellicle washing	22.72	0.008	0.202	2.614	0.0006
Sodium Phosphate	11.58	0.024	1.655	1.577	0.0012

Cradle-to-grave:

Material	ADF (MJ/f.u.)	AP (kg SO2 eq/f.u.)	FETP (kg DCB eq/f.u.)	GWP (kg CO2 eq/f.u.)	POPC (kg ethene eq/f.u.)
PLA	398.3	0.096	5.74	26.9	0.016
GF/PP	283.5	0.059	2.92	18.9	0.01
CNF/epoxy	295.5	0.061	2.13	19.9	0.097
BC/epoxy	442.2	0.11	4.52	27.1	0.014

Appendix D: copyrighted work permissions

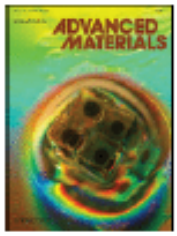

Title: Optically Transparent Composites Reinforced with Networks of Bacterial Nanofibers

Author: H. Yano,J. Sugiyama,A. N. Nakagaito,M. Nogi,T. Matsuura,M. Hikita,K. Handa

Publication: Advanced Materials

Publisher: John Wiley and Sons

Date: Jan 25, 2005

Logged in as:
Martin Hervy
Imperial College London

LOGOUT

Order Completed

Thank you for your order.

This Agreement between Imperial College London -- Martin Hervy ("You") and John Wiley and Sons ("John Wiley and Sons") consists of your license details and the terms and conditions provided by John Wiley and Sons and Copyright Clearance Center.

Your confirmation email will contain your order number for future reference.

printable details

License Number	4241820029640
License date	Dec 04, 2017
Licensed Content Publisher	John Wiley and Sons
Licensed Content Publication	Advanced Materials
Licensed Content Title	Optically Transparent Composites Reinforced with Networks of Bacterial Nanofibers
Licensed Content Author	H. Yano,J. Sugiyama,A. N. Nakagaito,M. Nogi,T. Matsuura,M. Hikita,K. Handa
Licensed Content Date	Jan 25, 2005
Licensed Content Pages	3
Type of use	Dissertation/Thesis
Requestor type	University/Academic
Format	Print and electronic
Portion	Figure/table
Number of figures/tables	1
Original Wiley figure/table number(s)	figure 2. A)
Will you be translating?	No
Title of your thesis / dissertation	Cellulose nanopaper as reinforcement for sustainable polymer composites
Expected completion date	Feb 2018
Expected size (number of pages)	160
Requestor Location	Imperial College London Department of Aeronautics South Kensington Campus London, London SW 7 2AZ United Kingdom Attn: Mr. Hervy
Publisher Tax ID	EU826007151
Billing Type	Invoice
Billing address	Imperial College London Department of Aeronautics South Kensington Campus

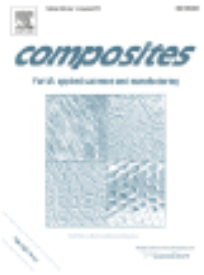

Title:	Strong and optically transparent biocomposites reinforced with cellulose nanofibers isolated from peanut shell
Author:	Baoxia Wang,Dagang Li
Publication:	Composites Part A: Applied Science and Manufacturing
Publisher:	Elsevier
Date:	December 2015

Logged in as:
Martin Hervy
Imperial College London
Account #:
3001225019

LOGOUT

Order Completed

Thank you for your order.

This Agreement between Imperial College London -- Martin Hervy ("You") and Elsevier ("Elsevier") consists of your license details and the terms and conditions provided by Elsevier and Copyright Clearance Center.

Your confirmation email will contain your order number for future reference.

printable details

License Number	4275940055739
License date	Jan 25, 2018
Licensed Content Publisher	Elsevier
Licensed Content Publication	Composites Part A: Applied Science and Manufacturing
Licensed Content Title	Strong and optically transparent biocomposites reinforced with cellulose nanofibers isolated from peanut shell
Licensed Content Author	Baoxia Wang,Dagang Li
Licensed Content Date	Dec 1, 2015
Licensed Content Volume	79
Licensed Content Issue	n/a
Licensed Content Pages	7
Type of Use	reuse in a thesis/dissertation
Portion	figures/tables/illustrations
Number of figures/tables/illustrations	1
Format	both print and electronic
Are you the author of this Elsevier article?	No
Will you be translating?	No
Original figure numbers	fig. 7
Title of your thesis/dissertation	Cellulose nanopaper as reinforcement for sustainable polymer composites
Expected completion date	Feb 2018
Estimated size (number of pages)	160
Requestor Location	Imperial College London Department of Aeronautics South Kensington Campus London, London SW 7 2AZ United Kingdom Attn: Mr. Hervy
Publisher Tax ID	GB 494 6272 12
Total	0.00 GBP

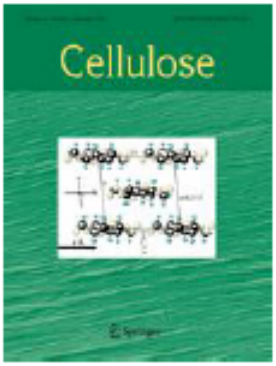

Title: A comparative study of energy consumption and physical properties of microfibrillated cellulose produced by different processing methods

Author: Kelley L. Spence, Richard A. Venditti, Orlando J. Rojas et al

Publication: Cellulose

Publisher: Springer

Date: Jan 1, 2011

Logged in as:
Martin Hervy
Imperial College London

LOGOUT

Order Completed

Thank you for your order.

This Agreement between Imperial College London -- Martin Hervy ("You") and Springer ("Springer") consists of your license details and the terms and conditions provided by Springer and Copyright Clearance Center.

Your confirmation email will contain your order number for future reference.

printable details

License Number	4241820242519
License date	Dec 04, 2017
Licensed Content Publisher	Springer
Licensed Content Publication	Cellulose
Licensed Content Title	A comparative study of energy consumption and physical properties of microfibrillated cellulose produced by different processing methods
Licensed Content Author	Kelley L. Spence, Richard A. Venditti, Orlando J. Rojas et al
Licensed Content Date	Jan 1, 2011
Licensed Content Volume	18
Licensed Content Issue	4
Type of Use	Thesis/Dissertation
Portion	Figures/tables/illustrations
Number of figures/tables/illustrations	1
Author of this Springer article	No
Order reference number	
Original figure numbers	figure 5
Title of your thesis / dissertation	Cellulose nanopaper as reinforcement for sustainable polymer composites
Expected completion date	Feb 2018
Estimated size(pages)	160
Requestor Location	Imperial College London Department of Aeronautics South Kensington Campus London, London SW 7 2AZ United Kingdom Attn: Mr. Hervy
Billing Type	Invoice
Billing address	Imperial College London Department of Aeronautics South Kensington Campus London, United Kingdom SW 7 2AZ Attn: Mr. Hervy